Orbital Free Ab Initio Molecular Dynamics Simulation Study of Static and Dynamic Properties of Liquid Binary Alloys

A dissertation presented

by

Mohammad Alamgir Hossain

to

The Department of Theoretical Physics

in partial fulfillment of the requirements

for the degree of

Doctor of Philosophy

in the subject of

Theoretical Physics

University of Dhaka

Shahabag, Dhaka-1000

September 2022

Professor G. M. Bhuiyan
(Ph. D.)
316, New Physics Building
Cell: +880-1911305306
E-mail:gbhuiyan@du.ac.bd

Department of Theoretical Physics
University of Dhaka
Ramna, Dhaka-1000, Bangladesh
Phone: +880-9666911463, Ext. 7050
Fax: +880-2-9667222
E-mail: theor_phys@du.ac.bd

Approval Sheet

This is to certify that the thesis entitled "Orbital Free Ab Initio Molecular Dynamics Simulation Study of Static and Dynamic Properties of Liquid Binary Alloys" has been written by Mohammad Alamgir Hossain who has successfully carried out this research under my supervision. He can now submit the dissertation to the concern authority for evaluation for his Ph. D. degree.

Dated, Dhaka
December 28, 2023

Dr. Golam Mohammed Bhuiyan
Professor

তাত্ত্বিক পদার্থবিজ্ঞান বিভাগ, ঢাকা বিশ্ববিদ্যালয়, রমনা, ঢাকা - ১০০০, বাংলাদেশ।
ফোন ঃ +৮৮০-৯৬৬৬৯১১৪৬৩, এক্স- ৭০৫০, ফ্যাক্স ঃ +৮৮০-২-৯৬৬৭২২২, ই-মেইল ঃ theor_phys@du.ac.bd

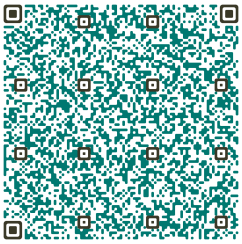

ISBN: 978-984-35-3007-3

Thesis supervisor

Dr. Golam Mohammed Bhuiyan

Author

Mohammad Alamgir Hossain

Orbital Free Ab Initio Molecular Dynamics Simulation Study of Static and Dynamic Properties of Liquid Binary Alloys

Abstract

Recently, *ab initio* molecular dynamics simulation has been an effective tool to study different physical properties of condensed matters. Simulation using the Kohn-Sham orbitals is much accurate in principle, but it demands very long computational time. As a consequence, it limits the number of particles (just few hundreds) in a periodic cell. This limitation may be largely overcome by employing the orbital free *ab initio* molecular dynamics (OF-AIMD) simulation method. This method is based on the Hohenberg-Khon version of the Density Functional Theory (DFT). Here the exchange and correlation functions are treated by the local density approximation (LDA). Specefically, in the present work we have studied some static and dynamic properties of NaK liquid metallic binary alloys. The static properties involve the static structure factors, isothermal compressibility, partial coordination number etc. The dynamic properties studied are dynamic structure factors, shear viscosity, diffusion coefficients, and velocity of sound. Static and dynamic properties calculated from the OF-AIMD simulation data are found to be good in agreement with the available experimental and other simulation data.

Contents

List of Figures

List of Tables

Acknowledgments

Praise be to Allah, the One and Only God, the Lord of the World. May Allah send blessings and peace upon the best of the chosen ones, Muhammad and upon his family and Companions.

Firstly, I would like to thank my supervisor Prof. Golam Mohammed Bhuiyan for his guidance and immense support through out my PhD research program. His vast knowledge, patience and motivation inspired me towards knowledge based development for understanding physical interpretation of natural phenomenons and the research methodology to explore new sciences. Prof. Bhuiyan is the most innovative, collaborative and friendly person who leading the theoretical condensed matter physics group at the Department of Theoretical Physics. I am honored and lucky enough to get the opportunity to work in this group. It is not possible for me to express my gratitude to him by any means.

Apart from my Supervisor, I won't forget to express the gratitude to Dr. Abu Zafur Ziauddin Ahmed. I found him as my mentor, without his cooperation my doctorate research would have been beyond my imagination. Although he is not my formal joint or co-supervisor but I always find him in such role. His encouragement and insightful suggestion exile my research and writing skills. It would be very hard for me to forgot his endless support and guidance in my entire life.

I would like to thank Dr. Md. Riazuddin Molla, Dr. Mohammad Abdur Rashid, Mohammad Saiful Alam and my teachers. I greatly acknowledge the support and cooperation of Dr. Riazuddin as a senior member of condensed matter research group. He is very generous and amicable person. Another wonderful person to acknowledge is Mohammad Saiful Alam. His assistance for drawing some figures is remarkable. I remember Dr. Rashid for his logistic and technical support. Dr. Md. Masud Rana is a nice dynamic person. I am thankful to him for his logistic support and continual encouragement.

I would also like to thank Professor Dr. Mohammed Arshad Momen and Prof. Dr. Tanvir Hanif, to extend their administrative support and to provide all the required facilities for me during my Ph.D study. I would also like to express my appreciation to all the faculty members and stuffs of the Department of Theoretical Physics, University of Dhaka for their warm cooperation.

Specially, I would like to mention the collaboration with Departamento de Física Teórica, Universidad de Valladolid, Valladolid, Spain. My profound gratitude goes to Prof. Dr. D. J. González and Prof. Dr. L. E. González, Departamento de Física Teórica, Universidad de Valladolid, Valladolid, Spain for providing us the orbital free *ab initio* molecular dynamics (OF-AIMD) simulation code. Their support and collaboration enriched my research.

I am thankful to Indian Institute of Technology, Kharagpur (IIT Kharagpur) for their support under the Center for Theoretical Studies (CTS) visitors programme. In

this regards I am very thankful to Prof. A. Taraphder for arranging this support to host me at IIT Kharagpur.

I acknowledge the financial support of Bose Center for Advanced Study and Research in Natural Sciences, University of Dhaka for my M.Phil. program. I also acknowledge the financial support of the Ministry of Science and Technology, Bangladesh under the project of Bangabandhu Science and Technology Fellowship Trust to carry out my PhD study.

I am greatly indebted to my wife Mahjabeen Islam and my daughters Nujhat Jabeen Hossain, Nabeeha Jabeen Hossain, because they are form the backbone and origin of my happiness. Their constant support and unparallel love have enabled me to complete the write up of this dissertation. I owe to all of them for my every achievement.

Finally, but most importantly, I acknowledge the support of my family. My sincere thanks goes to my father Mohammad Mafiz Uddin and also to my mother Most. Asmotar Nasa, my younger brother Mohammad Didarul Alam and his wife, my father in law Md. Mahbubul Islam, my mother in law Nilufa Islam, my brother in law Nasih-ul-Islam and his wife, my sister in law Farhana Islam and her husband Md. Mizanur Rahman.

Mohammad Alamgir Hossain,
September 11, 2022

Dedicated to my father Mohammad Mafiz Uddin,
my mother Most. Asmotar Nasa,
my Wife Mahjabeen Islam,
my daughters Nujhat Jabeen Hossain & Nabeeha Jabeen Hossain,
and my brothers & sisters

Chapter 1

Introduction

Now a days, there are three wide research fields in Physics. These fields are (i) the particle and high energy physics (ii) Cosmology and (iii) condensed matter physics and Non-Linear Physics. Field (i) deals with very tiny things, (ii) is associated with very big things and the third one deals with very complicated microscopic features of the surface and bulk systems. The topics of the present thesis covered part of the third field where alloys of liquid metals are investigated through studying several static and dynamic properties by deploying orbital free *ab-initio* molecular dynamic (OF-AIMD) simulation technique. OF-AIMD is a special case of general density functional theory (DFT) [1–3], where orbitals are approximated by taking local density approximation (LDA). Study of liquid systems poses difficulties due to the unavailability of perfect theoretical models as it is exist for the ideal gas or the harmonic solids at low temperature. Although, many theoretical models have been developed to explain different features of liquid systems having diverse nature. For instance, one can recall the quasi-lattice model [4], and the perturbative models [5]. In the former

one similarity between physical behaviours of liquids and solids are exploited, and in the latter model perturbation to a reference system is employed in a similar fashion as in other fields.

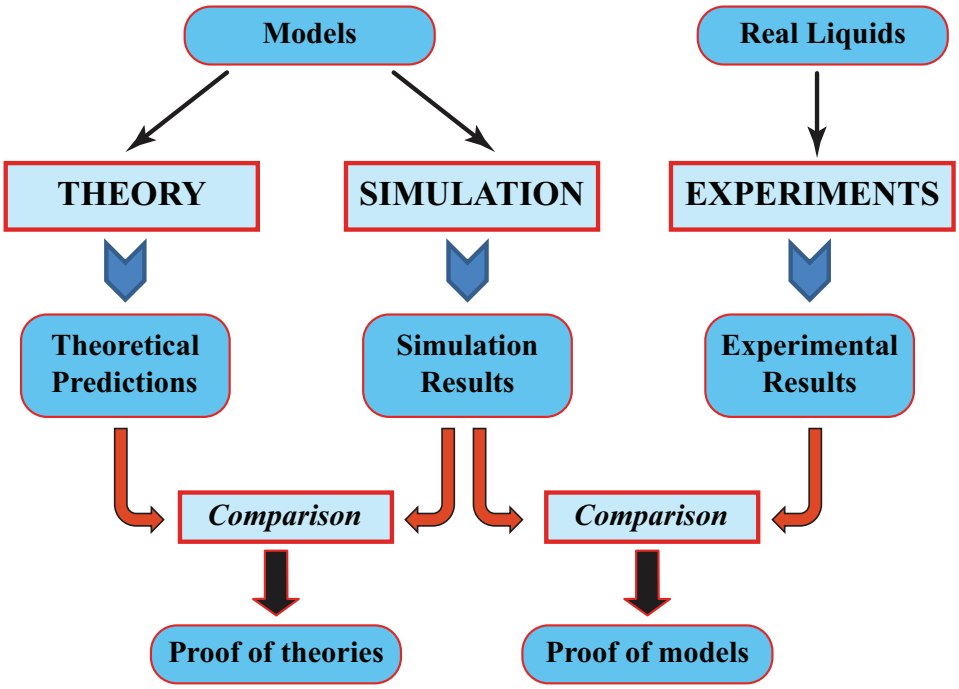

Figure 1.1: Connection among theory, experiment and simulation [6].

An approach to study physical properties of liquid systems that is different from the theory and the experiment is the simulation technique, in particular, the Molecular Dynamics (MD) simulation method. The MD simulation technique is, in fact, an extremely effective tool for the investigation of physical behaviour of the macroscopic systems of different dimensions. On the other hand, MD simulation allows to test the reliability of various theoretical models and also yields information which are difficult or impossible to gather experimentally. The computational power thus

enable us to perform complex calculations in order to solve equation of motion for a group of molecules keeping full control over the ambient conditions (external fields, pressure etc). More specifically, metals in the liquid state form a good sample to perform simulation in a precise way to obtain exact results without going to any approximation.

The first Molecular Dynamics (MD) study goes back to Alder and Wainwright. The solid-liquid phase transitions of a system of molecules interacting via a hard-spheres potential

$$v(r) = \begin{cases} \infty & r \leq a \\ 0 & r > a. \end{cases} \tag{1.1}$$

are studied by them in 1957 [7]. In equation (1.1) a denotes the hard sphere (HS) diameter. Two years latter Alder and Wainwright discuss in detail about the purpose, methodology, applications and limitations of MD simulation method [8]. Rahman in an article in 1964 presented results of MD simulation with 864 atoms in a sample at 94.4 K and material density of ρ=1.374 g.cm^{-3} [9]. Here, the inter-ionic interaction was described by the Lennard-Jones (LJ) potential [10]:

$$v(r) = 4 \in \left[\left(\frac{\sigma}{r} \right)^{12} - \left(\frac{\sigma}{r} \right)^{6} \right]. \tag{1.2}$$

The MD simulation data enabled him (Rahman) to evaluate different correlation functions that are microscopic in nature. For this seminal work and his productive career, in general, Rahman emerged as one of the pioneers for the study of physical problem employing simulation methods. Many codes developed by him are still being used now a days. Following the work of Rahman, Verlet performed simulations to calculate different structural [11], thermodynamic [12], and dynamic properties.

Verlet's work improved some technical aspects of MD simulation like algorithm for calculating coordinates and velocities, this algorithm has been established now and is known as the Verlets algorithm. An excellent review on the work done in 1970s is also there [13].

In 1970s computer simulation techniques were widely used by the physicists and chemists. At that time a question arose whether simulation fits in experimentation or in the theory. It is true that, the simulated system is not real but mimics the real system as far as time evaluation is concerned. On the other hand, simulations are prepared just like an experiment, both generates data after the run and these are finally analyzed to describe physical or chemical properties of the sample. From this point of view there is a similarity between simulation and experimentation. Theory, on the other hand, adopts other path based on mathematical formulae, reduction-ism and prediction of new phenomena. From these points of view simulation share several points with the theory. Therefore, the computer simulation forms a field of its own and plays a fundamental role in connecting both the theory and experiment, this is illustrated in figure 2.1.

The computer simulation method got a giant step forward in 1980s when the electronic states are explicitly entered in to the calculation. Before that the N-body inter-ionic interactions where modeled by effective pair potentials where the existing parameters were adjusted fitting the experimental data. Following the first simulation work performed by Rahman and Verlet (where the LJ pair potential was used for argon) recently much more sophisticated potential models are being developed in order to study different complicated systems. For instance, potential model to

describe interaction in water [14], in liquid metals [15], and in proteins [16], can be noted. Despite the success of the simulation methods namely the Classical Molecular Dynamics (CMD) some limitations still remains in the case of transfer-ability of the pair potentials. This limitation impeded to have a precise general description of the systems that can reproduce the experimental data.

The most remarkable event in the development of the simulation technique is the work of Car and Parrinello [17] in which they successfully introduced electrons in the simulation. As a result a new class of simulation methods is generated that are known as the *ab-initio* Molecular Dynamics (AIMD) or the first principles molecular dynamics. In AIMD the forces acting on the molecules were obtained from the electronic energy through the Hellmann-Feynmann theorem. Inter-ionic interactions are, therefore, handled at a much more fundamental level than the CMD. The complex phenomena such as formation of electronic bonds [18], distortion and polarization in water molecules have automatically emerged from the AIMD simulation. The *ab-initio* methods, on the other hand, are much more cumbersome and computationally expensive.

An *ab-initio* calculation gives the absolute energy of a system of fixed ionic configuration and moving electrons. The major disadvantage of the *ab-initio* methods is the demands on heavy computational power. The fundamental concept of AIMD techniqe is to solve the Schrödinger wave equation (SE). The resulting solutions then describe the quantum mechanical state, namely the ground state energy from which forces on the ions and other physical properties (structural and dynamic) of the system are obtained. Practically, the SE can not be analytically solved for systems

containing more than one electron. For this reason, different approximation methods have been introduced in the theory and, over the years these are evolved up to the level of satisfaction. All these methods have their own merits and demerits. These approximation methods are often classified into two groups; namely the wave mechanics based approach [19] and the density functional based approach [20].

In the present work, a method based on the density functional theory (DFT) within the framework of Hohenberg and Kohn theory [1] is applied to investigate the bulk properties of liquid simple metals alloys. The DFT is the most convenient technique to solve the SE for the ground state energy of a system. This is because the DFT method is capable of dealing with systems consisting of hundreds or even more atoms. Whereas, for coupled cluster and other wave mechanics based methods the cost of computation enhances severely with the increasing size of the system. One faces gridlock just for working with a few tens of particles using the largest supercomputers and most efficient algorithms. Definitely the DFT has already occupied the position of the most attractive *ab-initio* method recently for the simulations of the condensed matter. The DFT can be categorized into either orbital based or orbital free method. Explicit density dependent total energy functional of the DFT as proposed by Hohenberg and Kohn [1] is known as the orbital free DFT (OF-DFT). When the kinetic energy (KE) functional, $T_s[\{\psi_i\}]$, and all other terms including the exchange and correlation (XC), $E_{xc}[\rho(\mathbf{r})]$, depend implicitly on the orbitals in the total energy functional, this method is named as the Kohn and Sham DFT (KS-DFT) or orbital based DFT [2]. The KS-DFT method is time consuming and only been used for systems of small size (up to ≈ 100 particles), whereas OF-DFT can handle

a system having hundreds or thousands or even more particles without considerable time consumption. By construction the OF-DFT technique is less accurate than the KS-DFT because the former method does not take care of actual orbitals. But, in practice, to mimic a real system closely one should put particles, as more as possible, in the periodic cell. From this point of view the OF-AIMD method is favourable. We have employed OF-DFT in this study for a binary system. Here, 2000 particles are taken in a cell. The accuracy [21] level of our calculations is found to be comparable to that of the KS-DFT.

As the new generation of computers and relevant algorithms has been developed the OF-AIMD methods are being incorporated into the field of scientific research and, now, it has been a very powerful tool to study the behaviour of different physical properties [22, 23]. Liquid metal is a good example of systems that expose itself for the basic research and industrial applications. Research in liquid metals and their alloys has enhanced in recent years because their various applications in diverse fields such as in fusion energy, for tumor therapy, medicine, nerve connections and bone disease repair [24]; for low dimension electronic circuits; nanoelectronics, and soft robotics, for wearable technology [25].

Fusion energy production could meet the current energy crisis without any hazard and environmental challenges being faced by humankind today. This is why, many different research projects are now focused in inventing proper technology to maintain high temperature plasma without burning the machinery containing it. Metals in liquid phase are having a promising plasma facing component, because, their properties will remain unchanged by the displacement of atoms due to their collisions

with particles escaping from plasma. Additionally, liquid metals can withstand high temperature inside the fusion reactor. In this regard, the most promising materials are being sodium (Na) and potassium (K). Several experiments have already been performed to study their effectiveness at high temperatures. The computer simulations would be, however, of great help in understanding different physical properties at different thermodynamic and environmental situations.

Solids, liquids and gases are categorized as having various states of matter [26], because each of them organizes their atoms and molecules differently. While molecules in a gas move freely, those in a solid are closely packed. Condensed substance is referred to as a liquid [27, 28]. Although its symmetry is more like that of a gas, its density is comparable to that of the solid phase. Many properties of liquids, such as specific heat [29], are comparable to those of solids at similar temperatures, although they are typically far more challenging to calculate than those of solid states or gases. For instance, near the melting point, the specific heat of sodium (Na) at constant volume C_V is remarkably similar to the specific heat of the monoatomic solid $3Nk_B$. This is remarkable because transverse vibrational modes, which are accountable for a specific heat contribution, cannot exist in a perfect fluid. We get liquid metal alloy when we combine the atoms of two or more elemental liquid metals. Liquid alloys are significant from a metallurgical perspective because many solid binary alloys are initially created by cooling from a liquid alloy. This is crucial for understanding the energetics involved in the production of solid alloys. The stability of metallic glasses which are metastable amorphous systems created by fast quenching liquid alloys of favourable composition, may also be better understood with knowledge of liquid al-

loys. Additionally, liquid alloys are important in astrophysics and geophysics. White dwarfs may have even more unusual, quasi-metallic components. The innards of planets may contain a liquid mixture of metallic hydrogen and helium. For advanced bearing materials, alloys with a miscibility gap in the liquid state are very intriguing. Liquid alloys are widely used in many fields of science and engineering, which increases the importance of their geochemical characteristics. Numerous theoretical and experimental research [7-9] have been done on the wetting and other surface characteristics of alloys. The multicomponent alloys [10] are an emerging field of research.

Here the results of an OF-AIMD simulation study for the static and dynamic properties of Na_xK_{1-x} liquid binary alloy at a temperature near its melting point are reported. We have performed simulation for liquid Na_xK_{1-x} alloys at concentrations, x_{Na} = 0.1, 0.2, 0.3, 0.4, 0.5, 0.6, 0.7, 0.8 and 0.9. Our simulated results seem to be promising in comparison to available scientific literature both theoretical and experimental ones.

This thesis is organized as follows. Chapter 2 presents the general features of alkali metals. The computational method is described in Chapter 3. Chapter 4 and 5 present the density functional theory and liquid state theory, respectively. Chapter 6 include all the results obtained from our calculation. Finally, conclusions are drawn in chapter 7.

Chapter 2

General Features of the Alkali Metals

2.1 Periodic Alkali Metal Trends

Alkali metals are treated as simple metals due to their particular electronic structure. As their metallic behaviour in the liquid phase remains almost same they are called simple liquid metals. This feature of liquid alkali metals these attracted more attention of the physicists and chemists, and that led a large number of theoretical, experimental and computational studies available in the literature. On the contrary, their neighbour, liquid rare earth metals received much less attention in terms of availability in the literature. It is, however, worth noting that properties of alkali metals in the solid state specifically the phase diagram as a function of pressure and temperature are investigated both theoretically and experimentally. Some interesting phenomena also emerged from these studies.

Though a lot of experimental information is available for liquid alkali metals, there is scarcity of experimental information for the liquid alkali metallic alloys. This lack-

ing implicitly restricted dedications from the theoretical point of view. In order to gain more information and to understand clearly the structural and dynamic properties of liquid alkali metals alloy we have undertaken this project to study them through the molecular dynamics simulation (MD) method, near their melting points. Some salient features of alkali metals are:

- Soft, Shiny and Silvery.
- high reactivity at standard pressure and temperature.
- rapidly give up their outermost electron to create cations with a positive charge.

Due to the softness of alkali metals they can be cut into pieces just by a plastic knife. Shiny surface of them vanishes rapidly in the air because of oxidation. Alkali metals are therefore preserved under oil so that reaction with atmospheric air do not occur. Alkali metals in the periodic table lie in group 1, (excluding H). Alkali metals react with normal H_2O, but reaction of the latter is stronger than the former ones.

Lithium, sodium, potassium, rubidium, cesium, and francium alkali metals make up group 1 (1A) of the periodic table and are considered to be alkali metals. Due to the fact that their outermost electron is in an s-orbital, they belong to the s-block group of elements, which are located on the left side of the periodic table. The reason the alkali metals have that name is because they react with water to produce alkali's, which are powerful bases that may counteract acids. Sodium and potassium make up 2.6% and 2.4% of the crust of the Earth, making them the sixth and seventh most prevalent elements. The other alkali metals, cesium, lithium, and rubidium, which make up 0.03, 0.007, and 0.0007 percent of the Earth's crust, respectively, are

far rarer. The periodic table's group trends in attributes are best illustrated by the alkali metals, which contain elements that share many characteristics. For instance, all recognized alkali elements are displayed as you move down the table:

- expanding the atomic radius,
- the electronegativity is diminishing,
- expanding reactivity,
- melting and boiling points falling.

Moving down the periodic table generally causes their densities to increase, with the exception of potassium, which has a density that is lower than sodium. Alkali metals are only found as compounds and are particularly reactive. They are unit valence electropositive metals.

2.2 Alkali Metal Electronic Configurations

(i). In the valence shell of an alkali metal, there is just one electron.

(ii). ns^1 specifies the electronic configuration. As an illustration, the electronic configuration of sodium is $1s^2$, $2s^2$, and $3s^1$.

(iii). They frequently lose the outer shell electron to produce positively charged cations (monovalent ions).

(iv). As a result, they are the most electropositive elements. For the same reason, they are also the least pure elements.

Table 2.1: Position of simple, less simple and transition metals in the periodic table and their electronic configurations.

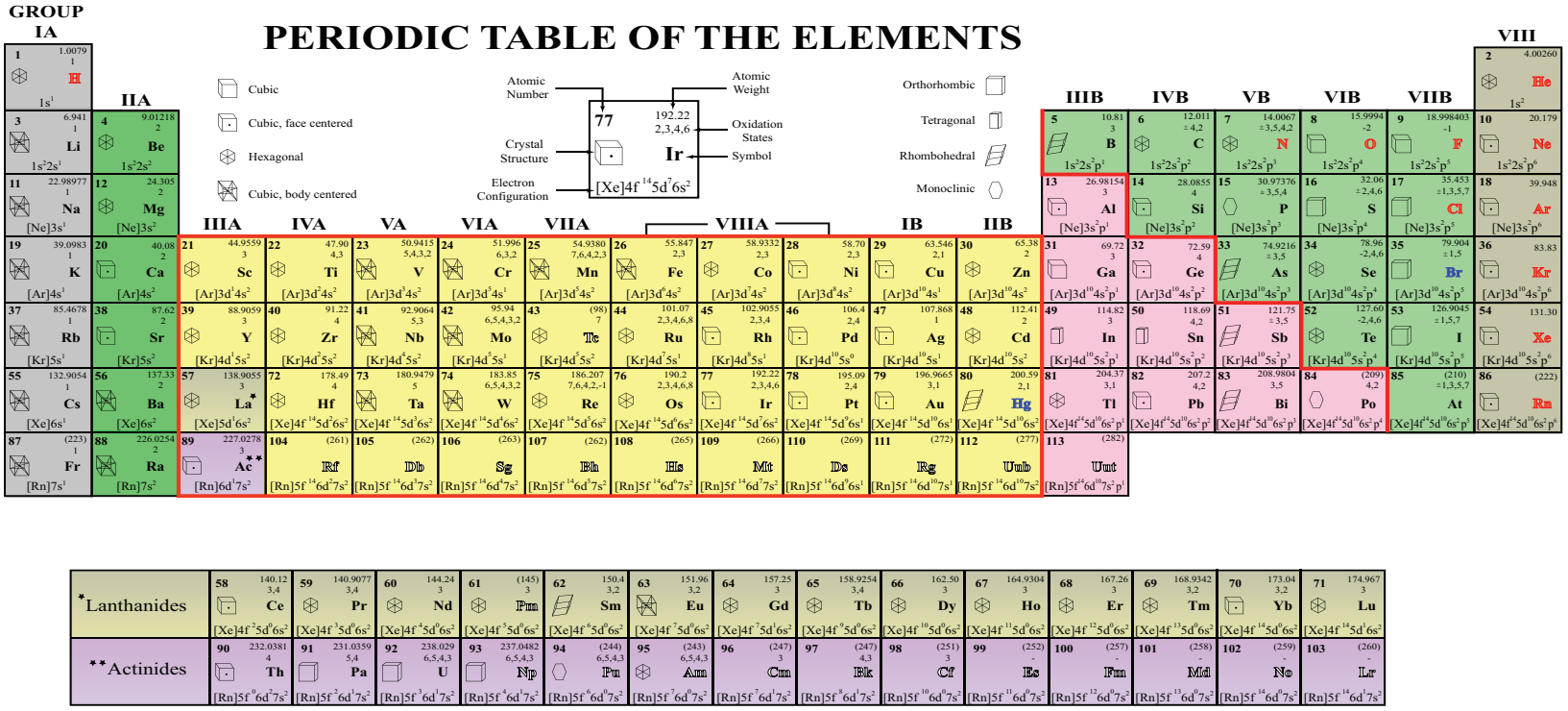

2.3 Sodium

The soft, silvery metal sodium interacts strongly with water and tarnishes quickly in the presence of air. The Earth's crust, contains 2.6%, the sea water contain 15% of sodium, it is the fourth most prevalent element. The name is taken from the English word soda, which is used to describe a variety of sodium compounds, including baking soda, washing soda, and sodium hydroxide (caustic soda). The symbol "Na" originates from the latin word *natrium*. It may be collected from saltwater and is present in the minerals trona (sodium carbonate) and halite (rock salt, or sodium chloride, NaCl). About 60% of the salt collected from these sources is turn into sodium carbonate, sodium hydroxide, another 20% is utilized as a preservative and flavoring agent in the food sector; the other 20% is used for other purposes, such as de-icing roadways. As it reacts with the moisture in the air to generate metallic sodium, sodium hydroxide it is typically kept in the mineral oil or another hydrocarbon.

Yellow light is produced when sodium atoms are energetically excited; the highest emissions are known as "sodium D-lines" wavelengths of which are 589.0 and 589.6 nm (including the sun). Street lighting using sodium vapor also use sodium. Sodium ions in human body control blood pressure and osmotic pressure, while sodium and potassium ions jointly play a significant role in nerve impulse transmission. Table salt, or sodium chloride, is one of the most significant substances. Commercially produced sodium chloride is either extracted from the earth as halite, from deposits left behind by long-defunct seabeds, or as a byproduct of the evaporation of seawater. In a device known as a Downs Cell, sodium chloride is electrolyzed to create metallic sodium and chlorine gas. The structure of the cell is intended to keep the sodium

and chlorine distinct as they are formed. Since ancient times, people have utilized sodium carbonate, also known as soda ash or sodium bicarbonate, to make glass, paper, detergents, and soda (which helps remove highly charged cations like calcium and magnesium from the hard water). Strong base sodium hydroxide, commonly known as caustic soda or lye, is used to make detergents and drain cleaners. It does this by degrading triglycerides, which are oils and fats like lard, vegetable oils, olive oil, etc. to create carboxylate salts, which are the building blocks of soap. Baking soda's major component, sodium bicarbonate, or $NaHCO_3$, commonly referred to as sodium hydrogen carbonate, is used to leaven bread and other baked goods.

In fast neutron reactors, sodium is a well-known Heat Transfer Fluid (HTF). Its melting and boiling points are 97.8 and 881.4 degrees Celsius, respectively. It is a good HTF because of its strong thermal conductivity and moderately high heat capacity, although it is very reactive with water. The United States of America started developing liquid metal fast breeder reactors in the 1950s of the previous century (LMFBR). Because of its excellent heat transmission and nuclear properties, sodium was chosen as the coolant [30].

2.4 Potassium

Potassium is a soft, silvery metal but tarnishes rapidly in atmospheric air and interacts quite violently with water. Its name comes from the English word "potash", which stands for potassium carbonate, a substance that is present in large quantities in wood ashes. The letter "K" is taken from the Latin word, *kalium*. In the Earth's crust, potassium is 4th most common element. The three primary potassium-containing

ores are sylvite (potassium chloride, carnallite and alunite).

Potassium is crucial for plant health and is widely used in producing fertilizers. In human body, potassium plays a crucial part in the contraction of muscular tissue, and the mobility of Na and K ions in nerve cells plays a significant role in the transmission of nerve impulses. Potassium salts are utilized in fireworks because they light a purple color when heated. Potassium is typically kept beneath mineral oil or another hydrocarbon as in the case of Na. Like sodium, it can also oxidize in dry air to form potassium superoxide, KO_2.

Potassium reacts chemically with water to form potassium hydroxide and hydrogen as the end products. This reaction generates a lot of heat energy, which frequently ignites the hydrogen gas that is created. Potassium-40, is radioactive and makes up 0.0117% of the total amount of K in the planet and its half-life is 1.25 billion years. By comparing the ratio of potassium-40 to argon-40 in rocks, one can estimate a rock's age. It goes through electron capture to make argon-40 (potassium-argon dating). All potassium sources contain trace levels of potassium-40, and in the human body about, 170,000 atoms of potassium-40 decay each second. Along with the decays of thorium and uranium, the energy generated by the potassium-40 decay contributes to the heat that exists inside the Earth.

Numerous potassium compounds are often utilized. Potassium chloride, also known as KCl, is a salt replacement that is combined with sodium chloride to enhance flavor and a component of fertilizers. It is also used in large quantities in fatal injections to hasten cardiac arrest and death. Glass is made using potassium carbonate, or potash, commonly known as K_2CO_3. Making soaps and detergents requires

the use of potassium hydroxide, sometimes referred to as caustic potash or KOH. A strong oxidizer and component of gunpowder, potassium nitrate, usually known as saltpeter, is used in fireworks and match heads. In order to manufacture oxygen for re breathers and other breathing apparatus, potassium superoxide, also known as KO_2, combines with CO_2 to form potassium carbonate and O_2 gas; it is also used in mines, submarines, and spacecraft.

2.5 Liquid metal properties

Liquid metals, in physics are composed of alloys with extremely low melting temperatures that, in the phase diagram, form a eutectic, meaning that the alloy is liquid at room temperature. For the purposes of reactor technology, liquid metallic alloys having low melting points can be used as reactor coolant within the working temperature ranges (usually above the room temperature). Because they have good heat transfer capabilities and can be used for systems with low-pressure as in the case of sodium-cooled fast reactors (SFRs). Regarding their structural peculiarities, metals are characterized by the existence of charge carriers, notably practically free electrons, which gives them great electrical and thermal conductivity. In power plants, a high rate of heat transfer and working surface temperatures that were close to coolant temperature were made possible by the use of liquid metal coolant.

Additionally, the liquid metals which are employed in the reactor as coolant are very poor neutron absorbers. So, this quality enables the operation of liquid metal reactors with a rapid neutron spectrum. Fast reactors based on liquid metal coolant have a high power density and do not require a neutron moderator. The drawback of

many liquid metals is that they retain the majority of their metallic properties when solidified for use in various technological devices.

2.6 Na_xK_{1-x} liquid alloy

The alkali metals sodium and potassium are combined to form the sodium-potassium alloy, often known as Na_xK_{1-x} . This alloy is typically liquid at room temperature. There are several commercial quality options. Na_xK_{1-x} needs to be handled carefully because it is highly reactive with water and can catch fire when exposed to air.

Na_xK_{1-x} is liquid at normal temperature and contains 40% to 90% potassium by mass. The eutectic mixture also known as Na_xK_{1-x}-77, which is a liquid from -12.6°C to 78.5°C and has a density of 0.866 g/cm^3 at 21°C and 0.855 g/cm^3 at 100°C, contains 77% potassium and 23% sodium by mass. It is less dense than water. Due to its high reactivity with water, it is typically stored under hexane or other hydrocarbons or under an inert gas (typically dry nitrogen or argon), if high purity and little oxidation are required. Na_xK_{1-x} pulls into a bun-like shape because of its extremely high surface tension. It has a specific heat capacity of 982 J/kg.K, which is about one-fourth that of water, but due to better thermal conductivity, heat transmission is higher along a temperature gradient.

It develops a yellow potassium super oxide layer when stored in the air, which could catch fire. With water and organic materials, this super oxide reacts violently. While mineral oil is lighter than most hydrocarbons, Na_xK_{1-x} is not thick enough to sink in them. If the super oxide has already developed, this method of storage is dangerous. On December 8, 1999, a sizable explosion occurred at the Oak Ridge Y-12

plant when Na_xK_{1-x} that had been improperly handled with mineral oil and cleaned up after an accidental spill was scratched with a metal instrument. PTFE (Teflon) is also damaged by the liquid alloy.

The Phase diagram of Na_xK_{1-x} binary alloy is shown in Figure 2.1 [31]. In the solid phase it exhibits β phase [32] after concentration, $x_{Na} = 0.7$. From the phase diagram it appears that the melting temperature of the alloy depends on the concentrations of the alloy. At concentration, $x_{Na} = 0.32$, the melting temperature becomes the lowest value of 260.53 K. The temperature at which we have performed the OF-AIMD calculations is 373 K which is above the melting temperature for all concentrations.

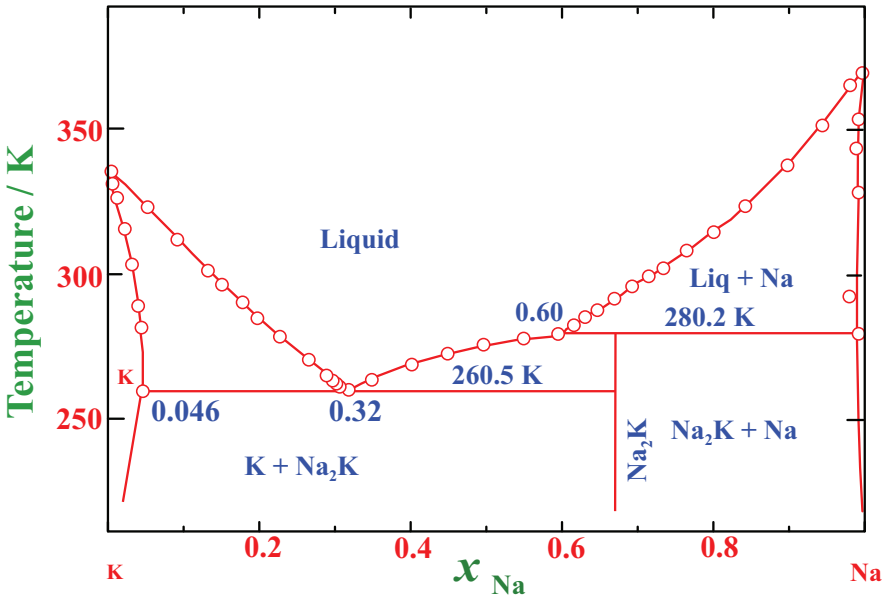

Figure 2.1: Phase diagram of Na_xK_{1-x} liquid alloy.

Experimental fast neutron nuclear reactors have employed Na_xK_{1-x} as its coolant. These get shut down and de-fueled more often than commercial plants. The other

materials used in practical reactors, lead or pure sodium, would need to be heated continuously in order to keep the coolant in a liquid state. Utilizing Na_xK_{1-x} helps to overcome this. As an example, consider the Dounreay Fast reactor. Na_xK_{1-x} has a relatively low vapor pressure, which is significant in the vacuum of space. Due to its advantageous thermal properties, liquid sodium-potassium alloy is a desirable heat

Table 2.2: Molar mass ($g.mol^{-1}$), melting point (K), boiling point (K), atomic number, electronic configuration, atomic radius and crystal structure of the group IA elements.

Element	Molar mass	Melting point	Boiling point	Atomic number	Electronic config.	Atomic radius	Crystal structure
Li	006.941	453.00	1620.00	3	$[He]2s^1$	1.52	bcc
Na	022.990	371.00	1154.00	11	$[Ne]3s^1$	1.86	bcc
K	039.100	336.00	1039.00	19	$[Ar]4s^1$	2.27	bcc
Rb	085.470	312.00	0961.00	37	$[Kr]5s^1$	2.47	bcc
Cs	132.900	301.00	0978.00	55	$[Xe]6s^1$	2.65	bcc
Fr	223.000	301.00	-	87	$[Rn]7s^1$	-	bcc

transfer medium for both the future generation of ground-based power plants [33] and the nuclear reactors used in space power systems [34]. However, sodium-potassium alloy shows incredible promise as a working fluid for heat pipes with improved thermal performance [35]. The low melting point of Na_xK_{1-x} coolant ($-12.6°C$) for a mixture of 32% Na and 68% K) and its comparatively strong heat conductivity are its key benefits.

Chapter 3

Computer Simulation

Computer simulation is the practice of mathematical modeling carried out on a computer and intended to forecast the behavior or result of a physical or real-world system. It also goes by the name "computer experiment". In computational physics, computer simulation has developed into a helpful tool for the mathematical modeling of numerous natural systems. Additionally, simulation can be used in situations when experiments are challenging, expensive, and risky. The prediction of material properties is one of the most often used molecular simulation applications, and it is typically accomplished using both the Monte Carlo (MC) and molecular dynamics (MD) computational techniques. Both molecular dynamics (MD) simulation and Monte Carlo (MC) methods are now often used to investigate the characteristics of materials, fabricate devices, and create new useful materials. In this instance, molecular dynamics simulations are our primary concern. In the upcoming section we will discuse Monte Carlo simulation in breif for the completeness of the description and we will describe molecular dynamic simulation in detail.

3.1 Monte Carlo Simulation

Probabilities are the foundation of the Monte Carlo method. Since it lacks dynamics, it does not follow the time evolution of configurations. It involves the computation of probabilities of generating arbitrary molecular configurations. In order to simulate a fluid system, we let the system transition between various configuration states. The subsequent three steps are used to make these transitions. The first step is the generation of a trial configuration at random. Calculating the change in energy and other attributes in the trial configuration is the next step in evaluating a "acceptance criterion". In order to determine whether to accept or reject the trial configuration, the acceptance criterion is finally compared to a random integer. In a finite amount of time, it is crucial to sample the states that contribute the most in order to precisely estimate the system's attributes. A Markov chain is created to achieve this. A Markov chain is a collection of trials where each subsequent trial's result only affects its immediately preceding trial. A new state in a Markov chain will be accepted with a higher probability if it is preferable to the current state. This typically indicates that the energy of the new trial state is lower.

In Monte Carlo simulations, a trial configuration is frequently created by shifting, exchanging, removing, or adding a molecule. The type and scope of the motion that is being attempted are both determined by probabilities. Probabilities are also used to determine the type and size of the motion that is being undertaken. Whatever ensemble is chosen, the transition probability always includes calculated energy of the new configuration and compared it to the energy of the previous state. When the attempted configuration is unsuccessful then the old state is counted as a new state.

3.2 Molecular Dynamics Simulation

Molecular simulation techniques are becoming more and more important in research and technology as a result of the advent of high speed computing. In this thesis, we examine various static and dynamic features of liquid Na_xK_{1-x} binary alloys using orbital free *ab initio* molecular dynamics (OF-AIMD) simulation methods.

For the study of material characteristics at the nano- and microscale, statistical mechanics is a crucial tool. The material properties of things can theoretically be derived from statistical mechanics if we have a good understanding of the interactions inside and between molecules. The analytical problems in statistical mechanics, with the exception of a few simple and ideal circumstances, can only be solved approximately or are insoluble. Molecular simulation can be a useful tool for delivering almost perfect solutions to statistical mechanics-related issues. Molecular simulation can be used to determine the material properties for a given tractable model. Theoretical hypotheses can be tested via molecular simulation. Additionally, one can determine the accuracy of a model by comparing the outcomes of molecular simulation to those of actual experiments. If the model is accurate, molecular simulation can also provide theoreticians and experimentalists with a wealth of knowledge that is currently difficult to obtain from either theory or experiment. Therefore, simulation serves two purposes: it connects models to theory and it connects models to experiment. One can use molecular simulation to determine the macroscopic properties of a system, such as thermodynamic quantities, transport coefficients, equations of state, etc., given microscopic information about the system, such as atomic mass, molecular structure, interactions between particles, etc. Both academically and technologically,

it is advantageous to understand the relationship between microscopic and macroscopic quantities. Additionally, molecular simulations can provide information on some crucial parameters that are difficult or even impossible to get through experiments. Extreme thermodynamic circumstances, for instance, make it challenging to conduct experiments. However, one can quickly acquire quantitative findings of, for example, a shock wave experiment, a high-temperature plasma, a nuclear reactor, star formation, and so on, utilizing molecular modeling.

A simulation technique for examining the actual motions of particles (molecules) and atoms is called molecular dynamics. where the evolution with time of a group of molecules that interact with each other is tracked by integrating the equation of motion. The core of the MD simulation is to solve the Newtonian equations of motion (NEM) for the system with a limited number of molecules. The MD method allows us to study the materials in molecular scale. By resolving Newton's equations for the motion of the molecules, it is possible to see how the locations, velocities, and orientations of the system's particles vary with time. For classical systems

$$\mathbf{F}_i(t) = m_i \frac{d^2\mathbf{r}_i}{dt^2}, i = 1, 2, \ldots, N, \tag{3.1}$$

where $\mathbf{r}_i$ and m_i are the position vector and mass of the i-th particle at time t, $\mathbf{F}_i$ denotes the force acting on the i-th particle and N is the overall number of molecules. In essence, MD is a motion image that tracks molecules as they move back and forth, twist, turn, and collide. An initial condition, which consists of the coordinates and momenta of each particle, is first applied N particles system. The coordinates and momenta of each molecule are then determined for each time step using the equations of motion. When the system has evolved in this fashion over time, we

can take the phase variables' time average. The system's time-dependent features can be discovered using MD simulation as it tracks time. Using the MD approach, we may examine a system's dynamical and equilibrium thermodynamic properties at a fixed temperature. The output of such simulation is simply the positions and corresponding velocities of the molecules of the sample in 'equilibrium', that is, at every simulation time step. By using these information, many physically interesting properties can be evaluated. The accuracy of a MD calculation widely depends on the method with which are the forces calculated. *Ab-initio* MD simulations method which will be briefly explained in the following part, to be employed in the current investigation.

3.2.1 Classical Molecular Dynamics Simulation

The forces in classical molecular dynamics are computed from a parameterized potential, either fitted to empirical data or computed from first principles. At least in compared to *ab initio* molecular dynamics, classical molecular dynamics is quick. Large systems with billions of atoms or more can be simulated, making it possible to model processes like grain formation, crack propagation, heat transfer, etc. Additionally, for modest system sizes, long simulation times can be obtained with many millions of time steps, allowing simulation of processes like diffusion that take a while to occur. Another benefit is that since the potential is known, it may be changed to investigate how variations in the potential affect the system's physical characteristics. As a result, it can be a useful model to comprehend the system's fundamental mechanics.

Despite the fact that there are numerous issues, the empirically fitted potential and forces come first. The exact quantum mechanical potential will always be better than the fitting. When fitting the parameters, compromises are a given. A decision must be made regarding which properties should be suited to and which ones should be reproduced. Due to the fact that the parameters are fitted to experimental or first-principles data for a specific set of conditions, there is also the issue of transfer ability. It's also unknown how well the model will capture a different set of circumstances when the potential is applied. This means that it is challenging to determine how accurate the potential is in an unidentified configuration. This is a serious restriction because the aim is to forecast attributes of that are unknown.

An alloy with a few elements will require a fast growing number of parameters because the majority of potentials are based on pair interactions and triplet interactions. Additionally, the number of parameters increases rapidly as the number of elements increases. Because of this, fitting takes a very long time. The fact that there are so many co-dependent factors and so few empirical data points to fit to them is an issue. Although parameters can frequently be fitted to *ab initio* results, this will need numerous expensive calculations.

3.2.2 *Ab initio* Molecular Dynamics Simulation

Typically an *ab initio* MD simulation technique (AIMD) uses force derived from electronic structure theory to change the dynamics of the system over time. Classical molecular dynamics (CMD), on the other hand, uses force obtained from (semi) empirical force fields. *Ab initio* is a Latin word and literally means "from the beginning".

When a calculation relies just on the tiny and well-established rules of nature without the use of any additional assumptions or special models,it is said to be *ab initio* or first principles. The AIMD is the name of the simulation technique that blends the traditional mo lecular dynamics of nuclei with electronic structure theory.

AIMD is one of the most significant numerical tools created in the past few decades and this technique is rapidly developing and expanding. In the AIMD computation, dynamical trajectories at finite-temperature are produced utilizing forces derived from calculations of the electronic structure that are done "on the fly" as the simulation develops. As a result, AIMD allows for the formation and breaking of chemical bonds and takes into consideration the effects of electronic polarization [36, 37]. AIMD is effectively applied to various physically significant problems in physics and chemistry. In recent years, AIMD has also been used to examine issues connected to biological systems. Numerous research have unearthed novel physical phenomena and microscopic mechanisms that cannot yet be discovered using empirical approaches. As a result, fresh interpretations of experimental data are produced, and in certain situations, new experiments are even suggested. Assuming that The Born-Oppenheimer approximation (BO) is true, dynamics of a system with K electrons and L nuclei, can be addressed classically and electrons in ground state quantum mechanically, which is the ideal case of an AIMD calculation [38]. In the current study, we applied the renowned Car-Parrinello technique to *ab initio* MD modeling.

3.3 The Car-Parrinello Method

The molecular dynamics developed by Car-Parrinello is an advancement of the Lagrangian formalism of classical molecular dynamics (CMD) in which the total electronic energy of a metallic system as provided by DFT replaces the model potential defining the interaction among atoms. We formally introduce the electronic wavefunctions as new dynamical variables. The Car-Parrinello method is frequently used to as the *ab initio* molecular dynamics. Because, it does not require an inter atomic potential to be supplied from outside as an input. Instead, it calculates the forces and potential directly from the electronic energy as the simulation proceeds. This method stands out as a new and more efficient one for calculating the physical properties of materials. To serve this purpose the electronic equations are solved by employing appropriate boundary conditions, plane wave basis sets and also from the approach of the DFT. The DFT's [39] orbital free (OF) version permits the application of the Car-Parrinello approach as well. In the Car-Parrinello [17, 40] method, self-consistency, nuclear movement, and electronic states are all addressed by a single algorithm that unifies MD and DFT. This approach relaxes both the electronic and ionic degrees of freedom concurrently by taking into account nuclear and electronic dynamics simultaneously. The Car-Parrinello approach, which is used to calculate the electrical structure, appears to have made four overall improvements. These are as follows [41]:

(i) Instead of using variational equations, use optimization techniques.

(ii) Instead of matrix diagonalization, use equations of motion.

(iii) Matrix operations are substituted with fast Fourier transformations (FFT).

(iv) In place of eigenvector operation, a trace of the occupied subspace.

Keep in mind that the overall energy in an orbital-free approach depends solely on charge density. Therefore, The Car-Parrinello technique can be used with the energy functional theory [39]. The pseudo-Lagrangian for OF-DFT approach is defined as

$$\mathcal{L}_{CP} = T_e + T_n - E[\rho, \{\mathbf{R}_i\}] + \mu\Big(\int \rho \, d\mathbf{r} - N\Big), \tag{3.2}$$

where N represents the overall amount of electrons, $\mathbf{R}_i$ stands for the coordinates of the i-th nucleus, and $E[\rho, \{\mathbf{R}_i\}]$ the entire potential energy of a system [see equation (4.89)]. The first term reflecting the imaginary KE linked to the electronic degrees of freedom is defined as

$$T_e = \frac{1}{2} M_e \int \dot{\psi}^2 d\mathbf{r}, \tag{3.3}$$

where $\dot{\psi} = \frac{d\psi}{dt}$ and $\rho = \mid \psi \mid^2$, and the model of classical motion of charge density, which is similar to the motion of electrons in their orbits, includes the fictitious mass M_e as a parameter. To keep the trajectory adiabatic and prevent energy from moving from the electronic to the ionic degrees of freedom, the imaginary mass of the electrons must be small enough. The time step must also be less than the typical values used in other MD algorithms in order for this to work. Kinetic energy of atoms makes up the second term in the Lagrangian

$$T_n = \frac{1}{2} \sum_i M_i \mid \dot{\mathbf{R}}_i \mid^2, \tag{3.4}$$

where, M_i denotes the mass of the i-th ion and the dot denotes time derivative. The total electronic energy of the coupled system of electrons and ions is represented by

the third term in equation (3.2). The following (Car-Parrinello) equations of motion are produced using the aforementioned Lagrangian

$$M_i\ddot{\mathbf{R}}_i(t) = -\nabla_{\mathbf{R}_i} E_g \tag{3.5}$$

$$M_e\ddot{\psi}(\mathbf{r},t) = -\frac{\partial E_g}{\partial \psi(\mathbf{r},t)} + \mu\psi(\mathbf{r},t), \tag{3.6}$$

for both classical ionic $\{\mathbf{R}_i\}$ and electronic $\psi(\mathbf{r},t)$ degrees of freedom, respectively, subject to the constraint

$$\int \mid \psi \mid^2 d\mathbf{r} = N, \tag{3.7}$$

and E_g is the ground state energy of the system. Following Hellmann-Feynman theorem the force actions on the i-th ion is provided by

$$\mathbf{F}_i = -\nabla_{\mathbf{R}_i} E_g \tag{3.8}$$

and so equation (3.5) becomes

$$\mathbf{F}_i(t) = M_i\ddot{\mathbf{R}}_i(t) \tag{3.9}$$

In equation (3.9), the force on the i-th ion at time t, $\mathbf{F}_i(t)$, depends on the positions of all of the other ions of the system at that time. After specifying the initial positions and velocities of each of the N molecules, the basic MD procedure follows, for which it repeats for the desired number of iterations according to the following steps:

(i) The force on each particle is calculated according to equation (3.8).

(ii) The positions of the particles of the system are updated gradually in time according to equation (3.9).

To solve the integration involved in step (ii) we have used the Verlet Leap-frog algorithm (VLFA) with time step δt for each atomic movement. Similar to this, the VLFA is used to solve numerically the motion of the electronic degrees of freedom in equation (3.6) with an electronic time step of δt_e. It is also crucial to choose the right time step, δt. A large time step results in atoms moving too far down a specified route, which produces a poor simulation of the motion. It takes longer to conduct the simulation because a too-small time step necessitates more iterations. So, the time step must be one order of magnitude smaller than the vibrational period or the interval between impacts. In order to simulate a liquid of solid molecules, time steps are chosen to be of the order of femtoseconds, and to simulate vibrating molecules, time steps on the scale of tenths of a femtoseconds are provided [42].

The time steps for evolving the ionic and electronic positions are not similar in evey detail. It is important to carefully select the time step δt_e and the fictitious mass M_e so that the electrons' dynamics stay adiabatic. This means that throughout the motion, the system should continue to be in its electronic ground condition. Due to the small fictitious mass M_e, it is necessary to integrate the electronic equations of motion with a smaller time step δt_e compared to the standard 1-10 fs time step used for CMD [43].

3.4 The Verlet Leap-frog Algorithm

In MD simulations, the integration algorithm is used to perform the step-by-step finite difference solution of the equations of motion. The Verlet leap-frog algorithm is one of the frequently used algorithms. An effective algorithm to incorporate Newton's

equations of motion (NEM) is important for an effective molecular dynamics program. In the current study, we have integrated NEM for ions and electrons using the VLFA. For application to MD simulations, the original Vrlet algorithm has been modified into the VLFA. The former one employs the location and forces at time t as well as the positions at time $t-\delta t$ to forecast the positional coordinates at time $t+\delta t$, where δt is the integration time step in the molecular dynamics scheme.

The Verlet algorithm combines two Taylor expansions. Taylor expansion is used to acquire the location from time t (forward) to $t+\delta t$ and (backward) to $t-\delta t$ up to the third order, one obtains

$$\mathbf{R}_i(t+\delta t) = 2\mathbf{R}_i(t) - \mathbf{R}_i(t-\delta t) + \frac{\mathbf{F}_i(t)}{M_i}\delta t^2 + O(\delta t^4). \tag{3.10}$$

The estimation of the new ionic locations contains an inaccuracy of the order δt^4. The velocities are obtained from the basic definition of differentiation

$$\mathbf{v}_i(t) = \frac{\mathbf{R}_i(t+\delta t) - \mathbf{R}_i(t-\delta t)}{2\delta t}, \tag{3.11}$$

and this velocity formula is only accurate to orders of δt^2. This is necessary in order to calculate kinetic energy. The time-reversal symmetry of the Verlet method results in good energy conservation, and it is easy and compact to code. The velocities, however, are not easily controlled. The VLFA is used for the velocities at half time step defined as

$$\mathbf{v}_i(t+\frac{\delta t}{2}) = \frac{\mathbf{F}_i(t)}{M_i}\delta t + \mathbf{v}_i(t-\frac{\delta t}{2}), \tag{3.12}$$

to obtain more accurate velocities. Then, the velocities at time t can be also computed from

$$\mathbf{v}_i(t) = \frac{\mathbf{v}_i(t+\frac{\delta t}{2}) + \mathbf{v}_i(t-\frac{\delta t}{2})}{2}, \tag{3.13}$$

where the ionic positions are then obtained from

$$\mathbf{R}_i(t+\delta t) = \mathbf{R}_i(t) + \mathbf{v}_i(t+\frac{\delta t}{2})\delta t. \tag{3.14}$$

Schematically, the VLFA can be shown as:

(1). Given current position, $\mathbf{R}_i(t)$ and velocity at last half-step, $\mathbf{v}_i(t-\frac{\delta t}{2})$.

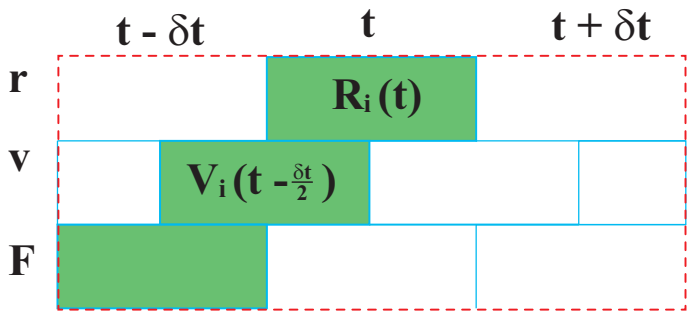

(2). Compute current force, $\mathbf{F}_i(t)$ via the Hellmann-Feynman theorem $\mathbf{F}_i = -\nabla_{\mathbf{R}_i} E_g$.

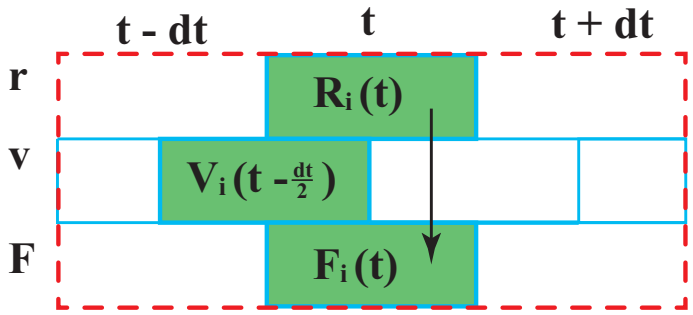

(3). Compute velocity at next half-step, $\mathbf{v}_i(t+\frac{\delta t}{2})$ via equation (3.12) using current force, $\mathbf{F}_i(t)$ and velocity at last half-step, $\mathbf{v}_i(t-\frac{\delta t}{2})$.

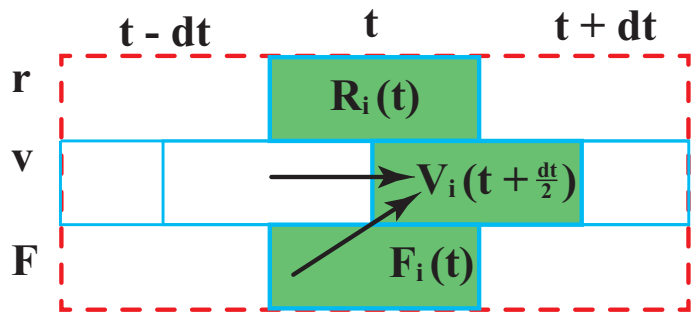

(4). Compute next position, $\mathbf{R}_i(t + \delta t)$ via equation (3.14) using current position, $\mathbf{R}_i(t)$ and velocity at next half-step, $\mathbf{v}_i(t + \frac{\delta t}{2})$.

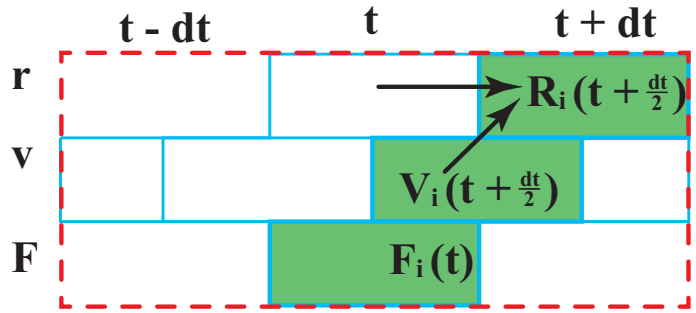

(5). Advance to next time step, repeat.

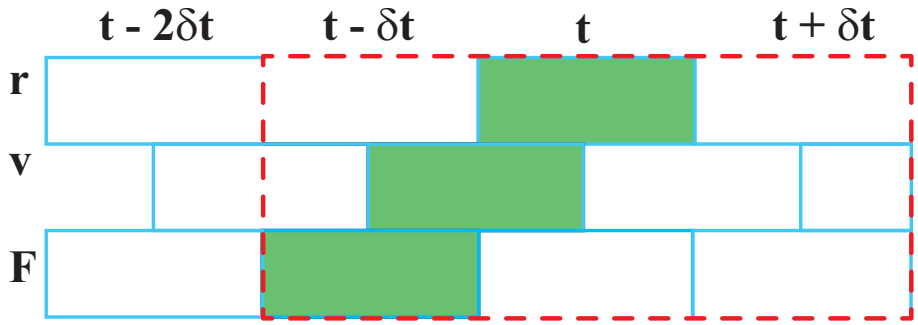

3.5 Periodic Boundary Conditions

Periodic boundary conditions (PBC) are frequently used in molecular dynamics, dislocation dynamics, and materials modeling to remove surfaces and prevent using a large number of molecules or a big simulation box. A collection of boundary conditions is known as periodic boundary conditions. The N particles (atoms, molecules, or ions) may be contained within a cubical cell, which stops them from drifting apart. However, because of fabricated surface effects, these configurations are bad for simulating bulk liquids. In such a simulation, the majority of molecules are found on the cube's surface where these particles are housed. The behaviour of particles in the bulk will differ from that of particles on the surface. In MD, PBCs are frequently employed to eliminate issues with false surface effects from computations for all system sizes. The entire space is filled with copies of the original cubic simulation box and the states of all the particles inside of it. An infinite lattice is created by the combination of the replication boxes and the simulation box. The fundamental tenet of the PBC is that if a particle changes position in the original box and its periodic images change position in the adjacent boxes as well. Since there are no walls or surface particles at the central box's edges, when a particle exits the central box (as in Figure 3.1), one of its images then enters via the opposite face with precisely the same speed. Because of this, the particles number in the central box (consequently in the whole system) remains conserved. Figure 3.1 is a 2-D representation of such a periodic system.

For normal liquids, the interaction potential is relatively short range in MD simulations. For example, such case the Lennard-Jones potential is often used in the case of CMD. This implies that only nearby particles make a major contribution to the

force acting on any given particle. As a result, MD simulations frequently include PBCs along with the "minimum image convention". The minimum image convention specifies that each molecule in the system interacts with the nearest molecule or its

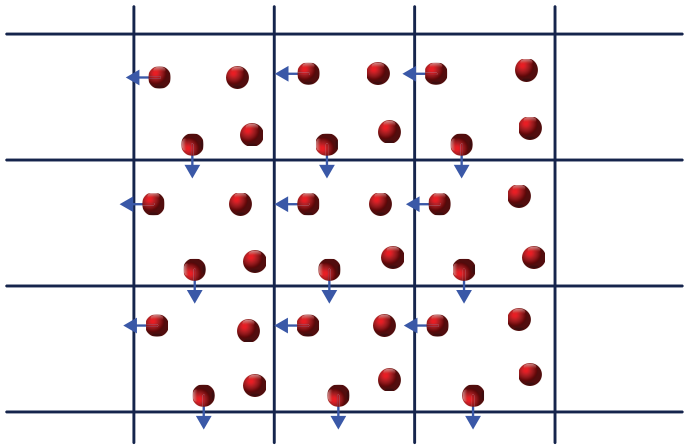

Figure 3.1: A two-dimensional PBC cell used in computer experiments [44].

image in the periodic array. An alternative is to employ a cut-off radius, which is typically taken to be considerably smaller than $\frac{L}{2}$ (the maximum radius of a sphere that can be packed into the cubic box) where L represents the cube's side. For long range potentials, these methods are likely to introduce serious errors in the force calculation, and therefore in the resulting trajectories of the particles. Instead, one must include the force contributions from all molecules in the main simulation box as well as from all the molecules in every periodic replica (*i.e.*, from an infinite number of particles). In reality, this is a very challenging task to handle it in computer simulation of particles; thus it is accomplished by the famous Ewald summation [45, 46]. Composite materials, particularly in the aerospace industry, are being employed

more and more due to their enticing qualities. The numerical method known as the finite element method has been very successfully used to research composite materials since it is both time and money efficient. For a very long time, researchers have preferred PBCs for simulating composite materials.

Chapter 4

Density Functional Theory

4.1 Theory of Electronic Structure

The study of electron energy in matter is known as electronic structure theory. This theory explains how electrons move within atoms or molecules. Which states that because electrons are lighter than nuclei and move more quickly as a result, they will distribute in the best way possible for any specific nuclear configuration [47]. The majority of a material's chemical and physical properties are governed by its electronic structure, particularly the structure of its outermost atomic shell. Therefore, study of the electronic structure of materials is an important part of research in material science. When the electronic issue is solved for a variety of nuclear configurations, the potential energy surface is revealed. The electronic energy for each nuclear configuration is the potential energy that the electrons feel. For the purpose of solving their equation of motion, one must apply quantum mechanics. According to quantum mechanics, electrons will not be confined at specific locations in space, but

are instead best viewed as interfering "matter waves" [48]. The Born-Oppenheimer approximation [49] is typically used to set the ions at predetermined sites, which is the core tenet of the electronic structure theory. Then we deal with the Hamiltonian of electronic motions and find all the eigen functions of that Hamiltonian eventually we get the eigen values which are the energy of the corresponding eigenstates. We will solely discuss the aspects of electronic structure theory that are relevant to our current work in this Chapter, including its theory, methodology, and applications. For the study of the electrical structure of many-body systems, the density functional theory (DFT) [1] is frequently acknowledged as the foundation. The Schrödinger equation for many-body systems can be roughly solved using DFT.

Although DFT theory is frequently referred to as "a first principle theory," there are still significant approximations that must be made to produce accurate simulation results. The present simulation is performed using the Hohenberg-Kohn (HK) version of the DFT [1], using the LDA [50], to treat correlation and the exchange energy and, the external potential of a system created by ions is approximated by the local model Pseudopotential [51]. The kinetic energy (KE) functional is the most important ingredient of HK version of DFT, and a reliable KE functional [52] is used in the present work to approximate it.

4.1.1 Schrödinger's Equation

The fundamental equation for explaining the electronic structure of matter in condensed matter physics is the Schrödinger equation (SE). It is also known as the Schrödinger wave equation, and is a partial differential equation which explains how

the wavefunction (Ψ) of a physical system evolves over time and space. In 1926 Erwin Schrödinger attempted to construct an equation for describing the so called wave behavior of matter (for example electron) using the de Broglie hypothesis. The equation was subsequently given the name Schrödinger equation, and its full name is the time-dependent Schrödinger equation [53]. For the systems of N particles it can be written as the form

$$i\hbar\frac{\partial}{\partial t}\Psi(\{\mathbf{r}_i\},t) = \hat{H}\Psi(\{\mathbf{r}_i\},t) \tag{4.1}$$

where $\mathbf{r}_i$ represents the positional coordinate of i-th particle and $\hat{H}$ is the Hamiltonian operator of the system defined as

$$\hat{H} = -\frac{\hbar^2}{2}\sum_{i=1}^{N}\frac{1}{m_i}\nabla_i^2 + V(\mathbf{r}_1,\mathbf{r}_2,\ldots,\mathbf{r}_N,t). \tag{4.2}$$

If the Hamiltonian itself has no time-dependency the Schrödinger equation becomes

$$\hat{H}\Psi(\mathbf{r}_1,\mathbf{r}_2,\ldots,\mathbf{r}_N) = E\Psi(\mathbf{r}_1,\mathbf{r}_2,\ldots,\mathbf{r}_N) \tag{4.3}$$

with the Hamiltonian $\hat{H}$ equal to

$$\hat{H} = -\frac{\hbar^2}{2}\sum_{i=1}^{N}\frac{1}{m_i}\nabla_i^2 + V(\mathbf{r}_1,\mathbf{r}_2,\ldots,\mathbf{r}_N) \tag{4.4}$$

where, E represents the system's overall energy. Equation (4.3) is known as the eigen value equation.

4.1.2 The Wave Function

In quantum physics, the quantum state of an isolated quantum system is mathematically described by a wavefunction. In most cases, the wavefunction is a probability

amplitude with complex values from which probabilities corresponding to the potential outcomes of measurements performed on the system can be determined. The wavefunction of a given system in quantum mechanics has all of the information. However, Ψ is a tremendously complex quantity that cannot be scientifically proven and depends on $4N$ factors, where N denotes the quantity of electrons. The time-independent wavefunction is considered for the stationary states. A question always arising with physical quantities is about its possible interpretations as well as observations. But the wavefunction itself has no physical interpretation. It is not a physically observable quantity, so that, the wavefunction is purely a mathematical notation. The probability interpretation of the wavefunction by Max Born provides a physical meaning of the wavefunction. The square of the wavefunction multiplied by volume elements gives the probability [54, 55] as

$$P = \mid \Psi(\mathbf{r}_1, \mathbf{r}_2, \ldots, \mathbf{r}_N) \mid^2 d\mathbf{r}_1 d\mathbf{r}_2 \ldots d\mathbf{r}_N. \tag{4.5}$$

Equation (4.5) describes the probability that particles 1,2,...,N are located simultaneously in the corresponding volume element $d\mathbf{r}_1 d\mathbf{r}_2 \ldots d\mathbf{r}_N$ [56]. All particles must be found some where in space so it follows that

$$\int d\mathbf{r}_1 \int d\mathbf{r}_2 \ldots \int d\mathbf{r}_N \mid \Psi(\mathbf{r}_1, \mathbf{r}_2, \ldots, \mathbf{r}_N) \mid^2 = 1, \tag{4.6}$$

which is generally known as the normalization condition for the wave function. Equation (4.6) also gives insight on the requirement that a wave function must fulfill some criteria in order to be physically acceptable. The wave function must be continuous over the full spatial range and square-integratable [57]. Another very important property of the wavefunction is that, calculation of the expectation values of operators

with respect to a wavefunction provides the average value of the corresponding observable for that wavefunction [58]. For an observable $O(\mathbf{r}_1, \mathbf{r}_2, \ldots, \mathbf{r}_N)$, one can generally write

$$O = \left\langle \hat{O} \right\rangle = \int d\mathbf{r}_1 \int d\mathbf{r}_2 \ldots \int d\mathbf{r}_N \Psi^*(\mathbf{r}_1, \mathbf{r}_2, \ldots, \mathbf{r}_N) \hat{O} \Psi(\mathbf{r}_1, \mathbf{r}_2, \ldots, \mathbf{r}_N). \tag{4.7}$$

4.1.3 The density of electrons

The fundamental variable in the density functional theory (DFT) is the electron density for N electrons. The density of electron in an electronic system is determined by the quantity of electrons present in a specific state per unit volume. If the spin coordinates are neglected, the electron density $\rho(r)$ can be expressed as measurable observable

$$\rho(\mathbf{r}) = N \int d\mathbf{r}_2 \ldots \int d\mathbf{r}_N \Psi^*(\mathbf{r}_1, \mathbf{r}_2, \ldots, \mathbf{r}_N) \Psi(\mathbf{r}_1, \mathbf{r}_2, \ldots, \mathbf{r}_N), \tag{4.8}$$

which only depends on spatial coordinates [1, 59]. The density of electrons $\rho(\mathbf{r})$ in the ground state can be measured by X-ray diffraction [60]. The density of electrons $\rho(\mathbf{r})d\mathbf{r}$ determines the probability of locating any electron within the volume element $d\mathbf{r}$ from the total number of N electrons, when quantum-mechanical effects are significant. Only the three spatial variables make up the non-negative function $\rho(\mathbf{r})$, which integrates to the overall amount of electrons and vanishes at infinity. These are some of the basic characteristics of the electron density:

(i.) When $\mathbf{r} \to \infty$, then $\rho(\mathbf{r}) \to 0$.

(ii.) The number of all electrons can be calculated by integrating the electron density, $\int \rho(\mathbf{r}) d\mathbf{r} = N$.

(iii.) It is possible to experimentally measure the observable $\rho(\mathbf{r})$.

It should be noted that the density, $\rho(\mathbf{r})$, only has three degrees of freedom. It is important to confirm that an approach actually contains the relevant system information before presenting it and using the electron density as a variable. Thus, it must include details about the total number of N electrons as well as the exterior potential denoted by V_{ext} [60]. The ground state electron density is the sole attribute that defines the external potential. The term uniquely means up to an additive constant as proved for the first time by Hohenberg and Kohn (HK) theorem. This proof will be discussed in the forthcoming subsection (4.2.2).

4.1.4 The many-body Hamiltonian of a Molecular System

The eigenfunctions of the many-body Hamiltonian can be used to explain a lot of the properties of atoms, molecules, and solids,

$$\hat{H} = \hat{T} + \hat{V}. \tag{4.9}$$

The Hamiltonian of the many-body system is the starting point of a quantum theory of materials. For the system containing N_n nuclei and N_e electrons neglecting external magnetic and electronic field is

$$\begin{aligned}\hat{H}_{ne}(\,\mathbf{r},\mathbf{R}\,) \;=\; & -\frac{\hbar^2}{2m_e}\sum_{i=1}^{N_e}\frac{1}{2}\nabla_i^2 - \frac{\hbar^2}{2M_I}\sum_{I=1}^{N_n}\nabla_I^2 + \frac{e^2}{4\pi\epsilon_0}\left[\sum_{i=1}^{N_e}\sum_{I=1}^{N_n}\frac{-Z_I}{\mid \mathbf{r}_i - \mathbf{R}_I \mid} + \sum_{i=1}^{N_e}\sum_{i<j}^{N_e}\frac{1}{\mid \mathbf{r}_i - \mathbf{r}_j \mid}\right. \\ & \left. \sum_{I=1}^{N_n}\sum_{J>I}^{N_n}\frac{Z_I Z_J}{\mid \mathbf{R}_I - \mathbf{R}_J \mid}\right]\end{aligned} \tag{4.10}$$

In atomic units, setting $\hbar = m_e = e = \frac{1}{4\pi\epsilon_0} = 1$, many-body Hamiltonian of the system reads,

$$\begin{aligned}\hat{H}_{ne}(\,\mathbf{r},\mathbf{R}\,) &= \sum_{i=1}^{N_e} -\frac{1}{2}\nabla_i^2 - \sum_{I=1}^{N_n}\frac{1}{2M_I}\nabla_I^2 + \sum_{i=1}^{N_e}\sum_{I=1}^{N_n}\frac{-Z_I}{\mid \mathbf{r}_i - \mathbf{R}_I \mid} + \sum_{i=1}^{N_e}\sum_{i<j}^{N_e}\frac{1}{\mid \mathbf{r}_i - \mathbf{r}_j \mid} \\ &\qquad + \sum_{I=1}^{N_n}\sum_{J>I}^{N_n}\frac{Z_I Z_J}{\mid \mathbf{R}_I - \mathbf{R}_J \mid} \\ &= \hat{T}_e + \hat{T}_n + \hat{V}_{ne} + \hat{V}_{ee} + \hat{V}_{nn}, \qquad (4.11)\end{aligned}$$

where, the nuclei are represented by I, J, and the indices i and j are used to represent the degrees of freedom for electronic systems. Nuclear masses and charges are M_I and Z_I, respectively. In the equation above, the sets of electronic and nuclear coordinates are denoted by $\mathbf{r}$ and $\mathbf{R}$, respectively.

We are particularly interested in the energy contributions made by electrons and nuclei for the relevant energy scale of such systems. As a result, the potential term $\hat{V}$ of the system is influenced by three different sorts of interaction between these parts: (i) Nucleus-nucleus interaction (fifth term) (ii) Nucleus-electron interaction (3rd term) (iii) Electron-electron interaction (4th term). According to theory, the KE term is the result of adding the kinetic energies of electrons (1st term) and nuclei (2nd term). But since the ions are millions of times heavier than the electrons, this is not surprising. Therefore, their contributions to the kinetic energy are typically ignored. The Born-Oppenheimer approximation is what is being discussed here. The first two terms on the right side of equation (4.11) are the descriptions of the kinetic energy operators for electrons and nuclei, respectively. The final three terms, which are repulsive potential caused by electron-electron and nucleus-nucleus interactions, respectively, are the electrostatic attraction between the electrons and the nuclei .

4.1.5 The Born-Oppenheimer Approximation

The hypothesis that it is possible to distinguish between the motion of atomic nuclei and electrons within molecules is known as the Born-Oppenheimer (BO) approximation in quantum physics and molecular physics. The BO approximation is physically justified by the fact that an atomic nucleus' mass is significantly more than an electron's mass in a given system (e.g. a proton is 1800 times as heavy as an electron). This implies that there must be a significant disparity in their respective speeds. Therefore, it makes sense to suppose that the nuclei are almost unchanged in relation to the mobility of the electrons in the system. As a result, the nucleus has no kinetic energy and just a constant potential energy (nucleus-nucleus). This is called the Born-Oppenheimer approximation. The BO approximation is used to simplify the Schrödinger equation (SE) for a molecule. Max Born and J. Robert Oppenheimer [49] proposed this approximation in 1927 during the early years of quantum mechanics, and it is still crucial in both quantum physics and molecular physics today. Probably the most basic approximation in physics and molecular physics is the Born-Oppenheimer (BO) approximation.

Practically speaking, it will enable us to precisely treat the electrical structure of molecules without worrying too much about their nucleus. The position of the nuclei determines the Hamiltonian that the electrons are experiencing at any particular time. Immediately after that, the full Hamiltonian $\hat{H}_{ne}$ is replaced by the so-called electronic Hamiltonian, which is

$$\begin{aligned} \hat{H}_{el}(\,\mathbf{r}\,;\mathbf{R}\,) &= \sum_{i=1}^{N_e} -\frac{1}{2}\nabla_i^2 + \sum_{i=1}^{N_e}\sum_{I=1}^{N_n} \frac{-Z_I}{\mid \mathbf{r}_i - \mathbf{R}_I \mid} + \sum_{i=1}^{N_e}\sum_{i<j}^{N_e} \frac{1}{\mid \mathbf{r}_i - \mathbf{r}_j \mid} \\ &= \hat{T}_e + \hat{V}_{ne} + \hat{V}_{ee}. \end{aligned} \tag{4.12}$$

where $\mathbf{R}$ indicates that $\hat{H}$ depends simultaneously on all $\mathbf{R}_I$ nuclear positions. The time-independent Schrödinger equation can be used to resolve any issue relating to the electronic structure of matter. However, the majority of problems involving stationary states focus on atoms and molecules devoid of time-dependent interactions [3]. Therefore, only the electronic time-independent Schrödinger equation is of our interest at this moment. The wave function only depends on the electronic coordinates [58] because the nuclear degrees of freedom (for example, the solid's crystal structure) only take the shape of a potential $V(\mathbf{r})$ influencing the electrons. The solution of the Schrödinger equation (SE)

$$\hat{H}_{el}\Psi_{el} = E_{el}\Psi_{el} \tag{4.13}$$

with electronic Hamiltonian ($\hat{H}_{el}$) gives the electronic wave function and the electronic

$$\Psi_{el} = \Psi_{el}(\mathbf{r}_1, \mathbf{r}_2, \ldots, \mathbf{r}_N; \mathbf{R})$$

energy E_{el}, where $\mathbf{R}$ is the ionic coordinates. Here, we have made it apparent that the Hamiltonian, as well as its eigenvalues and eigenstates, are all dependent on the specific nuclear configuration. This is the essential element of the BO approximation. Without mentioning the nuclei's quantum mechanics, it enables one to compute the electronic structure of a molecule. The sum of E_{el} and the nuclear repulsion term, which is constant, equals the total energy E for some fixed nuclei configurations

$$E_{II} = \sum_{I=1}^{N_n} \sum_{J>I}^{N_n} \frac{Z_I Z_J}{\mid \mathbf{R}_I - \mathbf{R}_J \mid}$$

leading to

$$E = E_{el} + E_{II}. \tag{4.14}$$

The Born-Oppenheimer approximation simplifies the complexity of the electronic structure problem to the solution of equation (4.13), and equations (4.13) and (4.14) yield the total energies. However, it should be remembered that the Born-Oppenheimer approximation is unquestionably not applicable in all circumstances. As a result, it is known that the BO approximation would fail when there are several potential energy surfaces that are either crossing each other [61] or are energetically close to one another.

The main challenge in solving equation (4.13) is the interaction between electrons, which hides all of the many-body quantum effects. Many approximate approaches for solving Schrödinger or Schrödinger-like equations have been devised by mapping the N electron SE into useful one-electron Schrödinger like equations, which are simpler to solve computationally. Finally, we point out that the classical treatment of the nuclei's masses can also be used to obtain the electronic Schrödinger equation.

The various approximation techniques used here can be categorized into the following main groups: (i) the DFT, in which density of electron is the key parameter, and (ii) methods based on the wave function, where the important element is the many electron wave function. In the current work, the electron density $\rho(\mathbf{r})$ is the important component, and DFT is employed to approximate the energy in the ground state of equation (4.13).

4.1.6 The Hellmann-Feynman Theorem

A helpful tool in solid state, atomic, and molecular physics is the Hellmann-Feynman theorem. The main focus of many molecular structural issues is forces. Typically,

energy and its changes with altering molecular configurations have been taken into account while thinking about these issues. In this study, the Hellmann-Feynman theorem is used to determine the forces that are exerted on the system's ions. This theorem is a popular and powerful method to efficiently calculate forces in a variety of dynamical processes. Let's now imagine a system of many bodies with an electronic Hamiltonian, $\hat{H}(\mathbf{r};\mathbf{R})$. The overall shape of the forces acting on the $I-th$ atom, denoted by the $\mathbf{F}_I$, is the downward gradient of the total electronic energy in relation to the $\mathbf{R}_I$ ionic position. Mathematically this force can be written as

$$\mathbf{F}_I = -\frac{\partial E}{\partial \mathbf{R}_I}, \tag{4.15}$$

where the system's overall energy is $E = \langle \Psi \mid \hat{H} \mid \Psi \rangle + E_{II}$. Therefore, the force can be written as

$$\mathbf{F}_I = -\frac{\partial E}{\partial \mathbf{R}_I} = -\big\langle \Psi \mid \frac{\partial \hat{H}}{\partial \mathbf{R}_I} \mid \Psi \big\rangle - \big\langle \frac{\partial \Psi}{\partial \mathbf{R}_I} \mid \hat{H} \mid \Psi \big\rangle - \big\langle \Psi \mid \hat{H} \mid \frac{\partial \Psi}{\partial \mathbf{R}_I} \big\rangle - \frac{\partial E_{II}}{\partial \mathbf{R}_I}. \tag{4.16}$$

since, $\big\langle \Psi \mid \frac{\partial \Psi}{\partial \mathbf{R}_I} \big\rangle = 0$, *i.e.* due to the variational principle the 2nd and 3rd terms of the above equation vanishes and then one finds

$$\mathbf{F}_I = -\big\langle \Psi \mid \frac{\partial \hat{H}}{\partial \mathbf{R}_I} \mid \Psi \big\rangle - \frac{\partial E_{II}}{\partial \mathbf{R}_I}. \tag{4.17}$$

This is often called the Hellmann-Feynman theorem or the force theorem [62, 63]. Further it is possible to show that $\mathbf{F}_I$ only based on the density of electron and the locations of the ion, so one can write

$$\mathbf{F}_I = -\int d\mathbf{r}\rho(\mathbf{r})\frac{\partial V_{ext}(\mathbf{r})}{\partial \mathbf{R}_I} - \frac{\partial E_{II}}{\partial \mathbf{R}_I}. \tag{4.18}$$

4.1.7 The Bloch's Theorem

The fact that plane waves are inherently periodic is one of their questionable characteristics. Clearly, this is a useful way to describe crystals. This is particularly true for systems made of condensed matter, like liquids, for which such periodic boundary conditions are frequently helpful and so taken for granted in simulations. However, extra attention must be paid when the periodic boundary conditions are not present, particularly for the electrostatic interaction.

The Bloch's theorem is the most common example to describe crystal's electrons. The ions are positioned in a regular periodic arrangement at 0 K in a flawless crystal. Bloch's theorem requires that the external potential experienced by the electrons be periodic as well, with the period being equal to the cell's length, **L**. Due to Bloch's theorem, plane wave basis sets have emerged as the obvious choice for the treatment of periodic systems, such as solids. According to Bloch's Theorem, the wavefunctions of electron's in a perfectly periodic potential can be expressed as

$$\psi_{n,\mathbf{k}}(\mathbf{r}) = e^{i\mathbf{k}.\mathbf{r}} u_{n,\mathbf{k}}(\mathbf{r}), \tag{4.19}$$

where the function $u_{n,\mathbf{k}}(\mathbf{r})$ has the same periodicity as the one-electron Hamiltonian's potential, $H = -\frac{1}{2}\nabla^2 + U(\mathbf{r})$, *i.e.* $u_{n,\mathbf{k}}(\mathbf{r}+\mathbf{R}) = u_{n,\mathbf{k}}(\mathbf{r})$, where $\mathbf{R}$ denotes the Bravais lattice vector. In computer simulation for a cell $\mathbf{R} = \mathbf{L}$, where $\mathbf{L}$ denotes the cell's size. In equation (4.19), $\mathbf{k}$ denotes a wavevector that is constrained in the first Brillouin Zone, and n denotes the band index. Since $u_{n,\mathbf{k}}(\mathbf{r})$ is a periodic function, we can expand it according to Fourier series by using plane waves

$$u_{n,\mathbf{k}}(\mathbf{r}) = \sum_{\mathbf{G}} C_{n,\mathbf{G}}\, e^{i\mathbf{G}.\mathbf{r}}, \tag{4.20}$$

where m is an integer and $C_{n,\mathbf{G}}$ are plane wave expansion coefficients, and $\mathbf{G}$'s are the reciprocal lattice vectors defined through $\mathbf{G}.\mathbf{R} = 2\pi m$. Therefore, the electron wavefunctions can be expressed as

$$\psi_{n,\mathbf{k}}(\mathbf{r}) = \sum_{\mathbf{G}} C_{n,\mathbf{k}+\mathbf{G}}\, e^{i(\mathbf{k}+\mathbf{G}).\mathbf{r}}, \tag{4.21}$$

which is a linear combining of plane waves.

4.2 Outline of the Density Functional Theory

Among the most common and effective quantum mechanical theories for matter is DFT. It is routinely used in physics and chemistry nowadays to determine the band structure of materials and the binding energy of molecules. Due to the use of functionals, (*i.e.* function of another function), in the equation for the density of electron $\rho(\mathbf{r})$, the theory is known as DFT. The DFT scheme depends on functionals of the electron density (for N electrons) defined as equation (4.8) alternative to the many-body wave function $\Psi(\{\mathbf{r}\})$. Therefore, in the DFT the electron density is the fundamental parameter that can be used to describe a quantum system with numerous electrons. To solve the Schrödinger equation of a system with numerous electrons directly in the calculations of the ground state electronic density and energy is an accurate way but it is an impossible task; so the use of the DFT is an approximate way. For this reason, another name of DFT is a theory of ground states and it is also called "a first principles theory".

At present, the DFT is a variational approach which is the most effective and promising method for calculating the electrical structure of matter. Simulations of

molecular dynamics calculate the movements of specific molecules in models of solids, liquids, and gases. The main concept in this case is motion, which explains how locations, velocities, and orientations change throughout the time. In essence, molecular dynamics depicts the motion of molecules as they travel back and forth, twisting, rotating, and colliding with one another.

In the fields of physics, chemistry, biology, and material science, the microscopic structure of molecules and systems in condensed phases is characterized by the arrangement of the electrons. The electronic structure theory provides a description of the arrangement of the electrons and their energy. The accuracy and effectiveness of the numerous applications of the electronic structure theory vary by orders of magnitude from one another. The Kohn-Sham density functional theory (KSDFT), one of several distinct electronic structure theory formalism, strikes the best balance between precision and effectiveness and is by far the most used one. The applicability of KSDFT to large systems with more than one thousand molecules is hampered by the fact that the computing cost of KSDFT still rises sharply with the number of electrons in the system. Knowledge of mathematics, physics, and computer science must be merged in order to reduce the computational cost of KSDFT.

DFT is applicable to a variety of systems, including atoms, molecules, solids, nuclei, and both classical and quantum fluids. The DFT is also well-liked for striking a balance between accuracy and computational expense. Since the density is a function of $\mathbb{R}^3$, the density functional theory (DFT) can easily be implemented in a much broader systems with hundreds or even thousands of atoms. Because of this, DFT has emerged as one of the most potent and effective methods for doing first principles

calculations intended to describe or even forecast the characteristics of molecular and condensed matter systems [3].

The density functional theory has two popular versions, these are [i] Kohn and Sham (KS) DFT and [ii] Hohenberg and Kohn (HK) DFT, the latter is also known as the orbital free (OF) DFT. According to DFT, any system's ground state energy is expressed as a function of its electron density, $\rho(\mathbf{r})$ as $E_g = E[\rho(\mathbf{r})]$. From a theoretical perspective, material science has advanced satisfactorily thanks to Hohenberg and Kohn's (HK) density functional theory [1]. They have demonstrated that a functional of the electron charge density, $\rho(\mathbf{r})$ may be used to express the overall energy of a system of N particles. Kohn and Sham (KS) [2] developed an equation for the total electronic energy of a system known as the KS-DFT by starting with the HK theory. In the KS-DFT, the Kohn-Sham equation, which is a one-particle SE, is used to compute the kinetic energy of the electrons. From the SE's form, it is clear that the energy functional consists of three terms: kinetic energy, contact with potential outside of oneself, and electron-electron interaction. An approximation of the kinetic energy functional was proposed by Kohn and Sham.

The distinction between the exact anticipated amount of the kinetic energy T_s and Hartree energy (E_H) of the auxiliary system is known as the exchange correlation energy, (E_{xc}). The E_{xc}, which is based on the homogeneous electron gas, was calculated by Kohn and Sham using the LDA. According to KS theory, electron charge density $\rho(\mathbf{r})$ is used to locally approximate the exchange correlation potential energy, E_{xc}. The so-called OF-DFT approach, which can be used instead of KS orbitals to approximate the kinetic energy (KE) term in KS-DFT, uses electron density. In

the present work, the OF-DFT method is the main tool to study different physical properties. OF-DFT methods will be dicussed in the section 4.5.

4.2.1 The Thomas-Fermi Model

A precise description of the contributions to the kinetic and potential energies in terms of the electron density $\rho(\mathbf{r})$ must be created in order to make OF-DFT approaches useful in computations. The development of orbital-free density functional theory is heavily focused on in order to make direct approximations for $T(\rho)$. In the beginning, Thomas [64] and Fermi (TF) [65] proposed that electrons are equally distributed (negatively charged clouds) around nuclei in a six-dimensional space in the 1927s (momentum and coordinates). The actual many-body problem has been greatly simplified by this. Before introducing a more precise theory, the DFT, it is instructive to take into account the fundamental concepts of the TF approximations.

Although the electron-nucleus and electron-electron interactions are handled classically in the TF model, the electrons' kinetic energy is generated from the uniform free electron gas using quantum statistical theory. In accordance with the TF approach, the system's total energy could be represented as a function (functional) of the electron density, $\rho(\mathbf{r})$. In a cube with side l, there are N electrons per square centimeter in actual space

$$\rho(\mathbf{r}) = \frac{N}{V} = \frac{N}{l^3}. \tag{4.22}$$

In this infinite well of three dimensions, the electron energy levels are provided by

$$E = \frac{h^2}{8ml^2}(n_x^2 + n_y^2 + n_z^2) = \frac{h^2}{8ml^2}(\tilde{R^2}), \quad n_x, n_y, n_z = 1, 2, 3, ... \tag{4.23}$$

The maximum energy of electrons and the Fermi energy E_F are determined by the sphere's radius, which is defined as $R = \widetilde{R}_{max}$ in the space (n_x, n_y, n_z) spanning all occupied states. The number of energy levels inside this maximum value at absolute zero provided by

$$N_F = \frac{1}{2^3}\frac{4\pi R^3}{3} = \frac{\pi}{6}\left(\frac{8ml^2E_F}{h^2}\right)^{\frac{3}{2}}. \tag{4.24}$$

The definition of the density of states is

$$g(E)dE = N_F(E+dE) - N_F(E) = \frac{\pi}{4}\left(\frac{8ml^2E_F}{h^2}\right)E^{\frac{1}{2}}dE. \tag{4.25}$$

At absolute zero, all energy levels below the Fermi energy are filled, including:

$$f(E) = \begin{cases} 1 & E \leq E_F \\ \\ 0 & E > E_F. \end{cases} \tag{4.26}$$

As a result, one cell's total electron energy will be provided by

$$\begin{aligned} E &= \int_0^{E_F} Ef(E)g(E)dE \\ &= \frac{4\pi}{h^3}(2m)^{\frac{3}{2}}l^3\int_0^{E_F} E^{\frac{3}{2}}dE \\ &= \frac{\pi}{5}\left(\frac{2l}{h}\right)^3(2m)^{\frac{3}{2}}{E_F}^{\frac{5}{2}}. \end{aligned} \tag{4.27}$$

The total number of electrons in a cell, denoted by ΔN, can be used to calculate the Fermi energy E_F:

$$\begin{aligned} N &= 2\int_0^{E_F} f(E)g(E)dE \\ &= \frac{\pi}{h^3}\left(\frac{2l}{h}\right)^3(2m)^{\frac{3}{2}}{E_F}^{\frac{3}{2}}. \end{aligned} \tag{4.28}$$

Combining equation (4.27) and (4.28) the source of the electrons' energy in a single cell is

$$\begin{aligned} E &= \frac{3}{10}(3\pi^2)^{\frac{2}{3}}\frac{l^3}{(2\pi)^2}\rho^{\frac{5}{3}} \\ &= C_F\frac{l^3}{(2\pi)^{\frac{5}{3}}} \\ C_F &= \frac{3}{10}(3\pi^2)^{\frac{2}{3}} = 2.871. \end{aligned} \tag{4.29}$$

Therefore, in TF model, the kinetic energy functional has the form

$$T_{TF}[\rho(\mathbf{r})] = C_F\int \rho^{\frac{5}{3}}(\mathbf{r})d\mathbf{r} = \frac{3}{10}\big(3\pi^2\big)^{\frac{2}{3}}\int \rho^{\frac{5}{3}}(\mathbf{r})d\mathbf{r}. \tag{4.30}$$

The well-known Thomas-Fermi kinetic energy functional, which is a function of the local electron density, is represented by equation (4.30). The electron-nucleus potential and the electron-electron potential in terms of electron density alone are determined using the classical theory to get the energy expression for an atom

$$E_{TF}[\rho] = \frac{3}{10}\big(3\pi^2\big)^{\frac{2}{3}}\int \rho^{\frac{5}{3}}(\mathbf{r})d\mathbf{r} - Z\int\frac{\rho(\mathbf{r})}{\mathbf{r}}d\mathbf{r} + \frac{1}{2}\int\int\frac{\rho(\mathbf{r}_1)\rho(\mathbf{r}_2)}{\mid \mathbf{r}_1 - \mathbf{r}_2 \mid}d\mathbf{r}_1 d\mathbf{r}_2. \tag{4.31}$$

Keep in mind that the nuclear charge Z is expressed in atomic units. The Thomas-Fermi theory of atoms' total energy functional is represented by equation (4.31). They used a variational technique to determine the ground state's energy and electron density, which had to be incorporated in the aforementioned equation. They presupposed that the system's ground state is linked to $\rho(\mathbf{r})$, for which the energy E_{TF} is minimized in accordance with the constraint

$$\int d\mathbf{r}\rho(\mathbf{r}) = N, \tag{4.32}$$

where N represents the amount of electrons overall in the atom. Therefore the variational principle must be satisfied by the ground state electron density

$$\delta\big\{E_{TF}[\rho] - \mu_{TF}\big(\int \rho(\mathbf{r})d\mathbf{r} - N\big)\big\} = 0, \tag{4.33}$$

which produces the chemical potential

$$\mu_{TF} = \frac{\delta E_{TF}[\rho]}{\delta\rho(\mathbf{r})} = \frac{1}{2}\big(3\pi^2\big)^{\frac{2}{3}}\rho^{\frac{2}{3}}(\mathbf{r}) - \phi(\mathbf{r}), \tag{4.34}$$

where the electrostatic potential caused by the nucleus and the entire electron distribution at location $\mathbf{r}$ is $\phi(\mathbf{r})$

$$\phi(\mathbf{r}) = \frac{Z}{\mathbf{r}} - \int d\mathbf{r}_2 \frac{\rho(\mathbf{r}_2)}{\mid \mathbf{r} - \mathbf{r}_2 \mid}. \tag{4.35}$$

Equation (4.34) and constraint (4.32) can be solved together to provide the electron density, which can then be entered into equation (4.31) to produce the total energy. This is the Thomas-Fermi theory [3] of the atom. The Thomas-Fermi technique might be thought of as an approximation to the more precise theory in light of contemporary DFT theory. It should be noted that the TF model doesn't lead to in any atomic binding to create solids or molecules.

4.2.2 The Hohenberg and Kohn Theory

The Hohenberg Kohn theorem, a core component of density functional theory (DFT), is now a vital instrument for the investigation of matter's electrical structure. The Hohenberg-Kohn theorem, which is at the core of modern science and engineering, has been greatly influenced by density functional theory, the most popular many-body technique for computations of electronic structure. The Hohenberg Kohn theorem is,

as we know, the theoretical foundation for DFT. The Hohenberg-Kohn (HK) theorems should therefore be the first topic of any discussion of DFT. Two well-known theorems based on the Thomas-Fermi (TF) model were developed and proven by P. Hohenberg and W. Kohn [1] and are typically referred to as the first and second HK theorems. The Hohenberg-Kohn theorem demonstrated that the ground state features of a system with a non-degenerate ground state are special functionals of the ground state electron density. The Kohn-Sham equations gives us a procedure for computing that density and thence those properties once the relevant functionals are known to sufficient accuracy. Beginning with the Thomas-Fermi theory, Hohenberg and Kohn established a link between the electron density and the many-electron Schrödinger equation (written in terms of $\psi(\mathbf{r}_1, \mathbf{r}_2, ..., \mathbf{r}_n)$).

Now let us consider the following discussions before starting the well-known Hohenberg-Kohn theorems. An electronic Hamiltonian for a system of N electrons is defined as $\mathbf{H}$. When a system is in the Ψ state, which may or may not meet the equation $\mathbf{H}\Psi = E\Psi$. The following formula provides the average of a number of energy measurements.

$$E[\Psi] = \frac{\langle \Psi \mid \mathbf{H} \mid \Psi \rangle}{\langle \Psi \mid \Psi \rangle} \tag{4.36}$$

where

$$\langle \Psi \mid \mathbf{H} \mid \Psi \rangle = \int \Psi^* \mathbf{H} \Psi d\mathbf{r} \tag{4.37}$$

and

$$E[\Psi] \geq E_{gs}. \tag{4.38}$$

Energy E_{gs} is the most crucial component of an electronic ground state. The variational principle allows us to calculate it. According to the variational principle, the

energy calculated from a speculated ψ is an upper bound to the ground state energy E_{gs}. The genuine ground state Ψ_{gs} and energy $E[\Psi_{gs}]$=E_{gs} will be obtained by fully minimizing of the functional $E[\Psi]$ with regard to all permitted N-electrons wave functions, that is,

$$E_{gs} = \min_{\Psi} E[\Psi] = \big\langle \Psi_{min} \mid \mathbf{T} + \mathbf{V}_{ne} + \mathbf{V}_{ee} \mid \Psi_{min} \big\rangle. \tag{4.39}$$

The variational principle thus specifies a method to ascertain the ground state wave function Ψ_{gs} and, consequently, the ground state energy and other desirable features, given a system of N electrons and nuclear potential V_{ext}. In another sense, the nuclear potential $V_{ext}(\mathbf{r})$ and the number of electrons N are both related to the ground state energy

$$E_{gs} = E_{gs}[N, V_{ext}(\mathbf{r})]. \tag{4.40}$$

In theory, each of these systems' characteristics can be thought of as a function of the external potential $V_{ext}(\mathbf{r})$. According to the first Hohenberg-Kohn theorem, up to a given constant, the non-degenerate ground-state density $\rho(\mathbf{r})$ defines the external potential $V_{ext}(\mathbf{r})$ in a unique manner [3]. This indicates that the external potential $V_{ext}[\rho(\mathbf{r})]$ is a clearly defined functional expression of the density. Currently, it is possible to write the system's energy as

$$\begin{aligned} E &= \big\langle \Psi \mid \mathbf{H} \mid \Psi \big\rangle \\ &= \big\langle \Psi \mid \mathbf{T} + \mathbf{V}_{ne} + \mathbf{V}_{ee} \mid \Psi \big\rangle \\ &= \int V_{ext}(\mathbf{r})\rho(\mathbf{r})d\mathbf{r} + \big\langle \Psi \mid \mathbf{T} + \mathbf{V}_{ee} \mid \Psi \big\rangle. \end{aligned} \tag{4.41}$$

The kinetic and interaction energy operators for the electrons are denoted by $\mathbf{T}$ and

$\mathbf{V}_{ee}$, respectively, and $\mathbf{H}$ is the total Hamiltonian corresponding to $V_{ext}(\mathbf{r})$. Equation (4.41) is used for the proof of Hohenberg-Kohn first theorem.

The electron density $\rho(\mathbf{r})$ and $V_{ext}(\mathbf{r})$ derived from it are known and all properties can be evalutated. If there is an additional external potential $V'_{ext}(\mathbf{r})$ that differs from $V_{ext}(\mathbf{r})$ by a larger amount than a constant, it can nevertheless produce the same electron density for the ground state $\rho(\mathbf{r})$. These would have two distinct Hamiltonians, $\mathbf{H}_1$ and $\mathbf{H}_2$, with the same ground state electron density but separate normalized wave functions, ψ_1 and ψ_2. Let us consider E_{gs} and E'_{gs} are the two ground-state energies for the Hamiltonian $\mathbf{H}_1$ and $\mathbf{H}_2$ respectively. Considering that wavefunction (ψ) is assumed to be non-degenerate [66], the Rayleigh Ritz minimal (variational) principle results in,

$$\begin{aligned} E_{gs} < \langle \Psi_2 \mid \mathbf{H}_1 \mid \Psi_2 \rangle &= \langle \Psi_2 \mid \mathbf{H}_2 \mid \Psi_2 \rangle + \langle \Psi_2 \mid \mathbf{H}_1 - \mathbf{H}_2 \mid \Psi_2 \rangle \\ &= E'_{gs} + \int [V_{ext}(\mathbf{r}) - V'_{ext}(\mathbf{r})]\rho(\mathbf{r}) d\mathbf{r}. \end{aligned} \tag{4.42}$$

In a Similar way, we obtain

$$\begin{aligned} E'_{gs} < \langle \Psi_1 \mid \mathbf{H}_2 \mid \Psi_1 \rangle &= \langle \Psi_1 \mid \mathbf{H}_1 \mid \Psi_1 \rangle + \langle \Psi_1 \mid \mathbf{H}_2 - \mathbf{H}_1 \mid \Psi_1 \rangle \\ &= E_{gs} - \int [V_{ext}(\mathbf{r}) - V'_{ext}(\mathbf{r})]\rho(\mathbf{r}) d\mathbf{r}. \end{aligned} \tag{4.43}$$

Addition of equation (4.42) and equation (4.43) leads to the contradiction

$$E_{gs} + E'_{gs} < E_{gs} + E'_{gs}. \tag{4.44}$$

As a result, it is established that the presence of a second potential, $V'_{ext}(\mathbf{r})$, which yields the same $\rho(\mathbf{r})$ but is not equal to $V_{ext}(\mathbf{r})$ + constant, must be incorrect. The quantity of electrons, N, is also determined by $\rho(\mathbf{r})$,

$$\int d\mathbf{r}\rho(\mathbf{r}) = N. \tag{4.45}$$

Consequently, the total energy can be expressed as a function of the electron density $\rho(\mathbf{r})$ for a given $V_{ext}(\mathbf{r})$:

$$\begin{aligned} E[\rho(\mathbf{r})] &= T[\rho(\mathbf{r})] + E_{ne}[\rho(\mathbf{r})] + E_{ee}[\rho(\mathbf{r})] \\ &= \int V_{ext}(\mathbf{r})\rho(\mathbf{r})d\mathbf{r} + F_{HK}[\rho(\mathbf{r})], \end{aligned} \tag{4.46}$$

where

$$F_{HK}[\rho(\mathbf{r})] = T[\rho(\mathbf{r})] + E_{ee}[\rho(\mathbf{r})]. \tag{4.47}$$

Here, it is important to notice that $F_{HK}[\rho(\mathbf{r})]$ is solely dependent on $\rho(\mathbf{r})$ and unaffected by any other potential $v_{ext}(\mathbf{r})$. Therefore, $F_{HK}[\rho(\mathbf{r})]$ is a general functional of $\rho(\mathbf{r})$. So, the main challenge facing DFT is the explicit form of the functional $F_{HK}[\rho(\mathbf{r})]$.

The second HK theorem introduces the energy variational principle into DFT (*i.e.* the density obeys a variational method). According to this, with a trail density of ρ_1, where $\rho_1(\mathbf{r}) \geq 0$ and $\int d\mathbf{r}\rho(\mathbf{r}) = N$,

$$E[\rho_1(\mathbf{r})] = \int v_{ext}(\mathbf{r})\rho_1(\mathbf{r})d\mathbf{r} + F[\rho_1(\mathbf{r})] \geq E_{gs}, \tag{4.48}$$

and

$$\int d\mathbf{r}\, v_{ext}(\mathbf{r})\rho_{gs}(\mathbf{r}) + F[\rho_{gs}(\mathbf{r})] = E_{gs} \tag{4.49}$$

where

$$E[\rho_1(\mathbf{r})] = T[\rho_1(\mathbf{r})] + E_{ne}[\rho_1(\mathbf{r})] + E_{ee}[\rho_1(\mathbf{r})]. \tag{4.50}$$

Therefore, $E_{gs} \leq E[\rho_1]$. Assume, in accordance with the first Hohenberg-Kohn theorem, that the ground-state wavefunction is ψ_{gs} and that it has a relationship to the

electron density $\rho(\mathbf{r})$. So, the external potential $v_{ext}(\mathbf{r})$ is determined exclusively by the ground-state $\rho(\mathbf{r})$.

Let us assume that the trail density $\rho(\mathbf{r})$ establishes its own wavefunction ψ_1 with a arbitrary variation from ψ_{gs}, We obtain

$$\int d\mathbf{r} v_{ext}(\mathbf{r})\rho(\mathbf{r}) + F[\rho] = \left\langle \Psi^{\rho}_{min} \mid v_{ext} + \mathbf{T} + \mathbf{V}_{ee} \mid \Psi^{\rho}_{min} \right\rangle \geq E_{gs} \tag{4.51}$$

corresponds to the ground state's bare minimum property. Once more using the minimal property, we obtain

$$E_{gs} = \left\langle \psi_{gs} \mid v_{ext} + \mathbf{T} + \mathbf{V}_{ee} \mid \Psi_{gs} \right\rangle \leq \left\langle \Psi^{\rho_{gs}}_{min} \mid v_{ext} + \mathbf{T} + \mathbf{V}_{ee} \mid \Psi^{\rho_{gs}}_{min} \right\rangle. \tag{4.52}$$

Now, when we remove the interaction from the external potential, v_{ext}, we obtain

$$\left\langle \psi_{gs} \mid \mathbf{T} + \mathbf{V}_{ee} \mid \Psi_{gs} \right\rangle \leq \left\langle \Psi^{\rho_{gs}}_{min} \mid \mathbf{T} + \mathbf{V}_{ee} \mid \Psi^{\rho_{gs}}_{min} \right\rangle. \tag{4.53}$$

The previous equation can only be accurate when

$$\left\langle \psi_{gs} \mid \mathbf{T} + \mathbf{V}_{ee} \mid \Psi_{gs} \right\rangle = \left\langle \Psi^{\rho_{gs}}_{min} \mid \mathbf{T} + \mathbf{V}_{ee} \mid \Psi^{\rho_{gs}}_{min} \right\rangle. \tag{4.54}$$

Thus we have

$$\begin{aligned} E_{gs} &= \int d\mathbf{r} v_{ext}(\mathbf{r})\rho_{gs}(\mathbf{r}) + \left\langle \psi_{gs} \mid \mathbf{T} + \mathbf{V}_{ee} \mid \Psi_{gs} \right\rangle \\ &= \int d\mathbf{r} v_{ext}(\mathbf{r})\rho_{gs}(\mathbf{r}) + \left\langle \Psi^{\rho_{gs}}_{min} \mid \mathbf{T} + \mathbf{V}_{ee} \mid \Psi^{\rho_{gs}}_{min} \right\rangle \\ &= \int d\mathbf{r} v_{ext}(\mathbf{r})\rho_{gs}(\mathbf{r}) + F[\rho_{gs}]. \end{aligned} \tag{4.55}$$

We can obtain

$$\begin{aligned} \left\langle \psi_1 \mid \mathbf{H} \mid \psi_1 \right\rangle &= \int \rho_1 v_{ext} d\mathbf{r} + T[\rho_1] + E_{ee}[\rho_1] \\ &= E[\rho_1] \geq E_{gs}[\rho]. \end{aligned} \tag{4.56}$$

Thus, the second Hohenberg-Kohn theorem is established. As a result, the energy will only be at its lowest when the electron density is that of the ground state. The basic assertion of density functional theory is reached by the two theorems mentioned above.

$$\delta\big\{E[\rho] - \mu\big(\int d\mathbf{r}\rho(\mathbf{r}) - N\big)\big\} = 0. \tag{4.57}$$

According to the restriction that $\int \rho(\mathbf{r})d\mathbf{r} = N$, the ground state electron density and energy correspond to the minimum of some functional $E[\rho]$, providing the appropriate amount of electrons. The system's electronic chemical potential μ serves as the Lagrange multiplier for this restriction. Let $\mu(\mathbf{r})=\frac{\delta E[\rho]}{\delta\rho(\mathbf{r})} = V_{ext}(\mathbf{r}) + \frac{\delta F_{HK}[\rho]}{\delta\rho(\mathbf{r})}$. Equation (4.57) thus gives the Euler-Lagrange equation

$$\mu(\mathbf{r}) - \mu = 0. \tag{4.58}$$

Due to the Hohenberg-Kohn theorems, the ground state characteristics can be evaluated using only electron density serving as the variational factor and a universal functional $F_{HK}[\rho]$. As the universal energy functional $F_{HK}[\rho]$ exists, but its explicit form is completely unknown. However, some approximations to $F_{HK}[\rho]$ are known to us and can be used in equation:

$$E_{gs}[N, V_{ext}] = \min_{\rho,\,\rho\to N} E[\rho, V_{ext}] = E_{gs}[\rho, V_{ext}], \tag{4.59}$$

for approximate solution, where $\rho \to N$ means $\int \rho d\mathbf{r} = N$. The energy functional $E[\rho, V_{ext}]$ contains the classical Coulomb interaction between the electrons and nucleus and between electrons and other electrons due to the density of electrons , which can be separated as

$$E[\rho(\mathbf{r}), V_{ext}(\mathbf{r})] = \int V_{ext}(\mathbf{r})\rho(\mathbf{r})d\mathbf{r} + \frac{1}{2}\int\int \frac{\rho(\mathbf{r}_1)\rho(\mathbf{r}_2)}{\mid \mathbf{r}_1 - \mathbf{r}_2 \mid} d\mathbf{r}_1 d\mathbf{r}_2 + G[\rho(\mathbf{r})]. \tag{4.60}$$

The difference between the actual electron-electron energy E_{ee} and the electrostatic interaction energy caused by the electron density $\rho(\mathbf{r})$ is represented by the symbol $G[\rho(\mathbf{r})]$,

$$G[\rho(\mathbf{r})] = T[\rho(\mathbf{r})] + E_{xc}[\rho(\mathbf{r})] \tag{4.61}$$

where $T[\rho(\mathbf{r})]$ is the kinetic energy of an electron system with a $\rho(\mathbf{r})$ electron density and $E_{xc}[\rho(\mathbf{r})]$ is the energy of exchange and correlation of an iteracting system.

4.2.3 The Kohn-Sham Equations

Density-functional theory was converted into a useful electronic structure theory by Kohn and Sham in a work that was published in 1965 [2]. The connection between a system's ground state density and ground state wavefunction is described by the Kohn and Sham equations. Kohn and Sham understood that the inaccurate description of kinetic energy was a major factor in the Thomas-Fermi theory's failure. The Thomas-Fermi model's kinetic energy functional, while provides a decent representation of a molecular system, is far from reality. Kohn and Sham reintroduced an auxiliary system of non-interacting electrons travelling in an effective field to overcome this issue (in a manner similar to the Hartree-Fock strategy). The functional form of $F_{HK}[\rho(\mathbf{r})]$ is expressed as a sum of non-interacting electrons kinetic energy (T_s), the Hartree energy (E_H), and the exchange and correlation energy (E_{xc}) is the result of combining all many-body quantum effects. As a result, the kinetic energy for this system is computed precisely, and the system's total functional energy may be divided into the following components:

$$E[\rho] = T_s[\rho] + E_{ext}[\rho] + E_H[\rho] + E_{xc}[\rho], \tag{4.62}$$

with the Hartree energy term $E_H = \frac{1}{2}\int\int \frac{\rho(\mathbf{r}_1)\rho(\mathbf{r}_2)}{|\mathbf{r}_1-\mathbf{r}_2|} d\mathbf{r}_1 d\mathbf{r}_2$ and external potential energy term $E_{ext}[\rho] = \int V_{ext}(\mathbf{r})\rho(\mathbf{r})d\mathbf{r}$. When compared to the first term, $T_s[\rho(\mathbf{r})]$ the kinetic energy functional of a system of electrons with density $\rho(\mathbf{r})$ and no interactions is given by equation equation (4.62), and the last term represents the exchange correlation energy functional defined as:

$$E_{xc}[\rho] = (T[\rho] - T_s[\rho]) + (E_{ee}[\rho] - E_H[\rho]). \tag{4.63}$$

Where the classical electrostatic energy of a charge density $\rho(\mathbf{r})$ is described by the Hartree term E_H, which stands for electrostatic energy of the electronic system under the mean-field approximation. The difference between the real electrostatic energy E_{ee} and the mean field term, also known as the Hartree term, E_H, makes up the majority of the exchange correlation energy ($E_{xc}[\rho]$), however it also includes kinetic energy $T[\rho] - T_s[\rho]$.

With the exception of the exchange correlation energy (E_{xc}), the Kohn-Sham equations can accurately express all of the aforementioned components in terms of the electronic density $\rho(\mathbf{r})$. The main goal of the Kohn-Sham technique is to estimate the kinetic energy of the real (interacting) system by taking into account an auxiliary system of N non-interacting electrons. They suggested that the electronic density may be described as the sum of a collection of N non-interacting single particle wavefunctions ψ_i, commonly known as KS orbitals

$$\rho(\mathbf{r}) = \sum_i^N \mid \psi_i \mid^2. \tag{4.64}$$

The Kohn-Sham kinetic energy functional term can be written as

$$T_s[\rho] = \sum_i^N -\frac{1}{2}\int \psi_i^*(\mathbf{r})\nabla^2\psi_i(\mathbf{r})d\mathbf{r}. \tag{4.65}$$

It has an orbital-specific dependence. The exchange correlation term $E_{xc}[\rho]$ and all other terms, which are derived from the single particle wave functions from which the density is determined, only implicitly depend on the orbitals. The reduction of $E[\rho(\mathbf{r})]$ with respect to the density of electrons $\rho(\mathbf{r})$ subject to the constraint that the amount of electrons must be constant, which leads to the central equation in Kohn-Sham density functional theory $(KS-DFT)$

$$\big[-\frac{1}{2}\nabla^2 + V_{KS}(\mathbf{r})\big]\psi_i = \varepsilon_i\psi_i, \tag{4.66}$$

with an one-body effective fictitious external potential,

$$V_{KS}(\mathbf{r}) = V_{ext}(\mathbf{r}) + \int \frac{\rho(\mathbf{r_1})}{\mid \mathbf{r}-\mathbf{r}_1 \mid} d\mathbf{r_1} + V_{xc}[\rho(\mathbf{r})]. \tag{4.67}$$

This equation has one electron orbitals ψ_i and is similar to Schrödinger equation for one electron. The energies of the Kohn-Sham one-electron orbitals are ε. This must be solved interactively because it is a single particle equation that resembles Hartree-Fock. It should be noted that the $V_{ks}(\mathbf{r})$ is dependent on the $\rho(\mathbf{r})$ via equation (4.64). As a result, the Kohn-Sham equation requires a self-consistent solution. To obtain the Kohn-Sham orbitals, the usual technique is to first create the $V_{ks}(\mathbf{r})$ using equation (4.66) as a starting point. A new density is derived from equation (4.64) based on these orbitals, and the procedure is repeated until convergence is reached. The ground state density $\rho(\mathbf{r})$ and the Kohn-Sham eigenenergies can be used to calculate the total energy as follows

$$E = \sum_{i=1}^{N}\varepsilon_i - \int d^3r\big[\frac{1}{2}V_H(\mathbf{r}) + V_{xc}(\mathbf{r})\big]\rho(\mathbf{r}) + E_{xc}[\rho(\mathbf{r})]. \tag{4.68}$$

We could precisely determine the ground state density and total energy if we knew the values of every term in the KS energy functional. Unfortunately, the undefined

term in equation (4.62) is the exchange-correlation energy functional E_{xc}. This term E_{xc} refers to both the component of the kinetic energy of the actual system that differs from the system of non-interacting electrons as well as the non-classical part of the electron-electron interaction (electron exchange and electron correlation). The main challenge facing modern DFT at this time is determining an approximation for the exchange correlation energy functional that is accurate enough. The local density approximation (LDA), which was proposed by Kohn and Sham [2,3], is an exact expression for the exchange correlation (XC) energy functional for the uniform electron gas (UEG) system. Since E_{xc} is not known precisely, it is required to approximation it, which is the subject of the following section.

4.3 Exchange-Correlation Energy Functionals

In order to treat the electronic energy precisely using the KS-AIMD approach, the exchange- correlation energy has been the focus of extensive research. The most important step is to approximate the electrical density by replacing many body terms with exchange-correlation interactions. As a result, it is assumed that the original many-body interacting system's ground state density is equivalent to that of an independent N electrons system. The exchange correlation functional is the ground state energy contribution in the KS-DFT technique that requires practical approximations. The OF-DFT approach, like the KS-DFT method, also employs the exchange correlation functional. The quality of the exchange correlation has a significant impact on how well a DFT computation system performs. Because of the Pauli exclusion principle, the exchange results from anti-symmetry. However, the correlation takes into

consideration the remaining complex many-body effects that require a large number of determinants to be properly explained. The problem of finding exact form of E_{xc} is the greatest challenge in the DFT because E_{xc} is not known that we have already mentioned before. It will be very difficult to express E_{xc} in a closed mathematical form. Finding of such mathematical form would be considered as a great success in the density functional theory. It is required to apply an approximation for E_{xc} since the form of exchange correlation energy in terms of the density $\rho(r)$ is typically unknown. There are two different kinds of approximations for E_{xc}. In particular, these are the local density approximation (LDA) and the generalized gradient approximation (GGA).

4.3.1 Local Density Approximation

The Local Density Approximation (LDA), which makes use of the results of calculations involving numerous bodies of the uniform electron gas. LDA is the first approximation for the exchange correlation (XC) functional $E_{xc}[\rho]$. It treats the electron gas locally at $\mathbf{r}$ as though it were a uniform electron gas (UEG) with a mean density of $\rho(\mathbf{r})$.

This approximation was first developed by Kohn and Sham [2]. Strictly speaking, the LDA is only valid if the density $\rho(\mathbf{r})$ fluctuates very slowly with $\mathbf{r}$. The system's total exchange-correlation energy, $E_{xc}[\rho]$, can be expressed using LDA to the DFT

$$E_{xc}^{LDA}[\rho(\mathbf{r})] = \int \rho(\mathbf{r}) d\mathbf{r} \varepsilon_{xc}^{LDA}[\rho(\mathbf{r})], \tag{4.69}$$

where, ε_{xc}^{LDA} denotes the exchange correlation energy per particle of the interacting homogeneous electron gas density $\rho(\mathbf{r})$. It is customary to divide the LDA exchange-

correlation energy per electron into an exchange part and a correlation part,

$$\varepsilon_{xc}^{LDA}[\rho(\mathbf{r})] = \varepsilon_{x}^{LDA}[\rho(\mathbf{r})] + \varepsilon_{c}^{LDA}[\rho(\mathbf{r})]. \tag{4.70}$$

The exchange component is straightforward and provided by the Dirac functional [67]

$$\varepsilon_{x}^{LDA}[\rho(\mathbf{r})] = -\frac{3}{4}\left(\frac{3}{\pi}\right)^{\frac{1}{3}}\rho(\mathbf{r})^{\frac{1}{3}}. \tag{4.71}$$

However, the correlation energy $\varepsilon_{c}^{LDA}[\rho(\mathbf{r})]$ to be more difficult. The precise outcomes for $\varepsilon_{c}^{LDA}[\rho(\mathbf{r})]$ have been established by Ceperley and Alder's [68] Quantum Monte Carlo (QMC) simulations. The common LDA functionals for $\varepsilon_{c}^{LDA}[\rho(\mathbf{r})]$ are the Perdew-Wang (PW) [69], Perdew-Zunger (PZ) [70], and Vosko-Wilk-Nusair (VWN) [71] functionals. The Perdew-Zunger approximation is typically used to approximate the correlation [70]. It has the form

$$\varepsilon_{c}^{LDA}[\rho(\mathbf{r})] = \begin{cases} 0.0311\,\mathrm{ln}r_s - 0.0480 + 0.0020\,r_s\,\mathrm{ln}r_s - 0.0116r_s & \text{for } r_s < 1 \\ -\frac{0.1423}{1+1.0529r_s^{\frac{1}{2}}+0.3334r_s} & \text{for } r_s \geq 1. \end{cases} \tag{4.72}$$

Where $r_s = \left(\frac{3}{4\pi\rho}\right)^{\frac{1}{3}}$. This is used in the present simulation. The functional derivative of $E_{xc}^{LDA}[\rho(\mathbf{r})]$ gives the exchange correlation potential within LDA,

$$V_{xc}^{LDA} = \frac{\delta E_{xc}^{LDA}[\rho(\mathbf{r})]}{\delta\rho(\mathbf{r})} = \varepsilon_{xc}[\rho(\mathbf{r})] + \rho(\mathbf{r})\frac{\partial\varepsilon_{xc}[\rho(\mathbf{r})]}{\partial\rho(\mathbf{r})}. \tag{4.73}$$

4.3.2 Generalized Gradient Appproximation

In addition to the local charge density, the exchange correlation energy is also influenced by the gradient of the local charge density. Generalized gradient approximations (GGA) are more complex approximations that take into account density gradients as

well as the density at $\mathbf{r}$; one that is frequently used is attributed to perdew *et.al*. In other words, for materials close to the homogenous electron gas, the LDA is suitable for smooth $\rho(\mathbf{r})$. However, inhomogeneous systems like molecules, clusters, or layers cannot be accurately predicted using LDA. GGAs are frequently referred to be semi-local functionals because of their reliance on $\nabla\rho(\mathbf{r})$. GGAs can produce more accurate findings than LDAs for a variety of parameters, such as molecular and solid ground state energies and geometries. Many GGAs are much better than LDA, particularly for covalent bonds and weakly bound systems. The generalized form of the GGA approximation to $E_{xc}[\rho(\mathbf{r})]$ is

$$E_{xc}^{GGA}[\rho(\mathbf{r})] = \int \rho(\mathbf{r})\varepsilon_{xc}^{GGA}\big[\rho(\mathbf{r}), \mid \nabla\rho(\mathbf{r}) \mid \big]d\mathbf{r} \tag{4.74}$$

as well as the standard method for creating a GGA functional is to express the correlation energy as

$$E_{xc}^{GGA}[\rho(\mathbf{r})] = \int \rho(\mathbf{r})\, \varepsilon_{xc}^{LDA}[\rho(\mathbf{r})]d\mathbf{r} + \int F_{xc}[\rho(\mathbf{r}), \mid \nabla\rho(\mathbf{r}) \mid]d\mathbf{r}, \tag{4.75}$$

where $F_{xc}[\rho(\mathbf{r}), \mid \nabla\rho(\mathbf{r}) \mid]$ is recognized as the exchange correlation enhancement factor. Contrary to the LDA, the GGA does not have a single form; rather, it is capable of a wide range of appropriate modifications [72–75], each of which corresponds to a different enhancement factor. Applying the GGA to molecules considerably improves its ability to mitigate the effects of LDA overbinding [76]. The most often used GGA is the Perdew-Burke-Ernzerhof (PBE) functional [74].

4.4 Pseudopotentials

The idea of pseudopotentials will be introduced in this section. It is commonly known that valence electrons rather than securely bonded core electrons play a major role in determining the most intriguing physical features of solids. Because of this, the theory incorporates the pseudopotential approximation. The pseudopotential approximation makes use of the fact to substitute weaker pseudopotentials for the core electrons, including the nucleus, acting on a set of fictitious wavefunctions rather than the actual valence wavefunctions. It is possible to optimize the pseudopotential so that it is actually even weaker than the potential of the frozen core [77].

The nuclei and core electrons are viewed as a single entity that interacts with the valence electrons via the external potential V_{ext}, which is often the pseudopotential. The solid is made up of lighter electrons and heavier nuclei. In many problems of molecular and atomic physics, the electrons of the system can be separated into the category of valence electrons and core electrons per atom.

The core electrons are tightly bound near the nuclei which known as core region. The fundamental concept involved in a pseudopotential calculation is that the ion core can be neglected. Because only the valence electrons are engaged in chemical bonding, the core electrons are strongly linked to their host nuclei, which is why pseudopotentials are used. The core electron density for isolated atoms is considered to have the same form in the pseudopotential approximation. The nuclear potentials that the valence electrons observe are screened by the core electrons. However, compared to valence electrons, core electrons have a far lower energy. As a result, valence electron wave functions have a significant oscillation component in the interior areas

due to the necessity of orthogonal wave functions. In order to adequately represent the valence electron wavefunctions, many more basis functions are required.

Pseudopotentials are fictional potentials that operate in the interior of an atom, replicating the screening action of the core electrons within the core area, which is governed by the cutoff radius. Outside of the core region, wave functions and potentials are both adapted to mimic the genuine ones. The ability of a pseudopotential to reproduce precise findings for all-electron computations is what is known as its transfer-ability, or quality.

The Kohn-Sham equation is then immediately inverted using the pseudo wave function ψ_{psl} to create the pseudopotential. Since a pseudopotential is not singular, many ways of creation are also available. There are various ways to generate a pseudopotential because it is not unique [78]. The four criteria that the pseudopotentials are required to follow in the reference configuration, or the atomic configuration for which the pseudopotential is generated, were developed by Hamann, Schlüter, and Chiang to guarantee the best smoothness and transfer-ability.

(i). The reference configuration is supported by both all-electron and pseudo eigenvalues.

$$\hat{H}|\psi_{nl}^{AE}\rangle = \epsilon_{nl}|\psi_{nl}^{AE}\rangle \tag{4.76}$$

$$\left(\hat{H} + \hat{V}_{nl}\right)|\psi_{nl}^{PS}\rangle = \epsilon_{nl}|\psi_{nl}^{PS}\rangle \tag{4.77}$$

(ii). Beyond a specific cutoff, R_c, AE and PS wavefunctions are in agreement.

$$\psi_{nl}^{AE}(r) = \psi_{nl}^{AE}(r) \qquad for \qquad r \geq R_c \tag{4.78}$$

(iii). The integration of real and fictitious norm squares from 0 to r for all $r < R_c$ is consistent.

$$\int_0^r |\phi_{nl}^{AE}|^2 r^2 dr = \int_0^r |\phi_{nl}^{PS}|^2 r^2 dr \tag{4.79}$$

(iv). For any $r < R_c$, the logarithmic derivatives and their energy derivatives are consistent.

$$[(r\phi^{AE}(r))^2 \frac{d}{dE}\frac{d}{dr} ln\phi^{AE}(r)]_R = [(r\phi^{ps}(r))^2 \frac{d}{dE}\frac{d}{dr} ln\phi^{ps}(r)]_R \tag{4.80}$$

Items 1 and 2 are self-evident. According to the Gauss theorem, item 3 is required in order for the electrostatic potential outside of the core region where $r < R_c$ is the same for the real and pseudo wavefunctions. To improve transfer-ability and replicate real potential phase changes in the scattering sense, 4 is finally required. The eigenvalues vary when we transition from an atom to another environment, like a solid or molecule. This shift in linear order is replicated by a pseudopotential that satisfies this item. A demonstration that item 4 is implied by item 3 can be made using the Friedel sum rule. The actions listed below must be taken in order to create a pseudopotential that preserves norms:

(1). The all-electron atomic system must be resolved.

(2). Choose which states should be considered valence and which should be considered core.

(3). Create the pseudopotentials $V_{nl}(r)$, for the valence states. There are various ways to do that. Here, we provide a description of the Kerker approach. For the core region, we use a parameterized analytical function in this approach.

Kerker's preferred analytical form is $\phi_{nl}^{ps} = e^p(r)$, where $e^p(r)$ is a fourth-order polynomial matching the genuine solution and its numerous derivatives at R_c.

(4.) Inverting the Schrödinger equation after obtaining a form for the pseudowavefunction results.

$$V_{nl,total}(r) = \epsilon - [\frac{l(l+1)}{2r^2} - \frac{\frac{d^2}{dr^2}\phi_{nl}^{PS}(r)}{\phi_{nl}^{PS}(r)}]. \tag{4.81}$$

Remember that the variable we are working with, $\phi(r)$, has the definition $\psi(r) = r\phi(r)$.

(5.) Inversion of the SE equation yields a potential $V_{l,total}(r)$ that is not only the desired ionic potential but also takes into account contributions from the Hartree and exchange-correlation factors. Therefore, these two contributions must be subtracted.

$$V_{nl}(r) = V_{l,total}(r) - V_{Hxc}^{PS}(r) \tag{4.82}$$

where it is determined for the pseudowavefunctions what the Hartree and xc contributions are un-screening is the name of this procedure. The $V_{nl}'s$ cannot be found in any particular way. Two competing factors are present:

(1.) adequate transfer-ability $\Rightarrow$ small r_c.

(2.) Large $r_c \Rightarrow$ more fluid pseudopotentials.

These two limitations should be balanced in a decent pseudopotential.

The pseudopotential potential may be either local or non-local. Both the non-local and local form of pseudopotential give accurate prediction for the properties of materials [79]. Particularly, the non-local pseudopotentials are depending on the

energy eigenvalue. Therefore, the precise form of pseudopotential is rather complex and its formulation is therefore often difficult. The two most popular non-local pseudopotential are norm conserving pseudopotentials and ultrasoft pseudopotential. The all-electron and pseudo wave functions must concur outside of a specified radius R_c in order for the pseudopotentials to be norm-conserving. Additionally, the integral density inside R_c is the same for both the all-electron wave function and the pseudo wave function ("norm conservation"). Numerous writers have created various types of norm-conserving pseudopotentials, including Troullier and Martins [80], Kerker [81], Hamann, Schlüter and Chiang [82], Vanderbilt [83], and Goedecker-Teter-Hutter [84]. Ion locations are the only factors that affect the local model pseudopotential. As a result of the computations' simplicity, they are typically employed to examine the properties of the matter. Up till present we have observed that for the construction of the local potential one must consider:

(i). The interaction between electrons and ions through the bare-ion local potential.

(ii). In Hartree screening, Coulomb interactions with the other conduction electrons are taken into consideration.

(iii). Correlation and exchange effects.

The KS-AIMD approach often uses non-local pseudopotentials that are fitted to certain free atom properties [80, 86–88]. But the fundamental variable in the OF-AIMD technique is the valence electron density. Since there are no orbitals, the pseudopotential must simply be a function of radius and be independent of angular momentum. They cannot be employed in the OF technique since they are nonlocally specified.

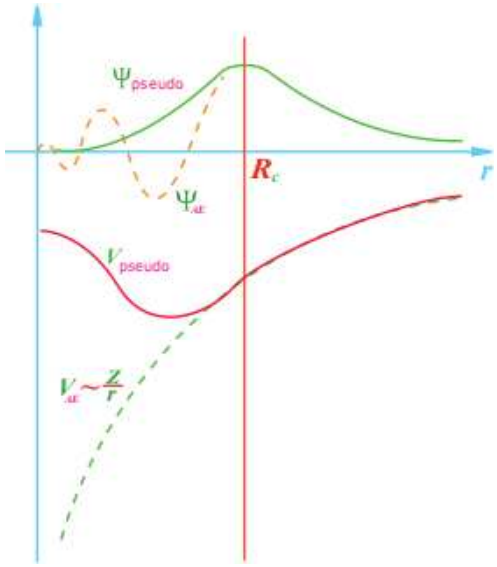

Figure 4.1: Schematic diagram of pseudopotential method [85], V_{AE}, Ψ_{AE} are the all electron potential and wave function, respectively.

For the OF-AIMD simulation method, local pseudopotentials (LPS) are therefore required. As a result, we have here utilized a local ionic pseudopotential proposed by Bhuiyan *et al.* [51]. Figure 4.1 depicts the idea of pseudopotential in a schematic manner [85]. The pseudopotential is clearly shown in Figure 4.1 to be significantly less than the all-electron potential, and the pseudo wave function lacks a radial node inside the core region. Additionally, we observe that the pseudopotential and wave function outside the core region match up with the equivalent all-electron ones. When used in conjunction with the OF-AIMD approach, the current local ionic pseudopotential has produced a good description of a number of static and dynamic features of the liquid Na_xK_{1-x} binary alloy at thermodynamic states above and close to their respective melting temperatures. The pseudopotential used in our purpose has the

form

$$v_{ps}(r) = \begin{cases} A + B\,\exp(-r/a) & \text{for } r < R_c \\ -\frac{Z}{r} & \text{for } r > R_c, \end{cases} \tag{4.83}$$

where a stands for softness parameter, R_c stands for the core radius, A and B stands for constants. Additionally, the requirement that the logarithmic derivative of the potential inside and outside the core precisely corresponds at the core radius has established the parameter B. By requiring that the OF-AIMD simulation replicate the observed static structure factor, the other parameters R_c, A and a have been fixed. The values of the parameters R_c, A and a used in our calculations are listed in the Table 6.1. The form factor of $v_{ps}(r)$ in reciprocal space is

$$\begin{aligned} v_{ps}(q) \;=\; & \frac{1}{V}\Big[\cos qR_c\Big\{-\frac{4\pi AR_c}{q^2} - \frac{4\pi}{q^2} - \frac{4\pi Ba^2R_ce^{-\frac{R_c}{a}}}{(1+a^2q^2)} - \frac{8\pi Ba^3R_ce^{-\frac{R_c}{a}}}{(1+a^2q^2)^2}\Big\} + \\ & \sin qR_c\Big\{\frac{4\pi A}{q^3} - \frac{4\pi BaR_ce^{-\frac{R_c}{a}}}{q(1+a^2q^2)} + \frac{4\pi Ba^4qe^{-\frac{R_c}{a}}}{(1+a^2q^2)^2} - \frac{4\pi Ba^2e^{-\frac{R_c}{a}}}{q(1+a^2q^2)^2}\Big\} + \\ & \frac{4\pi}{q^2} + \frac{8\pi Ba^3}{(1+a^2q^2)^2}\Big] \end{aligned}$$

where, the constant B is given by $B = \frac{Aae^{\frac{R_c}{a}}}{R_c - a}$ and V is the volume of a system.

4.5 Orbital Free Density Functional Theory

The electron density is still used as the primary variable in the OF approach [52, 89, 90], which is based on the KS evolution of DFT. As a result of the removal of the KS orbitals, memory requirements scale with system size linearly rather than quadratically as they would have under the KS strategy. With the assumption that the $T_s[\rho]$ is straightforward to calculate, there are also significant computational time savings

because just the electronic density distribution needs to be adjusted rather than the entire collection of orbitals. There is no longer a need for expensive Brillouin zone sampling and orbital orthogonalization. The OF scheme's reductions in processing time and memory enable simulation of considerably larger systems for longer simulation times than would otherwise be achievable. Nevertheless, an explicit form for $T_s[\rho]$ is necessary, and since only approximations for $T_s[\rho]$ are available, errors in the kinetic energy are created, which can have major consequences given that the kinetic energy is of the same magnitude as the total energy. The total energy function of OF-DFT is construct by taking approximations in the KE functional and the external potential energy functional of KS-DFT. Therefore, the functional approximations for kinetic energy (KE) and external potential energy are the primary distinction between KS-DFT and OF-DFT. In KS-DFT theory, the KE depends on the KS fictitious orbitals for non-interacting system while the external potential energy is described by the non-local pseudopotentials. On the other hand the KE in OF-DFT depending on the density of electrons and external potential energy is described by the local pseudopotentials.

In KS-DFT, the numerical value of $T_s[\rho]$ might be precisely determined although it is not directly derived from density. It is accomplished by using a collection of N one electron wave functions (KS orbitals) to resolve the N linked KS equations that characterize the imaginary non-interacting system. The resulting KS-DFT has been successful in many applications by applying these results combined with the comparatively straightforward approximations for the minor contribution term E_{xc}. Multiple approximations to the exchange correlation term exist [69–71] which provide

acceptable accuracy in simulation to study specific properties for specific class of materials. Different approximations are used in different applications. As there are more electrons than orbitals, KS-DFT requires that at least that many orbitals be computed (or pairs thereof). As V_{KS} relies on ρ, the KS equation must also be solved iteratively. The orbitals' basis sets must be expanded significantly as the part of the solution. The $O(N^3)$ scaling of computing cost with the amount of electrons that results from the utilization of the KS orbitals is often quite expensive. The use of DFT to very large systems is hampered by this cubic scaling. Despite of all limitations we need for a routine *ab initio* calculation on large systems. The basic algorithm of KS-DFT to determine the ground state energy and the density of a system of N electron moving in a specific $V_{ext}(\mathbf{r})$ is then as follows:

(i). Guess an initial density, $\rho(\mathbf{r})$.

(ii). Computation of the potential using

$$V_{KS}(\mathbf{r}) = V_{ext}(\mathbf{r}) + \int \frac{\rho(\mathbf{r_1})}{\mid \mathbf{r} - \mathbf{r}_1 \mid} d\mathbf{r_1} + V_{xc}[\rho(\mathbf{r})].$$

(iii). Find the N lowest-energy solutions of SE

$$\big[-\frac{1}{2}\nabla^2 + V_{KS}(\mathbf{r}) \big] \psi_i = \varepsilon_i \psi_i.$$

(iv). Construct a new density from the wave functions for all occupied states,

$$\rho(\mathbf{r}) = \sum_i^N \mid \psi_i \mid^2.$$

(v). If the density does not converge, go to step (ii).

(vi). Determine the ground state energy based on

$$E = \sum_{i=1}^{N} \varepsilon_i - \int d^3r \big[\frac{1}{2} V_H(\mathbf{r}) + V_{xc}(\mathbf{r})\big] \rho(\mathbf{r}) + E_{xc}[\rho(\mathbf{r})].$$

The bottleneck of KS-DFT could be removed if there were a proper treatment of the KE using the electron density only. The goal of Hohenberg and Kohn's DFT was to represent the ground state energy in terms of charge density without the use of wave functions; this type of DFT is known as orbital free DFT. The scaling of OF-DFT is linear. This idea was inspired by an earlier theory of density functional put out by Thomas [64] and Fermi (TF) [65], which states an accurate energy for the system of a homogeneous electron gas with no interactions. The name of this functional is TF energy functional. Depending on the number of orbitals, the KS theory requires a lengthy computation time. The total energy can be calculated quickly if the kinetic energy can be calculated without having to solve the KS equations. The most effective method for addressing big systems ($>$ 1000 particles) within realistic processing time frames [91–100] among all first-principles techniques for calculations dependent on DFT [1, 2] is the linear scaling OF-DFT. The OF-DFT approach does not solve self-consistently for one-electron orbitals and only uses the electron density, a function of three coordinates, as its major variational parameter [90], in contrast to conventional orbital-based first-principles techniques like Hartree-Fock [101–103] and KS-DFT [2] . As a result, all expenses related to orbital manipulation, such as orthonormalization, are removed. The benefit of adopting OF-DFT for periodic systems is even more significant because no k-point sampling is required, resulting in orders of magnitude savings for metallic systems in particular [91].

Although the first version of OF-DFT, the TF model [64, 65], first appeared far

earlier than it is now employed, KS-DFT and OF-DFT have not yet taken over as the most popular quantum mechanics technique for usage in real-world applications. The inability of kinetic energy density functional (KEDF) to be transferred is the main barrier to implementing OF-DFT. The original Hohenberg-Kohn theorems [1] may be used to their full potential if this roadblock could be overcome. There are several KEDF approximations exist in literature [20, 64, 65, 104–106]. The TF kinetic

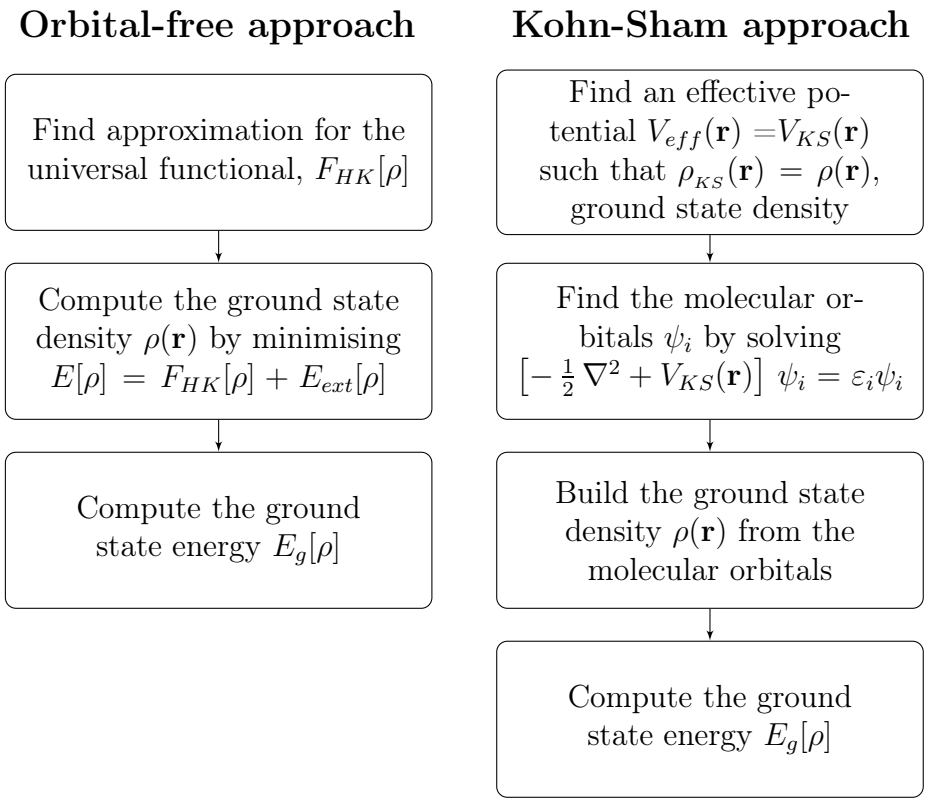

Figure 4.2: Orbital-free approache *vs.* Kohn-Sham DFT approache.

energy functional $T_{TF}[\rho(\mathbf{r})] = \frac{3}{10}\left(3\pi^2\right)^{\frac{2}{3}} \int \rho^{\frac{5}{3}}(\mathbf{r})d\mathbf{r}$ is true for gradually changing densities but not enough for application in rapidly diverse densities. Therefore, von Weizsäcker [104] developed a correction term for the TF energy functional that is $T_W[\rho(\mathbf{r})] = \frac{1}{8}\int \frac{|\nabla\rho(\mathbf{r})|^2}{\rho(\mathbf{r})}d\mathbf{r}$. It is known as the von Weizsäcker kinetic energy functional

and is for the singlet states [104] with one and two electrons. The T homas-Fermi-von Weizsäcker KE functional is a linear mixture of these two simplest approximations, the TF and von Weizsäcker KE functional. It has seen to appear in many OF-DFT applications [107]. According to Jones and Young [108, 109], the von Weizsäcker energy functional provides the proper second-order kinetic energy for the fast varying density limit while the TF energy functional provides the correct one for the slowly varying density limit. Figure 4.2 displays the processes in the OF-DFT and KS-DFT calculations.

4.5.1 Kinetic Energy Functional Approximmation

The major characteristic that sets apart the OF from the whole KS scheme is the inclusion of an explicit electron kinetic energy functional, $T_s[\rho]$. The theorems of Hohenberg and Kohn demonstrate the existence of such a functional, but little is known about its form. In comparison to the work on the electronic exchange-correlation energy functional, $E_{xc}[\rho]$, little progress has been made on $T_s[\rho]$; however, the possibility of an accurate OF-AIMD scheme has sparked interest, leading to the proposal of several approximative functional. In some limited circumstances, approximate forms have developed based on the known forms of $T_s[\rho]$.

A crucial component of a system's total energy functional is the kinetic energy functional, $T_s[\rho]$. The von Weizsäcker term $T_{vW}[\rho(\mathbf{r})]$ is usually regarded as being necessary for an accurate description of kinetic energy [104]. It is accurate for systems with one or two electrons and applies when densities are quickly changing. To accurately duplicate certain precisely known boundaries [52], additional terms are

typically added to the functional. The Thomas-Fermi functional yields the precise kinetic energy in the limit of uniform density

$$T_{TF}[\rho] = \frac{3}{10}\int \rho(\mathbf{r})k_F(\mathbf{r})^2 d\mathbf{r}, \tag{4.84}$$

Here, $k_F(\mathbf{r}) = \left(3\pi^2\rho\right)^{\frac{1}{3}}$ represents the local Fermi wave vector. The Lindhard function $\chi_L(q,\rho_0)$ [10,110], which corresponds to a uniform non-interacting electron gas, is used to calculate the response function in the case of approximately uniform density, where the linear response theory (LRT) is true.

The enormous benefits of the OF-AIMD simulation have sparked a growing interest in the creation of precise kinetic energy functional. Based on Perrot's [106] research as a starting point, Madden and co-workers [111, 112] improved functionals that accurately recover the Thomas-Fermi and linear-response limits and additionally include the quadratic response. Following their examination of these functionals, Wang *et al.* [113,114] proposed a linear combination of these functionals as a suitable form for T_s. They also obtained another expression that has kernels that rely on the density. These functionals' lack of positive definiteness is an undesirable trait, which means that minimizing the energy functional could result in an irrational amount of negative kinetic energy. A third kind of kinetic energy functional was created by Chacón *et al.* [115]. It uses a "averaged density" to recover the uniform density and LRT limitations. García-González *et al.* [116–118] explored and generalized their functional. Although they have the advantage of being positive definite, these functionals are more difficult to apply and call for N orders more fast Fourier transformations (FFT) than simpler functionals. Due to this, the OF-AIMD technique loses some of its advantages over the entire Kohn-Sham method [52].

4.5.2 Simplified Average Density Form for $T_s[\rho]$

The KE functional is the key portion for OF-DFT method. Therefore, a valid density functional for the kinetic energy (KE) is required for an accurate OF-DFT computation. We have employed a precise yet explicit functional of the valence electron density for $T_s[\rho]$. The averaged density methodology developed by Chacón, Alvarellos and Tarazona and García- González *et al.* has been simplified by González *et al.* and employed in the majority of applications of the OF-AIMD method discussed in this thesis. There were a number of formulas suggested for $T_s[\rho]$, and in the neighborhood of the current study, we employed an averaged density model [52, 116–119] with the following form

$$T_s[\rho] = T_{vW}[\rho] + T_\beta[\rho] \tag{4.85}$$

$$T_{vW}[\rho(\mathbf{r})] = \frac{1}{8}\int \frac{\mid \nabla\rho(\mathbf{r}) \mid^2}{\rho(\mathbf{r})} d\mathbf{r} \tag{4.86}$$

$$T_\beta[\rho] = \frac{3}{10}\int d\mathbf{r}\rho(\mathbf{r})^{\frac{5}{3}-2\beta}\tilde{k}(\mathbf{r})^2 \tag{4.87}$$

where,
$$\tilde{k}(\mathbf{r}) = (2k_F^0)^3 \int d\mathbf{s}k(\mathbf{s})w_\beta(2k_F^0 \mid \mathbf{r}-\mathbf{s} \mid) \equiv \omega_\beta(2k_F^0 r) * k(\mathbf{r}) \tag{4.88}$$

$$k(\mathbf{r}) = (3\pi^2)^{\frac{1}{3}}\rho(\mathbf{r})^\beta. \tag{4.89}$$

Here k_F^0 being the Fermi wave vector associated with the average electron density $\rho_0 = \frac{N_e}{V}$. In equation (4.87), the weight function $w_\beta(x)$, is selected to ensure that the linear response theory and Thomas-Fermi limits are accurately recovered. It is important to note that $\tilde{k}(\mathbf{r})$ appears as a convolution that can be quickly executed using standard FFT techniques. This functional, which was employed by Gómez *et al.* [120] to analyze extended liquid Cs earlier, is one of the generalizations with $\beta = \frac{1}{3}$.

González *et al.* [52] provide the functional details, which are replicated in Appendix B. The following are the key features of the KE functional:

(i). The largest value of the real positive number β that still results in a weight function that behaves mathematically is ≈ 0.6.

(ii). The limit of LRT and uniform density are recovered by the functional, which is positive definite.

(iii). The von Weizsäcker term is recovered if $\beta = 4/9$, however for other values of β, the limit is $T_{vW} + CT_{TF}$ when the mean electron density vanishes at $k_F^0 \to 0$ (for a finite system, for example).

(iv). It is anticipated that for values of $\beta > 0.5$, the driving force for the dynamic minimization of the energy, $\mu(\mathbf{r})\psi(\mathbf{r})$ [see equation 4.73], will stay finite even for extremely low electronic densities $\rho(\mathbf{r})$.

Due to the presence of significant inhomogeneities in the atomic distribution and, consequently, in the electron density, which has parts where it decreases significantly, the last two qualities described above are crucial in the case of expanding liquid metals. In fact, this circumstance has already been seen in iterative *ab initio* simulations of expanding liquid Na [121]. A functional with a value of β as close as feasible to 4/9 would be advised in systems where the occurrence of solitary atoms or clusters is likely. The von Weizsäcker term would be appropriate in these systems. For the current simulations, we used $\beta = 0.51$, which yields $C = 0.046$ [52] in the limit $\rho_0 \to 0$ and ensures that, at least for the preferred thermodynamic states, $\mu(\mathbf{r})\psi(\mathbf{r})$

stays finite and is not excessively large everywhere so that energy minimization can be accomplished.

4.5.3 Energy Minimization Technique in OF-DFT

The key components of the energy functional as well as its calculation methodology are covered in this section. The majority of models for liquid metals that can be thrown into the category of simple liquids depict them as organized in the short term but disordered in the long term. Take into account that each of the N valence Z ions is maintained in a volume V and interacts with the $N_{\mathrm{e}} = NZ$ valence electrons via the potential $v(r)$. Within the Born-Oppenheimer approximation, the total potential energy of the system can be expressed as the product of the energy of direct ion-ion Coulombic interactions and the energy of the electronic system's ground state under the external potential provided by the ions, $V_{\mathrm{ext}}(\mathbf{r}, \{\mathbf{R}_l\}) = \sum_{i=1}^{N} v(|\mathbf{r} - \mathbf{R}_i|)$,

$$E[\rho, \{\mathbf{R}_l\}] = \sum_{i<j} \frac{Z^2}{|\mathbf{R}_i - \mathbf{R}_j|} + E_g[\rho(\mathbf{r}), V_{\mathrm{ext}}(\mathbf{r}, \{\mathbf{R}_l\})]\,, \tag{4.90}$$

where $\rho(\mathbf{r})$ represents the ground state valence electronic density and $\mathbf{R}_l$ $(l = 1, 2, \ldots N)$ represents the ionic locations. Now, in accordance with the DFT, the energy functional $E[\rho]$ as specified in equation (4.43) is minimized by the ground state valence electronic density, $\rho(\mathbf{r})$. The ground state is derived from the variational principle for a certain set of ionic locations $\{\mathbf{R}_l\}$, that is, for a specific external potential V_{ext},

$$\frac{\delta \mathcal{F}}{\delta \rho(\mathbf{r})} \equiv \frac{\delta}{\delta \rho(\mathbf{r})}(E[\rho, \{\mathbf{R}_l\}] - \mu \int \rho(\mathbf{r}) d\mathbf{r}) = 0, \tag{4.91}$$

where, μ is an electron's chemical potential that is selected to produce the appropriate number of electrons N_{e}. We define the position dependent chemical potential, $\mu(\mathbf{r})$,

by the equation given as:

$$\begin{aligned}\mu(\mathbf{r}) &= \frac{\delta E}{\delta\rho(\mathbf{r})} \\ &= \frac{\delta T_s}{\delta\rho(\mathbf{r})} + \frac{1}{2}\int\int \frac{\rho(\mathbf{r}_2)}{\mid \mathbf{r}-\mathbf{r}_2 \mid} d\mathbf{r}_2 + V_{\text{ext}}(\mathbf{r}) + V_{xc}(\mathbf{r}),\end{aligned} \tag{4.92}$$

with $V_{xc} = \frac{\delta E_{xc}}{\delta\rho(\mathbf{r})}$, the density and energy of the ground state are found self-consistently by solving the equation

$$\frac{\delta\mathcal{F}}{\delta\rho(\mathbf{r})} \equiv \mu(\mathbf{r}) - \mu = 0, \tag{4.93}$$

together with the normalization constraint

$$\mathcal{G}[\rho(\mathbf{r})] = \int_v \rho(\mathbf{r}) d\mathbf{r} = N_e. \tag{4.94}$$

We have discovered that working in terms of a single effective orbital, $\psi(\mathbf{r})$ rather than $\rho(\mathbf{r})$, is more convenient, such that

$$\rho(\mathbf{r}) = \mid \psi(\mathbf{r}) \mid^2, \tag{4.95}$$

and to vary $\psi(\mathbf{r})$ rather than $\rho(\mathbf{r})$ [89, 111, 112, 122–127]. If ψ is genuine, this has the benefit of maintaining $\rho(\mathbf{r}) \geq 0$.

The effective orbital, $\psi(\mathbf{r})$ can be expanded into Fourier series in plane waves that are acceptable to the simulation's basic cubic periodic boundary conditions as

$$\psi(\mathbf{r}) = \sum_{\mathbf{G}} c_{\mathbf{G}} e^{-i\mathbf{G}.\mathbf{r}} \tag{4.96}$$

$$c_{\mathbf{G}} = \frac{1}{V}\int_{\text{v}} d\mathbf{r}\psi(\mathbf{r}) e^{i\mathbf{G}.\mathbf{r}} \tag{4.97}$$

$$\mathbf{G} = \frac{2\pi}{L}(n_1, n_2, n_3), \tag{4.98}$$

where, V denotes the cell's volume, L denotes the cube's side, and $\mathbf{G}$ denotes the super lattice's reciprocal lattice vector. With respect to wave vectors, this expansion is terminated at E_{cut} cutoff energies. An actual $\psi(\mathbf{r})$ means that, given a real c_0, $c_{-\mathbf{G}} = c^*_{\mathbf{G}}$. As a result it is just necessary to treat the half-set $\{c_{-\mathbf{G}}\}$ as variables. Instead of focusing on the electron density, the energy minimization now takes into account$\{c_{-\mathbf{G}}\}$. This results in the equations below

$$\frac{\partial \mathcal{F}}{\partial c_0} = 2\int_{\text{v}} d\mathbf{r}\mu(\mathbf{r})\psi(\mathbf{r}) - 2\mu V c_0 = 0, \tag{4.99}$$

$$\frac{\partial \mathcal{F}}{\partial c_{\mathbf{G}}} = 4\int_{\text{v}} d\mathbf{r}\mu(\mathbf{r})\psi(\mathbf{r})e^{i\mathbf{G}.\mathbf{r}} - 4\mu V c_{\mathbf{G}} = 0. \tag{4.100}$$

A simple quenching method is employed to perform the minimization energy functional at every step in time of the simulation. A fictitious kinetic energy for electrons

$$T_e = \frac{1}{2}M_e \sum_{\mathbf{G}} |\ \dot{c}_{\mathbf{G}}\ |^2 \tag{4.101}$$

is introduced following Car and Parrinello [17], where M_e is the fictitious mass of electrons and the dot stands for the derivative in relation to the imaginary time t_e. This kinetic energy is translated in terms of the set $c_{\mathbf{G}}$, and when combined with the "potential energy" $\mathcal{F}$ it yields the equation of motion for the electron density ($\forall$ $c_{\mathbf{G}} \in \{c_{\mathbf{G}}\}$) shown as [52]

$$M_e\ddot{c}_{\mathbf{G}} = -2\int_{\text{v}} d\mathbf{r}\mu(\mathbf{r})\psi(\mathbf{r})e^{-i\mathbf{G}.\mathbf{r}} + 2\mu V c_{\mathbf{G}}. \tag{4.102}$$

By employing the Verlet Leap-frog technique [6] and an electronic time step, Δt_e, these equations are numerically solved. Every time step, the velocities are reduced until the minimum is attained while staying within the predetermined tolerances T_e for the gradient of the potential energy, $\mathcal{F}$. Since the chemical potential μ is

unknown prior to the minimization, its stationary value should be substituted for μ in equation (4.102).

$$\frac{\int d\mathbf{r}\mu(\mathbf{r})n(\mathbf{r})}{\int d\mathbf{r}n(\mathbf{r})}, \tag{4.103}$$

yields a satisfactory convergence to the ground state with the "displaced" density $n(\mathbf{r}) = \rho(\mathbf{r}) - \rho_0$ at each time step [52]. Using the Hellmann-Feynman theorem, the inter atomic forces can be calculated from the electronic ground state

$$\mathbf{F}_i = -\nabla_{\mathbf{R}_i} E_g[\rho(\mathbf{r}), \{\mathbf{R}_l\}], \ (i = 1, \ldots, N), \tag{4.104}$$

and the Newton's equations of motion for the ions

$$\frac{d^2\mathbf{R}_i}{dt^2} = \frac{\mathbf{F}_i}{M_i} \tag{4.105}$$

numerically solved through the Verlet Leap-frog algorithm [6] with a suitable time step, Δt.

Chapter 5

Liquid State Theorey and Properties of Liquid Metals

Understanding and forecasting the characteristics of dense fluids and materials requires a molecular description of matter that is based on statistical mechanics theories and computer simulation. This chapter describes the theories relating to the static properties and the dynamic properties of the liquid systems and their alloys. We have also discussed the technique how these properties of the liquid systems are being calculated. In the present work the description of the properties namely, the static structural factor, $S_{ij}(q)$, the pair correlation function, $g_{ij}(r)$, isothermal and adiabatic compressibility, χ_T, coordination number, n_{ij}, self-intermediate scattering function (SISF), $F^s(q,t)$, intermediate scattering function (ISF), $F(q,t)$, self-diffusion coefficient, D^s, dynamic structure factor (DSF), $S_{ij}(q,\omega)$ and shear viscosity, η, are given. The transport coefficient of the system such as the adiabatic sound velocity (ASV), c_s, is determined by the dispersion curve's slope, which is derived from the

side peaks of the DSF. The structural and dynamic characteristics of the systems under thermodynamic equilibrium will be the main focus.

5.1 The Static Properties

This section offers a concise summary of the theories relating to static features such as the coordination number, paircorrelation function (PCF), isothermal and adiabatic compressibilities and static structure factor (SSF). We now focus on the challenge of analyzing the data from the MD simulation in order to investigate the characteristics derived from the phase-space trajectory. This section can be split into two parts: the static properties and the dynamic properties. Dynamic properties rely on correlations between two different time points, whereas static properties depend on a single time point. The pair distribution function (PDF), which represents the spatial arrangement of particles around a central particle, is connected to the static structure factor (SSF), that can be directly evaluated by X-ray or neutron diffraction experiments. This function is crucial to the theory of dense fluids and can be used to determine the crystalline solid's lattice structure.

The pair distribution function (PDF) is a very important tool in the theory of liquids and is used to determine how crystalline solids' lattice structures are organized. To have the detailed information regarding the structure of atomic systems different static distributions are oftenly used. Among them PDF is the most important one and this can not be measured directly from the experiment. Therefore, we may calculate pair distribution function either from the molecular dynamics (MD) simulation or from the numerical Fourier transformation (FT) of the static structure factor. Due

to the mathematical complexity, the PDF obtained from the MD simulation is more convenient than that obtained from the numerical Fourier transformation (FT). In the current study, the phase-space trajectory produced by MD simulation is used to directly calculate the static structure factor and the pair distribution function. We can compute the isothermal compressibility and coordination number using only the static structure factor and the PDF, respectively.

5.1.1 The Pair Distribution Function

In the MD simulation we may compute the PDF, $g(r)$, in two different ways, firstly it can be calculated directly from the trajectory generated in molecular dynamic (MD)

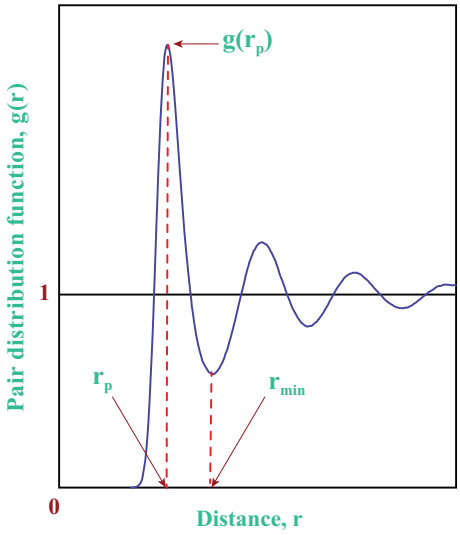

Figure 5.1: Schematic diagram of PDF, $g(r)$ in liquid state.

simulation and secondly $g(r)$ can be acquired from the Fourier Transformation [44] of the static structure factor, $S(q)$, directly found from the MD trajectory. The physical

definition of $g(r)$ is the probability of finding a particle at the same time and place at a distance $\mathbf{r}$ from a reference particle located at the origin.

The pair distribution function is a dimensionless quantity. A typical form of the PDF, $g(r)$, is depicted in Figure 5.1. The figure displays which the first peak of $g(r)$ occurs at r_p having a value of $g(r_p)$. As a result, the likelihood of discovering two particles at a distance of $r \approx r_p$ is $g(r_p)$. The pair distribution function then falls for $r > r_p$ and passes through a minimum point at around $r \approx r_{min}$. This indicates that there is a lower chance of discovering two particles at this distance.

Integration over each momentum component for a system of constant N, V and T results in a factor $(2\pi m k_B T)^{1/2}$, and the distribution function for the n bodies, $f_0^{(n)}$, may be represented as

$$f_0^{(n)}(\mathbf{r}^n, \mathbf{p}^n) = \rho_N^{(n)}(\mathbf{r}^n) f_M^{(n)}(\mathbf{p}^n), \tag{5.1}$$

where

$$f_M^{(n)}(\mathbf{p}^n) = \frac{1}{(2\pi m k_B T)^{\frac{3n}{2}}} \exp\big(-\beta \sum_{i=1}^{n} \frac{(|\mathbf{p}_i|)^2}{2m}\big), \tag{5.2}$$

is the result of n distinct independent momenta the Maxwell distributions. The equilibrium n-particle density $\rho_N^{(n)}$ is,

$$\begin{aligned} \rho_N^{(n)}(\mathbf{r}^n) &= \frac{N!}{(N-n)!} \frac{1}{h^{3N} N! Q_N} \int \int \exp\big(-\beta \mathcal{H}\big) d\mathbf{r}^{(N-n)} d\mathbf{p}^N \\ &= \frac{N!}{(N-n)!} \frac{1}{Z_N} \int \exp\big(-\beta V_N\big) d\mathbf{p}^N. \end{aligned} \tag{5.3}$$

The chance of finding n system particles using coordinates from the volume element $d\mathbf{r}^n$, independent of the remaining particle locations and independent of any momenta, is given by the number $\rho_N^{(n)}(\mathbf{r}^n) d\mathbf{r}^n$. Describe the n-particle density

$$\int \rho_N^{(n)}(\mathbf{r}^n) d\mathbf{r}^n = \frac{N!}{(N-n)!}. \tag{5.4}$$

Thus,

$$\int \rho_N^{(1)}(\mathbf{r})d\mathbf{r} = N. \tag{5.5}$$

Consequently, the overall number density and the single-particle density of a homogeneous fluid are the same:

$$\frac{1}{V}\int \rho_N^{(1)}(\mathbf{r})d\mathbf{r} = \frac{N}{V} = \rho. \qquad \text{(uniform fluid)} \tag{5.6}$$

It is known that $Z_N = V^N$ in the exceptional the instance of a homogeneous ideal gas. As a result, the pair density is

$$\int \rho_N^{(2)} d\mathbf{r}_1 d\mathbf{r}_2 = \rho^2(1 - \frac{1}{N}). \qquad \text{(ideal gas)} \tag{5.7}$$

The distribution function $g_N^{(n)}(\mathbf{r}^n)$ of n-particles characterized by the corresponding particle density as

$$g_N^{(n)}(\mathbf{r}^n) = \frac{\rho_N^{(n)}(\mathbf{r}_1, ...\mathbf{r}_n)}{\prod_{i=1}^{n} \rho_N^{(1)}(\mathbf{r}_i)}. \tag{5.8}$$

Regarding a uniform system

$$\rho^n g_N^{(n)}(\mathbf{r}^n) = \rho_N^{(n)}(\mathbf{r}^n). \tag{5.9}$$

For isotropic system, $g_N^2(\mathbf{r}_1, \mathbf{r}_2)$ is the pair distribution function. It is frequently known as the pair distribution function or correlation function and is represented as just $g(r)$ is a function that only depends on the separation $r_{12} = |\mathbf{r}_2 - \mathbf{r}_1|$.

The RDF gets close to the ideal-gas limit when $\mathbf{r}$ is significantly bigger than the inter-particle potential's range; according to equation (5.7), this limit is defined as $(1 - \frac{1}{N}) \approx 1$. It is also possible to express the particle densities specified by reference equation (5.3) according to δ-functions of position in a way that is highly useful for

further uses. It follows from the definition of a δ-function that

$$\begin{aligned}\langle\delta(\mathbf{r}-\mathbf{r}_1)\rangle &= \frac{1}{Z_N}\int\delta(\mathbf{r}-\mathbf{r}_1)\exp[-\beta V_N(\mathbf{r}_1,\mathbf{r}_2,.....,\mathbf{r}_n)]d\mathbf{r}^N \\ &= \frac{1}{Z_N}\int.....\int\exp[-\beta V_N(\mathbf{r}_1,\mathbf{r}_2,.....,\mathbf{r}_n]d\mathbf{r}_2.....,d\mathbf{r}_N. \quad (5.10)\end{aligned}$$

Despite being independent of the particle label(here taken to be 1), the ensemble average in equation (5.10) is a function of the coordinate $\mathbf{r}$. As a result, a total over all particle labels is equal to N times the contribution from each particle. The comparison with the definition (5.3) therefore demonstrates that

$$\rho_N^{(1)}(\mathbf{r}) = \langle\sum_{i=1}^{N}\delta(\mathbf{r}-\mathbf{r}_i)\rangle. \quad (5.11)$$

This is the ensemble average of a microscopic particle density, denoted by the symbol $\rho(\mathbf{r})$. Comparatively, the average of the result of two δ-functions is

$$\begin{aligned}\langle\delta(\mathbf{r}-\mathbf{r}_1)\delta(\mathbf{r}^{'}-\mathbf{r}_2)\rangle &= \frac{1}{Z_N}\int\delta(\mathbf{r}-\mathbf{r}_1)\delta(\mathbf{r}^{'}-\mathbf{r}_2)\exp[-\beta V_N(\mathbf{r}_1,\mathbf{r}_2,.....,\mathbf{r}_n)]d\mathbf{r}^N \\ &= \frac{1}{Z_N}\int.....\int\exp[-\beta V_N(\mathbf{r},\mathbf{r}_{\prime},\mathbf{r}_3...,\mathbf{r}_n]d\mathbf{r}_3....,d\mathbf{r}_N \quad (5.12)\end{aligned}$$

it suggests that

$$\rho_N^{(2)}(\mathbf{r},\mathbf{r}^{'}) = \langle\sum_{i=1}^{N}\sum_{j=1}^{N}{}'\delta(\mathbf{r}-\mathbf{r}_i)\delta(\mathbf{r}^{'}-\mathbf{r}_j)\rangle \quad (5.13)$$

where the prime on the summation sign denotes that terms with $i = j$ must be excluded. Finally, it is possible to describe the radial distribution function with a meaningful δ-function. It is obvious to conclude that

$$\langle\frac{1}{N}\sum_{i=1}^{N}\sum_{j=1}^{N}{}'\delta(\mathbf{r}-\mathbf{r}_j+\mathbf{r}_i)\rangle = \langle\frac{1}{N}\int\sum_{i=1}^{N}\sum_{j=1}^{N}\delta(\mathbf{r}^{'}+\mathbf{r}-\mathbf{r}_j)\delta(\mathbf{r}^{'}-\mathbf{r}_i)d\mathbf{r}^{'}\rangle. \quad (5.14)$$

As a result, if the system is homogeneous and isotropic:

$$\langle\frac{1}{N}\sum_{i=1}^{N}\sum_{j=1}^{N}\delta(\mathbf{r}-\mathbf{r}_j+\mathbf{r}_i)\rangle = \frac{\rho^2}{N}\int g_N^{(2)}(\mathbf{r},\mathbf{r}^{'})d\mathbf{r}^{'} = \rho g(r). \quad (5.15)$$

A crucial aspect of the physics of monoatomic liquids is the radial distribution function. This is due to a number of factors, the first of which is that radiation-scattering tests can measure $g(r)$. When, $r \to 0$, $g(r) = 0$ and $r \to \infty$, $g(r) = 1$. Second, at least at the level of pair correlations, the form of $g(r)$ sheds light on what is meant when something is said to have a liquid structure. According to the definition of $g(r)$, the average number of particles inside the range between r and $r+dr$ from a reference particle is $4\pi r^2 \rho g(r) dr$, and the peaks in $g(r)$ represent "shells" of neighbors around the reference particle. Therefore, integration of $4\pi r^2 \rho g(r)$ up to the first minimal position yields an estimate of the number of nearest neighbors, often known as the "coordination number".

With the partial pair potential known, the total correlation function $h_{ij}(r)$ of a binary alloy can be determined from the solution of the Ornstein-Zernike equation as

$$\gamma_{ij}(r) \equiv h_{ij}(r) - c_{ij}(r) = \sum_{k=1}^{2} c_k \rho \int h_{ik}(r) c_{kj}(r) dr, \tag{5.16}$$

where $h_{ij}(r) = g_{ij}(r) - 1$ and $c_{ij}(r)$ is the direct correlation function. To solve the Ornstein-Zernike integral equation, one needs a closer between $h_{ij}(r)$ and $c_{ij}(r)$. Using Rogers-Young approximation [128] defined as

$$g_{ij}(r) = \exp[\beta u_{ij}(r)] \left[1 + \frac{\exp[f_{ij}(r)\gamma_{ij}(r)] - 1}{f_{ij}(r)}\right] \tag{5.17}$$

where $\beta = \frac{1}{k_B T}$, k_B is the Boltzmann constant, T is the temperature, and $f_{ij}(r)$ is the mixing function given by

$$f_{ij}(r) = 1 - \exp(a_{ij} r) \tag{5.18}$$

Here we place $a_{ij} r = a$ and we calculated from the relation suggested by Lia *et al.* [129]. Thus for binary alloy, the partial pair distribution function $g_{ij}(r)$ can be

written as

$$g_{ij}(r) = 1 + \frac{1}{(2\pi)^3 \rho \sqrt{x_i x_j}} \int_0^\infty (S_{ij}(q) - \delta_{ij}) \exp(i\bar{q}.\bar{r}) d^3r \tag{5.19}$$

where the momentum transfer is represented by q and $S_{ij}(q)$ is the partial static structure factor.

5.1.2 Static Structure Factor

Static structure factor (SSF), $S(q)$, can also be estimated using two different methods as we have mentioned it for $g(r)$ in the previous section. Firstly, we may calculate static structure factor $S(q)$ directly from the trajectory generated in molecular dynamic (MD) simulation in momentum space. Secondly, we may get $S(q)$ from the Fourier transformation of $g(r)$ generated from MD simulation. A material's ability to scatter incident radiation is described by its SSF. Particularly for deciphering the interference patterns discovered by X-ray or neutron diffraction experiments, the structure factor is a very helpful tool. Figure 5.2 displays the schematic representation of $S(q)$.

A system's particle density can be described microscopically as [44]

$$\rho(\mathbf{r})) = \sum_{i=1}^{N} \delta(\mathbf{r} - \mathbf{r}_i) \tag{5.20}$$

where N denotes the number of particles and $\rho(\mathbf{r})$ denotes the average density at location $\mathbf{r}$ (single particle density) in this instance, it is the ensemble average: $\rho^{(1)}(\mathbf{r}) = \langle \rho(\mathbf{r}) \rangle$. The mean number density is the average throughout all of space: $\frac{1}{V} \int \rho^{(1)}(\mathbf{r}) d^3\mathbf{r} = \rho$. The static structure factor is the name for the density auto-correlation function of

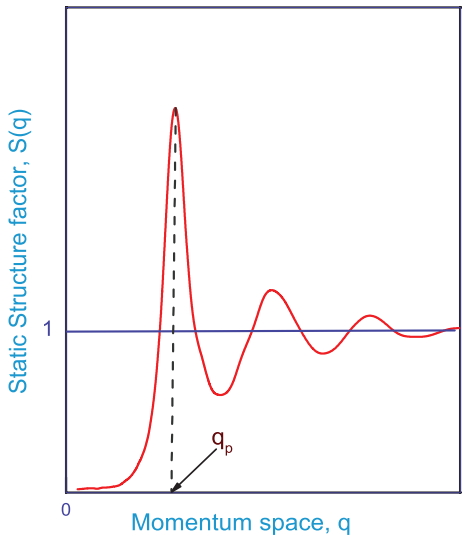

Figure 5.2: Schematic diagram of the SSF, $S(q)$, in the liquid state.

the Fourier components of the particle density. Mathematically, this auto-correlation function is defined as

$$S(\mathbf{q}) = \frac{1}{N}\langle \rho_{\mathbf{q}} \rho_{-\mathbf{q}} \rangle. \tag{5.21}$$

The structure factor from a molecular simulation can be calculated using this equation. Here, the particle density's Fourier component, denoted by the symbol $\rho_{\mathbf{q}}$, is written as

$$\rho_{\mathbf{q}} = \sum_{i=1}^{N} \exp(-i\mathbf{q}.\mathbf{r}_i), \tag{5.22}$$

and this quantity can be obtained easily and quickly from a given configuration. The atomic form factor equation (5.22) is the building block of the construction of the static structure factor. The structure factor contains all the information regarding the position of the particles. Another strategy is to represent the structure factor in

isotropic systems as the Fourier transform of $g(r)$

$$\begin{aligned} S(\mathbf{q}) &= \frac{1}{N}\sum_{i=1}^{N}\sum_{j=1}^{N}\left\langle e^{-i\mathbf{q}.\mathbf{r}_i}e^{i\mathbf{q}.\mathbf{r}_j}\right\rangle \\ &= 1+\frac{1}{N}\sum_{i=1}^{N}\sum_{j\neq i}^{N}\left\langle \int\int e^{-i\mathbf{q}.(\mathbf{r}_1-\mathbf{r}_2)}\delta(\mathbf{r}_1-\mathbf{r}_i)\delta(\mathbf{r}_2-\mathbf{r}_j)d\mathbf{r}_1 d\mathbf{r}_2\right\rangle \\ &= 1+\frac{1}{N}\frac{N(N-1)}{V^2}\int\int e^{-i\mathbf{q}.(\mathbf{r}_1-\mathbf{r}_2)}g(\mathbf{r}_1-\mathbf{r}_2)d\mathbf{r}_1 d\mathbf{r}_2 \\ &= 1+\rho\int e^{-i\mathbf{q}.\mathbf{r}}g(\mathbf{r})d\mathbf{r}. \end{aligned} \tag{5.23}$$

Due to the asymptotic behavior of $g(\mathbf{r})$, one finds that

$$S(\mathbf{q}) = 1+\rho\int e^{-i\mathbf{q}.\mathbf{r}}[g(\mathbf{r})-1]d\mathbf{r}. \tag{5.24}$$

For an isotropic system, $g(\mathbf{r}) \equiv g(r)$, and $S(\mathbf{q}) \equiv S(q)$. Thus one obtains

$$S(q) = 1+\rho\int e^{-i\mathbf{q}.\mathbf{r}}[g(r)-1]d\mathbf{r}. \tag{5.25}$$

The quantity $S(q)$ is callled the static structure factor because it describes the average distribution of molecular separations in momentum space in the fluid. It is the quantity of central interest in the equilibrium theory of fluids. The behavior of $S(q)$ often mimics that of $g(r)$, despite the fact that the physical significance of the individual features in the wave vector domain is entirely different. As a result, the first peak of $S(q)$ indicates that there is a dominant, nearly regular particle arrangement in real space. The asymptotic value of $S(q)$ at large q is also unity and indicates the vanishing of pair correlations at short wavelengths. Eventually, for large wave vectors, the "hard core" area is probed by $S(q)$ where $g(r)$ is vanishingly small. In contrast, $S(q \to 0)$ exhibits the characteristics of $g(r)$, particularly its asymptotic approach to unity for very large separations, in an average sense. As a result, it is reasonable to

assume that $S(0)$ is connected to a system's macroscopic property [43]. The principal peak of $S(q)$ is called the first diffraction maximum. Since $S(q)$ is a measure of the spatial correlation effects in the liquid, the position of the first maximum in liquid q_p, gives the distance $\frac{2\pi}{q_p}$ over which the correlation effects are strongest. There is no obvious direct connection between r_p and $\frac{2\pi}{q_p}$, where r_p is the position where $g(r)$ has its first maximum. We therefore expect $\frac{2\pi}{q_p}$ to be somewhat less than d (hard sphere diameter), while r_p should be somewhat greater than d [130].

In the current OF-AIMD simulation, the static structure factor is calculated directly from MD trajectory via

$$S(\mathbf{q}) = \frac{1}{N}\Big\langle \sum_{i,j} e^{-i\mathbf{q}.(\mathbf{r}_i - \mathbf{r}_j)} \Big\rangle, \tag{5.26}$$

where N denotes the total number of atoms in the spherical cell and $\mathbf{r}_i$ and $\mathbf{r}_j$ denote the coordinates of the particles with the indexes i and j, respectively. The q-vectors that are connected to the reciprocal lattice vectors of the simulation for a simple cubic cell should be provided, *i.e.* $q = \frac{2\pi}{L}(n_1, n_2, n_3)$, where L denotes the simulation cell's size. This implies that as q increase in size, we will obtain a histogram representation of $S(q)$ with improved resolution. In a simulation, the lowest amount of q that may be accessed is $q_{min} = \frac{2\pi}{L}$. The isothermal compressibility, which measures the proportional change in volume of a system when the pressure varies while the temperature stays constant, is another crucial thermodynamic quantity. The static structural factor is related to the isothermal compressibility. Throughout the range

$q \to 0$, the structure factor yields the important compressibility equation [130]

$$\begin{aligned} \lim_{q\to 0} S(q) &= 1 + \rho \int [g(r) - 1] d^3r \\ &= \frac{\left\langle N^2 \right\rangle - \left\langle N \right\rangle^2}{\left\langle N \right\rangle} = \rho k_B T \kappa_T, \end{aligned} \tag{5.27}$$

where, $\left\langle N^2 \right\rangle - \left\langle N \right\rangle^2$ is the mean square fluctuation in the number of particles and κ_T is the isothermal compressibility. Thus, it is noticed from equation 5.14 that, the limit $q \to 0$ of $S(q)$ is sensitive to temperature and density. In the present work, we do not calculated partial isothermal compressibility instead we have computed the alloys isothermal compressibility from the total structure factors (S_T) of Bhatia-Thornton . The isothermal compressibility is calculated from the relation

$$\chi_T = \frac{S_T(0)}{\rho k_B T}. \tag{5.28}$$

Here ρ, k_B, and T denote total ionic number density, Boltzmann's constant and temperature, respectively. The magnitude of $S_T(0)$ is determined by fitting the simulated q at lower q with

$$S(q) = S_0 + S_1 q^2, \tag{5.29}$$

where S_0 and S_1 are fitting constant. In the same way the isothermal compressibility could also be found from the experimental $S(q)$. From the inverse Fourier transformation of the static structure, $S(q)$, after subtracting the "self-correlation" [44] one may get PDF as follows

$$\rho[g(\mathbf{r}) - 1] = \frac{1}{(2\pi)^3} \int d\mathbf{q}\, e^{i\mathbf{q}.\mathbf{r}} [S(\mathbf{q}) - 1]. \tag{5.30}$$

Simple liquids are isotropic by nature. Thus, one finds

$$\rho[g(r) - 1] = \frac{1}{(2\pi)^3} \int d\mathbf{q}\, e^{i\mathbf{q}.\mathbf{r}} [S(q) - 1]. \tag{5.31}$$

After the calculation of pair distribution function, we computed the Ashcroft-Langreth's partial structure factors [131] by

$$S_{ij}(q) = 1 + \sqrt{x_i x_j}\rho \int [g_{ij}(r) - 1] \exp(-i\vec{q}.\vec{r})\vec{dr} \tag{5.32}$$

where x_i is the concentration of the ith components. From the knowledge of partial structure factor of $S_{ij}(q)$, we are able to compute the total structure factors by

$$S(q) = \frac{x_1 f_1^2 S_{11}(q) + 2\sqrt{(x_1 x_2)} f_2 S_{12}(q) + x_2 f_2^2 S_{22}(q)}{x_1 f_1^2 + x_2 f_2^2} \tag{5.33}$$

where f_1 and f_2 are atomic scattering factors and are taken from the literature [132]. The Bhatia-Thornton partial structure factors, $S_{NN}(q)$, $S_{CC}(q)$ and $S_{NC}(q)$ are presented in the Appendix B in equation B.1. Where the partial dynamic structure factors $S_{ij}(q, \omega)$ are obtained from the Fourier transformation of partial intermediate scattering function $F_{ij}(q, t)$ as given in equation A.2.

5.1.3 Coordination Number

The coordination number, n, is a significant quantity in the solid and liquid systems that provides a useful representation of the total number of nearest-neighbour atoms in the liquid structure. The strong spatial correlations exist in the liquid state is clearly indicated by the sharp structure in $g(r)$, where the first peak is representing the coordination shell of the nearest neighbours, the second peak is representing the next nearest neighbours, and so on [130]. The initial coordination number largely determines a liquid's characteristics. It is commonly employed as a parameter in the analysis of non-crystalline materials' structural properties. Therefore, the concept of the coordination number, particularly refers to the first coordination number. When

compared to crystals, this idea is a little hazy in liquids because of the atomic vibration that exists there naturally. The correlation functions will typically display double subscripts with each one corresponding to a different species in the alloy. This will describe the relationship between atoms of various types and particles of the same type. For illustration, three partial distribution functions that describe the particles of type j that surround particles of type i can be written as $g_{ij}(r)$.

We can investigate the local atomic structure of the alloy using these functions. The nearest neighbours' (NNs) distribution can be easily determined from the understanding of $g_{ij}(r)$. While the reference particle is positioned at the origin, the quantity $\rho g_{ij}(r)$ provides the average density of particles at a distance, r. There are few popular schemes [133] to estimate the first coordination number. Among them a common method is the integration of the RDF, $G(r)$, from $r = r_0$ either the first minimum of $g(r)$ or the first minimum of $G(r)$, with each option producing slightly different results for n. If a sphere with a radius of r_{ij} contains n_{ij} particles, which represent the number of j-type particles around a i-type particle, then

$$n_{ij} = 4\pi\rho x_j \int_{r_0}^{r_{ij}} r^2 g_{ij}(r) dr, \tag{5.34}$$

where r_{ij} corresponds to the location of the first minimum of the associated radial distribution function $G(r) = 4\pi r^2 g_{ij}(r)$ and x_j is the concentration of particles of type j. The formula (5.34) is used to calculate the coordination number in this study [133–135]. The Wanger [136] short range order (SRO) parameter for the first neighbour shell, α, provides a way to quantify the aforementioned ordering patterns,

$$\alpha = 1 - \frac{n_{ij}}{x_j(x_i n_j + x_j n_i)} \qquad (j \neq i = 1, 2) \tag{5.35}$$

where $n_i = n_{ii} + n_{ij}(i, j = 1, 2)$ and x_j represent the concentration of particles of type j. In a sphere with a radius of r_{ij}, there are n_{ij} particles of type j around each i particle. If $\alpha(\alpha > 0)$ is positive, the liquid has a homo-coordinating tendency, meaning that particles of the same type are more likely to be surrounded by atoms of the same kind. However, a negative value of $\alpha(\alpha < 0)$ denotes the opposite, *i.e.* a predisposition toward hetero-coordination. Atoms are distributed at random, therefore, $\alpha = 0$. Similarly, one can also get the experimental coordination number from the RDF, $G(r)$, plugging in the experimental $g(r)$.

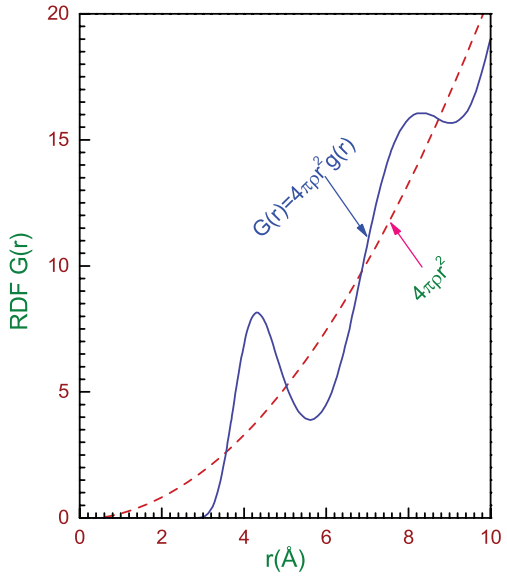

Figure 5.3: Typical curve of the radial distribution function (RDF) and parabolic function ($4\pi r^2\rho$). These are shown in arbitrary unit.

5.2 Dynamic Properties

Time correlation functions among the atomic velocities are used in liquid systems to provide information about various transport features linked to particle mobility and

coupling between the velocity of different particles. These functions must be determined via alternative methods, such as MD simulations, as they cannot be determined empirically. The relative velocity correlation functions (VCFs), $Z_{ij}(t)$, are the main subject of our attention. Numerous dynamic features have been estimated, including single-particle (self-intermediate scattering functions, self dynamic structure factors, velocity autocorrelation function, and mean square displacement) and collective ones (intermediate scattering functions, dynamic structure factors, longitudinal and transverse currents and shear viscosity).

5.3 Single Particle Dynamics

5.3.1 Self-diffusion Coefficient

Diffusion is the process of atomic mass transport which mostly occurs due to the existence of concentration gradient in the system. In such process the kinetic energy is acquired from the interactions with the neighboring atoms. A concentration gradient exists until the diffused substance is evenly distributed. While the self-diffusion coefficient describes the motion of molecules in the same material in the absence of any gradient that could cause mass transfer in the system [137]. Estimation and prediction of diffusivity of substances is of great importance in industrial processes. It finds its application in rating of existing units, designing and developing new units and equipment's and also in research [138]. There are two common methods to calculate the self-diffusion coefficient. The first one is from the positions of particles and the second one is from velocities of particles. The Green-Kubo relation, which

involves integrating the velocity auto correlation function, is a method for determining the self-diffusivity from particle velocities [139]. The locations of the particles are used, however, when calculating the self-diffusion coefficient from the Einstein relation [139]. The velocity auto correlation function (VACF) is one of the prime example of a time dependent correlation function. Understanding the fundamental nature of the dynamical process at work in the molecular system is crucial. The VACF is the measurement how quickly a grain velocity becomes decorrelated with its initial velocity. The normalized VACF is described as

$$Z(t) = \frac{\langle \mathbf{v}\,(0).\mathbf{v}\,(t)\rangle}{\langle v^2\rangle}, \tag{5.36}$$

where $\langle .....\rangle$ denotes the ensemble average and $Z(t)$ represents a projection of the particle's velocity at time t with respect to its original direction of motion. The schematic diagram of the normalized VACF is displayed in Figure 5.4.

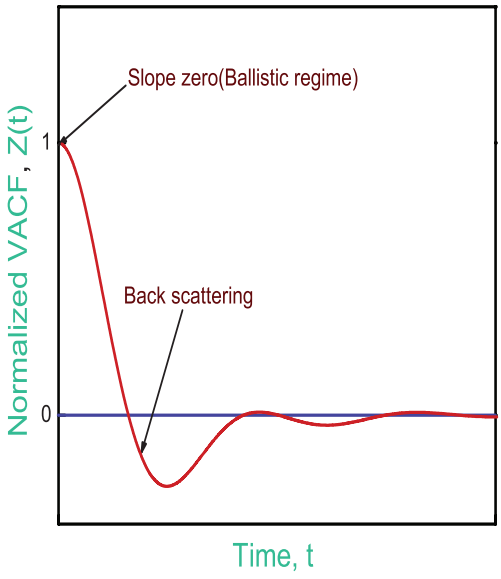

Figure 5.4: Schematic diagram of the normalized VACF of liquid metal near the melting point.

The VACF is a slowly decaying function which is not a simple exponential. The negative value of $Z(t)$ implies a high possibility of significant angle deflections (near 180 °) in colliding particles, which occurs due to cage effects. The cage effect describes how the properties of molecules are affected by the surrounding. In the first region, which occurs ($t \to 0$), the VACF shows slow decay as particles move in free flight. This means the particle velocity remains essentially the same as its initial value. The region $t \to 0$ is called ballistic regime. In the second region, which occurs at short to moderate time, the VACF decays rapidly due to the onset of collisions with surrounding particles. The third region, represents for time $t \to \infty$, the VACF decays to zero, indicating the absence of any residual correlation. The plot of VACF in this area is nearly horizontal, suggesting that the liquid system is being acted upon by relatively weak forces.

5.3.2 Generalized Einstein Relation of Self-diffusion

The self-diffusion coefficient of liquid systems can be calculated by using time-dependent correlation functions referred to as the Einstein relation (ER) [43]. The mean square displacement (MSD) is connected to this relationship. The MSD is a measurement of the typical distance covered by a particle and is defined as

$$\langle \delta r^2(t) \rangle = \langle \mid \mathbf{r}_i(t + t_0) - \mathbf{r}_i(t_0) \mid^2 \rangle. \tag{5.37}$$

The MSD also contains information on the diffusion of particles and may be independent of the t_0 in the thermal equilibrium condition. A typical form of the MSD function is illustrated in Figure 5.5. In liquid system, quadratic behaviour holds only for a very short time interval ($t \to 0$), which is on a par with the average collision

duration. Beyond this time scale, the particle's movement is defined as a random walk, for which the MSD only rises linearly with time.

Consider a collection of N particles having time-dependent position coordinates $\mathbf{r}_i(t)$, where $i = 1, 2, \ldots, N$ and t is the time. The van Hove distribution function $G(\mathbf{r}, t)$ [140], comes after the name of van Hove who characteristics the dynamical structure measured in inelastic neutron scattering experiments.

The real-space dynamical correlation function $G(\mathbf{r}, t)$ is used to describe the spatial and temporal distributions of particle pairs in a fluid. It is possible to generalize time

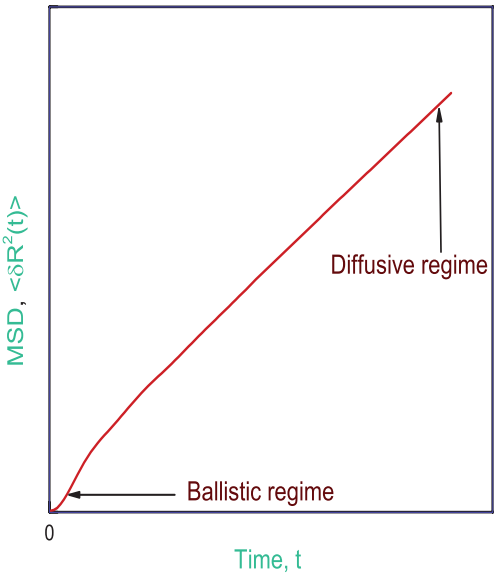

Figure 5.5: Schematic diagram of the MSD function of liquid metals near its melting point.

correlation functions to space and time correlation functions. Take the microscopic number density into consideration

$$\rho(\mathbf{r}, t) = \sum_{i=1}^{N} \delta(\mathbf{r} - \mathbf{r}_i(t)), \tag{5.38}$$

with the average defined as

$$\langle \rho(\mathbf{r},t)\rangle = \lim_{T\to\infty}\frac{1}{T}\int_0^T dt\ \frac{1}{V}\int_v d\mathbf{r}\,\rho(\mathbf{r},t),$$

and stated by

$$\langle \rho(\mathbf{r},t)\rangle = \frac{N}{V} = \rho.$$

Let's create the density-density correlation

$$G(\mathbf{r}'',\mathbf{r}';t'',t_0) = \frac{1}{\rho}\langle \rho(\mathbf{r}'',t'')\rho(\mathbf{r}',t_0)\rangle, \tag{5.39}$$

which generalizes the equilibrium density-density correlation function, which is defined as [44]

$$H(\mathbf{r},\mathbf{r}') = \frac{1}{N}\big\langle \big[\rho(\mathbf{r}') - \langle\rho(\mathbf{r}')\rangle\big]\big[\rho(\mathbf{r}'+\mathbf{r}) - \langle\rho(\mathbf{r}'+\mathbf{r})\rangle\big]\big\rangle. \tag{5.40}$$

For homogenous system at equilibrium equation 5.41 only depends on the time and space differences, $t \equiv t'' - t_0$ and $\mathbf{r} \equiv \mathbf{r}'' - \mathbf{r}'$. Then

$$G(\mathbf{r},t) = \frac{1}{N}\big\langle \sum_{i=1}^{N}\sum_{j=1}^{N}\delta\big(\mathbf{r} + \mathbf{r}_j(t_0) - \mathbf{r}_i(t+t_0)\big)\big\rangle, \tag{5.41}$$

where $\delta(\mathbf{r})$ represents the three-dimensional Dirac delta function. Equation (5.41) is known as the van Hove correlation function (vHCF). Physically, the van Hove function can be interpreted as being proportional to the likelihood that a particle i will be found at location $\mathbf{r}''$ at time t'', whereas the reference particle j was found at position $\mathbf{r}'$ at time t_0.

It is possible to naturally divide the vHCF, $G(\mathbf{r},t)$, into two terms. By distinguishing between the scenarios $i = j$ and $i \neq j$, which are referred to as "self" and

"distinct", respectively. Thus one finds

$$\begin{aligned} G(\mathbf{r},t) &= \frac{1}{N}\langle\sum_{i=1}^{N}\delta(\mathbf{r}+\mathbf{r}_i(t_0)-\mathbf{r}_i(t+t_0)\rangle + \frac{1}{N}\langle\sum_{i\neq j}^{N}\delta(\mathbf{r}+\mathbf{r}_j(t_0)-\mathbf{r}_i(t+t_0))\rangle \\ &= G_s(\mathbf{r},t)+G_d(\mathbf{r},t). \end{aligned} \tag{5.42}$$

The self part, $G_s(\mathbf{r},t)$, explains the average motion of the particle that was initially at the origin, while the distinct part, $G_d(\mathbf{r},t)$, depicts the actions of the remaining N-1 particles. Furthermore, simple liquids are isotropic by nature and hence $G(\mathbf{r},t)$ only be affected by the scalar quantity $\mid \mathbf{r} \mid = r$. In the hydrodynamic limit of long distances and times, the self part of the distribution function $G_s(r,t)$ obeys the equation [141]

$$\frac{\partial}{\partial t}G_s(r,t) = D^s\nabla^2 G_s(r,t), \tag{5.43}$$

where the self-diffusion coefficient is represented by D^s. The solution of equation (5.43) with the Dirac delta initial condition $G_s(r,t_0) = \delta(\mathbf{r})$ is of the Gaussian form [141]

$$G_s(r,t) = (4\pi D^s t)^{-\frac{3}{2}}\exp[-\frac{r^2}{4D^s t}]. \tag{5.44}$$

Therefore, the mean square displacement of a tagged particle over time t is given by

$$\begin{aligned} \langle\delta r^2(t)\rangle &= \langle\mid \mathbf{r}(t+t_0)-\mathbf{r}(t_0)\mid^2 \\ &= \int r^2 G_s(r,t)d\mathbf{r} \\ &= 6D^s t. \end{aligned} \tag{5.45}$$

Taking the limit of $t\to\infty$ such that the ratio $\frac{\langle\delta r^2(t)\rangle}{t}$ becomes constant, one can obtain the self-diffusion coefficient as

$$D^s = \lim_{t\to\infty}\frac{\langle\delta r^2(t)\rangle}{6t} = \lim_{t\to\infty}\frac{1}{6t}\langle\mid \mathbf{r}_i(t)-\mathbf{r}_i(0)\mid^2\rangle = \lim_{t\to\infty}\frac{1}{6t}\Delta_{MSD}(t). \tag{5.46}$$

This equation is the well known Einstein relation for self-diffusion coefficient.

5.3.3 Green-Kubo Relation of Self-diffusion

The Green-Kubo (G-K) relation is the another technique to calculate the self-diffusion coefficient from the time-dependent correlation functions [44]. If $\mathbf{v}(t)$ represents the particle's velocity at any arbitrarily chosen time t, one obtains

$$\delta\mathbf{r}\,(t) = \int_0^t \mathbf{v}\,(t')dt'. \tag{5.47}$$

By squaring and averaging equation (5.47) over time origins gives

$$\begin{aligned} \langle \delta r^2 \rangle &= \int_0^t dt'' \int_0^t dt' \langle \mathbf{v}\,(t').\mathbf{v}\,(t'') \rangle \\ &= 2\int_0^t dt'' \int_0^{t''} dt' \langle \mathbf{v}\,(t').\mathbf{v}\,(t'') \rangle. \end{aligned} \tag{5.48}$$

The factor 2 in equation (5.48) appears due to the symmetric property of the integrand in time t' and t''. The velocity auto correlation function $\langle \mathbf{v}\,(t').\mathbf{v}\,(t'') \rangle$ based on the disparity in time. By introducing $\tau = t'' - t'$ one may write equation (5.48) as [139]

$$\begin{aligned} \langle \delta r^2 \rangle &= 2\int_0^t dt'' \int_0^{t''} d\tau \big\langle \mathbf{v}\,(\tau).\mathbf{v}\,(0) \big\rangle \\ &= 2\int_0^t d\tau \big\langle \mathbf{v}\,(\tau).\mathbf{v}\,(0) \big\rangle \int_\tau^t dt'' \\ &= 2\int_0^t d\tau \langle \mathbf{v}\,(\tau).\mathbf{v}\,(0) \rangle (t-\tau) \\ \text{or, } \frac{\langle \delta r^2 \rangle}{2t} &= \int_0^t d\tau \langle \mathbf{v}\,(0).\mathbf{v}\,(\tau) \rangle (1 - \frac{\tau}{t}) \end{aligned} \tag{5.49}$$

Taking the long-time limit, we find

$$\lim_{t\to\infty} \frac{\langle \delta r^2 \rangle}{2t} = \int_0^\infty d\tau \langle \mathbf{v}\,(0).\mathbf{v}\,(\tau) \rangle. \tag{5.50}$$

Using equation (5.46) we may arrive at

$$D^s = \frac{1}{3}\int_0^\infty dt \langle \mathbf{v}\,(0).\mathbf{v}\,(t) \rangle. \tag{5.51}$$

Using equation (5.36) one finds

$$D^s = \frac{k_B T}{m} \int_0^\infty Z(t) dt. \tag{5.52}$$

In equation (5.52), the factor $\frac{k_B T}{m}$ is derived from the particle's average kinetic energy [141] as follows

$$\frac{1}{2} m \langle \mid v \mid^2 \rangle = \frac{3}{2} k_B T. \tag{5.53}$$

The Green-Kubo formula and the Einstein relation are identical theories. They are very important theories for liquid state. The Einstein relation and Green-Kubo formula are often known as MSD and VACF methods, respectively. Many theories are suggested to describe the transport phenomena namely the mass, momentum or energy transfer in simple dense fluids. None of these theories are capable to predict exact result. Alongside with the theoretical values of self-diffusion coefficients we have a little experimental data available in the literature at different thermodynamic states. Therefore, MD simulation has become an useful method for studying self-diffusion coefficients of real fluids composed of relatively simple molecules [138]. In this instance we have calculated the self-diffusion coefficients of liquid systems from $Z(t)$ and $\langle \delta r^2(t) \rangle$ through the Green-Kubo and Einstein relations, respectively. It is worth noting that $Z(t)$ and $\langle \delta r^2(t) \rangle$ are obtained from OF-AIMD simulation method in the present work.

5.3.4 Stokes-Einstein Relation

The Stokes-Einstein (SE) relation connects the self-diffusion coefficient, D, shear viscosity, η, and effective hard sphere diameter of the particle, d, *i.e.* the location of

the first peak of the PDF [43, 44, 130]

$$D = \frac{k_B T}{C\pi\eta d}, \tag{5.54}$$

where C is a constant that is dependent on the flow's boundary conditions and k_B is the Boltzmann constant. This relationship was first presented to explain the diffusive motion of a big Brownian particle in a continuous fluid with shear viscosity, η. The stick boundary condition ensures that the fluid velocity at the surface matches the particle velocity, and in this instance, $C = 3$. In contrast, the slip boundary condition causes a non-tangential force to act on the sphere, setting the normal component of the fluid velocity equal to the normal component of the particle velocity. In this instance, $C = 2$ is found. The SE relation was solely obtained from macroscopic factors. Surprisingly, it has been discovered to function effectively at the atomic level in simple liquids. If the slip boundary condition is applied, the values of the effective hard sphere diameter, d that are more logically calculated can be discovered.

5.3.5 Diffusion Coefficients for Alloys

The time correlation functions among the atomic velocities provide information about several transport features in liquid systems, including the mobility of the particles and the coupling between the velocities of different particles. It is necessary to use alternative methods, such as MD simulations, because this functions cannot be determined empirically. We are primarily interested in relative velocity correlation functions (VCFs), also known as $Z_{ij}(t)$, which are defined as the time correlation function of the relative velocity of the center of mass of species i with respect to the center of

mass of species j [34,35] *i.e.*,

$$Z_{ij}(t) = \frac{1}{3} x_i x_j N \langle [\mathbf{v}_i(t) - \mathbf{v}_j(t)].[\mathbf{v}_0 - \mathbf{v}_j(0)] \rangle, \tag{5.55}$$

where, $\mathbf{v}_i(t)$ denotes the mean molecular velocity of the ith component and N represents the total number of particles,

$$\mathbf{v}_i(t) = \frac{1}{N_i} \sum_{l(i)=1}^{N_i} \mathbf{v}_{l(i)}(t), \tag{5.56}$$

The total number of i-type particles is N_i, and the velocity of the i-type particle is $\mathbf{v}_{l(i)}(t)$. Separating the $Z_{ij}(t)$ into self-contributions ($Z^0_{ij}(t)$) and distinct contributions ($Z^d_{ij}(t)$) as follows

$$Z_{ij}(t) = (1 - \delta_{ij}) Z^0_{ij}(t) + x_i x_j Z^d_{ij}(t), \tag{5.57}$$

where, the Kronecker's delta is δ_{ij}, $Z^0_{ij}(t) = x_j Z^s_i(t) + x_i Z^s_j(t)$, $Z^s_i(t)$ being the velocity autocorrelation function of a i-type particle that has been placed in the fluid, and $Z^d_{ij}(t)$ accounts for the contribution of the distinct velocity correlations.

The associated diffusion coefficients, D_{ij}, D^0_{ij}, D^d_{ij} and D^s_i, are obtained from the time integrals of $Z_{ij}(t)$, $Z^0_{ij}(t)$, $Z^d_{ij}(t)$ and $Z^s_i(t)$, where D^s_i is the common self-diffusion coefficient. We can write binary mixes as

$$D_{12} = D^0_{12} + x_1 x_2 D^d_{12} \equiv D^0_{12}(1 + \gamma_{12}), \tag{5.58}$$

When all species are identical, $\gamma_{12} = 0$, and $D^0_{12} = x_2 D^s_1 + x_1 D^s_2$, γ_{12} is a measure of the deviation from a perfect mixing. The interdiffusion coefficient is expressed using the following formalism:

$$D_{int} = \theta D_{12} = \theta(1 + \gamma_{12}) D^0_{12}, \tag{5.59}$$

where, $\theta = \frac{x_1 x_2}{S_{CC}(q \to 0)}$. For a composition that comes close to being optimal $\theta \approx 1$, $\gamma_{12} \approx 0$ and, consequently, $D_{int} \approx D^0_{12}$.

5.3.6 Self-intermediate Scattering Function

The self intermediate scattering function (SISF), $F_s(\mathbf{q},t)$, is one of the most basic time-dependent quantities. The probability that a tagged particle has travelled a specific distance from its original position at time t is given by the expression $F_s(\mathbf{q},t)$. As a result, the most comprehensive data regarding the motion of a single particle is provided by the SISF. This refers to the dynamics of a single particle at various length scales, from the hydrodynamic limit to the limit of free particles. Area under $F_s(\mathbf{q},t)$ can be used to define a relaxation time τ. The dynamical variable for i-th particle reads as

$$\rho_{s,i}(\mathbf{R},t) = \delta(\mathbf{R} - \mathbf{R}_i(t)), \tag{5.60}$$

which is usually referred to as the i-th single-particle (or self-) density at time t and location $\mathbf{R}$. The interpretation of $\rho_{s,i}(\mathbf{R},t)$ as a 'density' comes from the integration of equation (5.60) over the full range of $\mathbf{R}$. We write the normalization condition as

$$\int \rho_{s,i}(\mathbf{R},t)\, d\mathbf{R} = 1, \tag{5.61}$$

which simply states that the tagged particle certainly be counted somewhere in the volume V at any time [43]. As is clear from its definition, $\rho_{s,i}(\mathbf{R},t)$ is expected to change dramatically depending on t and $\mathbf{R}$. The gross measure of this variable is provided by its statistical average that yields [43]

$$\langle \rho_{s,i}(\mathbf{R},t) \rangle = \langle \rho_{s,i}(\mathbf{R},t_0) \rangle = \frac{1}{V}, \tag{5.62}$$

which is consistent with the previous interpretation of $\rho_{s,i}(\mathbf{R},t)$ as a number density. The space Fourier transformation of the i-th self-density is

$$\rho_{s,i}(\mathbf{q},t) = \int d\mathbf{R} e^{-i\mathbf{q}.\mathbf{R}} \rho_{s,i}(\mathbf{R},t) = e^{-i\mathbf{q}.\mathbf{R}_i(t)}. \tag{5.63}$$

We have calculated $F_s(q,t)$ from the the particles positions. The time correlation associated with $\rho_{s,i}(\mathbf{R},t)$ is usually referred to as the self intermediate scattering function and is characterized as [43, 44, 52]

$$\begin{aligned} F_s(\mathbf{q},t) &= \langle \rho_{s,i}(\mathbf{q},t+t_0)\rho^*_{s,i}(\mathbf{q},t_0) \\ &= \frac{1}{N}\Big\langle \sum_{i=1}^{N} e^{-i\mathbf{q}.\mathbf{R}_i(t+t_0)} e^{i\mathbf{q}.\mathbf{R}_i(t_0)} \Big\rangle, \end{aligned} \tag{5.64}$$

where N denotes the total number of particles, $\mathbf{R}_i(t)$ denotes the location of the i-th particle at time t, and $\langle ... \rangle$ is the average over time origins and wave vectors with the same modulus. Equation (5.64) has been used in OF-AIMD simulation for calculating self intermediate scattering functions. The present work is concerned with isotropic

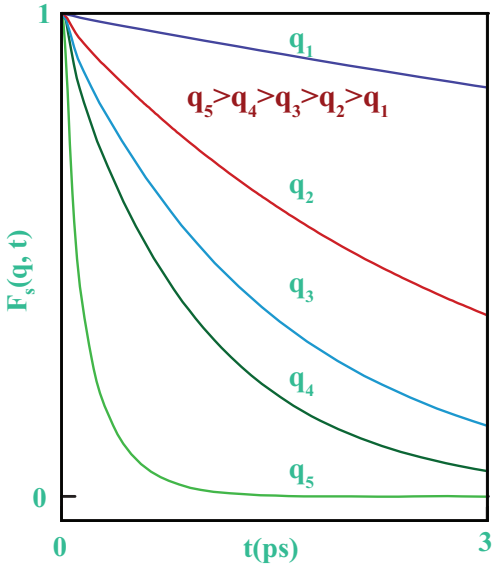

Figure 5.6: Schematic diagram of the SISF in the liquid state.

systems only, for which the self intermediate scattering function depends only on the values q of $\mathbf{q}$. Alternatively, $F_s(q,t)$ can be calculated by taking the Fourier

transformation of the self part of vHCF, $G_s(R,t)$ defined as

$$F_s(q,t) = \int d\mathbf{R}\, \exp\left[-i\mathbf{q}.\mathbf{R}\right] G_s(\mathbf{R},t). \tag{5.65}$$

This method, however, has the disadvantage to involve Fourier transformation artefacts due to the limited size of our simulation box. The general behaviour of $F_s(q,t)$ is shown schematically in Figure 5.6. $F_s(q,0) = 1$, due to the facts that the tagged molecule is localized to the origin at time t=0. As time evolves and the molecule begins to move away from its initial position, $F_s(q,t)$ decreases in a smooth manner. The decay rate seems to be increased with q, indicating that the short-wavelength fluctuations die out much more rapidly [130]. The self-intermediate function and the self diffusion coefficient, which is also referred to as the self intermediate scattering function's Gaussian approximation, have an intriguing relationship. A Gaussian function of R can be used to represent the self part of the van Hove function $G_s(\mathbf{R},t)$, which is represented as [44, 142]

$$\begin{aligned} G_s(\mathbf{R},t) &= \frac{1}{\sqrt{4\pi D\, t}} \exp\left[-\frac{R^2}{4Dt}\right] \\ &= \frac{1}{(2\pi)^3} \int d\mathbf{q} e^{-Dq^2 t} e^{i\mathbf{q}.\mathbf{R}}, \end{aligned} \tag{5.66}$$

where, D is the self-diffusion coefficient. By using equation (5.66), one can read from equation (5.65)

$$\begin{aligned} F_s(q,t) &= \exp\left[-q^2 Dt\right] \\ &= \exp\left[\frac{-\langle \delta R^2(t)\rangle q^2}{6}\right]. \end{aligned} \tag{5.67}$$

It represents a popular Gaussian approximation for $F_s(q,t)$. The $F_s(q,t)$ obtained from the Gaussian approximation agrees well with that directly calculated from the

molecular dynamics simulations for both small and large wave vectors. This approximation agrees quite well with simulated $F_s(q,t)$ for $q \to 0$. This implies that the self diffusion coefficient regulates the self-intermediate scattering function. In the liquid range, the discrepancies between them are found to be rather small, and mainly occur in the intermediate range of times and wave vectors as expected [43]. Even, on the basis of these direct comparisons the overall results predicted by the Gaussian ansatz are quite acceptable. As expected, the main shortcomings are found to occur at the intermediate wave vectors, where the deviations may even rises up to about 20% [43].

5.4 Collective Dynamics

5.4.1 Intermediate Scattering Function and Dynamic Structure Factor

The particles density at time t at a point $\mathbf{R}$ is defined as equation (5.38) and in the collective case with Fourier components defined as

$$\rho_{\mathbf{q}}(t) = \sum_{i=1}^{N} e^{-i\mathbf{q}.\mathbf{R}_i(t)}. \tag{5.68}$$

An example of a density autocorrelation function is the intermediate scattering function (ISF), which is denoted by $F(\mathbf{q},t)$. This gives information on the overall dynamics of density variations on both long and short-term time scales. Due to the isotropy of the system under investigation, $F(\mathbf{q},t)$ only depends on the magnitude of the $\mathbf{q}$ parameter and not its direction. As a result, the function $F(\mathbf{q},t)$ depends entirely on the wavenumbers $q = \mid \mathbf{q} \mid$ and time t.

We have directly calculated the ISF, $F(q,t)$, using the atomic trajectories in the current OF-AIMD simulation. It's described as [43, 44, 52]

$$\begin{aligned} F(q,t) &= \frac{1}{N}\langle \rho_{\mathbf{q}}(t+t_0)\rho_{-\mathbf{q}}(t_0)\rangle \\ &= \frac{1}{N}\Big\langle \Big(\sum_{i=1}^{N} e^{-i\mathbf{q}.\mathbf{R}_i(t+t_0)}\Big)\Big(\sum_{j=1}^{N} e^{i\mathbf{q}.\mathbf{R}_j(t_0)}\Big)\Big\rangle, \end{aligned} \tag{5.69}$$

where N denotes the overall particle count and $\mathbf{R}_j(t)$ denotes the location of the j-th particle at time t. Instead of direct computation, one can determine $F(q,t)$ by applying the Fourier transformation (FT) of the vHCF generated in MD simulation, *i.e.*

$$F(q,t) = \int d\mathbf{R}\, \exp[-i\mathbf{q}.\mathbf{R}]\, G(\mathbf{R},t). \tag{5.70}$$

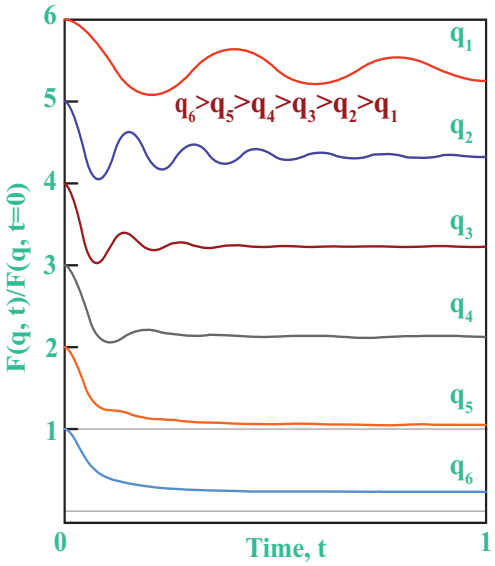

Figure 5.7: Schematic diagram of the ISF of liquid metal near the melting point.

Accuracy of $F(q,t)$ acquired from FT is less than that obtained from direct calculation of $F(q,t)$. This is as a result of the mathematical complexity of FT. The quantity

$F(q,t)$ is readily available in light and neutron-scattering investigations [44]. A typical behaviour of $F(q,t)$ for liquid metal is shown in Figure 5.7.

Fluctuations of $F(q,t)$ implies dynamical heterogeneities. $F(q,t)$ exhibits oscillatory behaviour, with the oscillations' amplitudes increasing with decreasing q values for liquid metals near melting points [43]. The liquid is unable to support any collective excitation as q rises and the length scale $\frac{2\pi}{q}$ gets ever-more microscopic, therefore $F(q,t)$ should decrease monotonically [43]. The term "de Gennes narrowing" refers to the gradual deterioration of $F(q,t)$ at $q \approx q_p$, which is brought on by the strong spatial correlations that arise at those q values close to q_p [43]. $F(q,t)$ decays more slowly in the limit $q \to 0$ than the self intermediate scattering function, $F_s(q,t)$. when q is large, the intermediate scattering function, $F(q,t) \to F_s(q,t)$ [130].

The dynamic structure factor (DSF), a mathematical function, provides details on the temporal evolution of inter-particle interactions. The intermediate scattering function $F(q,t)$ is connected to the DSF. It is described by the Fourier transform of the $F(q,t)$ into the frequency domain with the addition of an appropriate window to eliminate the effects of truncation as

$$S(q,\omega) = \frac{1}{2\pi}\int_{-\infty}^{\infty} F(q,t)\exp[-i\omega t]dt. \tag{5.71}$$

This technique has been used to evaluate the dynamic structure factor in the current OF-AIMD simulation. The DSF represents thermal fluctuations in a material that are relevant for experiments because they are correlated with the intensity of scattered neutrons in inelastic neutron scattering (INS) or the inelastic X-ray scattering (IXS). It is important to note that the dynamic structure factor will be even in ω since $F(q,t)$ is a true function that is even in t.

The DSF exhibits well defined side peaks for lower values of q and exist up to $q \approx q_p$, where the major peak of the function $S(q)$ is represented by q_p. The presence of clearly defined side peaks suggests collective density excitation, and after nearly $q > q_p$, the side peak of $S(q,\omega)$ looks to be a shoulder rather than a peak and then monotonically diminishes at large q values. Eventually, at the largest value of q where $S(q) \approx 1$, $S(q,\omega)$ approaches the 'self' spectrum $S_s(q,\omega)$ [43]. An estimation of the dispersion relation can be made from the locations of the side peaks of the function $S(q,\omega)$, and the adiabatic sound velocity can be calculated from the slope of the dispersion curve at the value of $q \to 0$. The ISF and therefore the DSF, is more challenging to compute than static properties like $g(r)$ and $S(q)$. Because the static

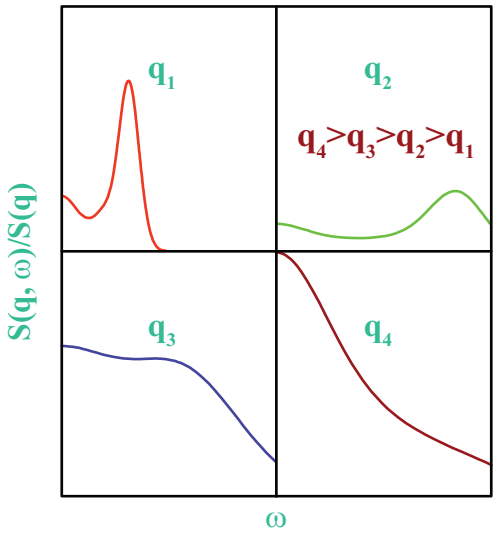

Figure 5.8: Schematic diagram of the normalized DSF of liquid metal near the melting point.

properties are defined as an ensemble average of a dynamical variable at certain time, whereas the ISF involves the ensemble average at two different times. The general behaviour of the normalized DSF is illustrated in Figure 5.8.

5.4.2 Viscosity

Viscosity gives the measurement of resistance to flow [143]. Viscosity is the result of internal friction between two adjacent layers that occurs when they slide past one another and each applies a frictional resistive force to the other. The system's reaction to a shearing force is used in non-equilibrium molecular dynamics to calculate the shear viscosity, η. However, in the context of AIMD, equilibrium methods are desirable since they maintain the opportunity to calculate all other physical parameters within the same simulation. In the context of equilibrium simulations, a common method of obtaining η is by the Green-Kubo formalism, which involves the temporal integration of the stress autocorrelation function generated from the off-diagonal component of the stress tensor [144]. The current work incorporates a different approach based on the transverse time correlation function $J_t(q,t)$. It has the benefit of producing a generalized q-dependent viscosity, which allows for the detection of the hydrodynamic regime and the evaluation of the finite size effect [144]. Figure (5.9) roughly depicts the basic behaviour of $J_t(q,t)$. The directorial parameter

$$\mathbf{j}(q,t) = \sum_{j=1}^{N} \mathbf{v}_j(t) e^{i\mathbf{q}.\mathbf{R}_j(t)}, \tag{5.72}$$

is referred to as the current density linked to the total motion of the particles. A possible division of the current density is

$$\mathbf{j}(q,t) = \mathbf{j}_l(q,t) + \mathbf{j}_t(q,t), \tag{5.73}$$

where, respectively, $\mathbf{j}_l(q,t)$ and $\mathbf{j}_t(q,t)$ denote the longitudinal component parallel to $\mathbf{q}$ and the transverse component perpendicular to $\mathbf{q}$.

Let us assume that waves are propagating in the z-direction. When the particle

motion (velocity) and wave propagation (direction) are parallel to one another, longitudinal current results. Contrarily, transverse current occurs when the direction of the particle motion is perpendicular to the direction of the wave propagation [43].

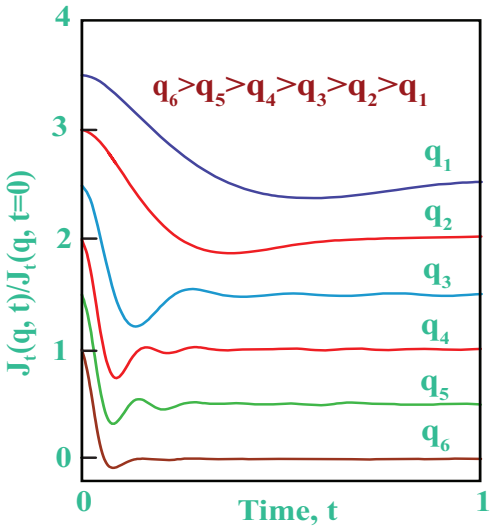

Figure 5.9: Schematic diagram of the transverse time correlation function, $J_t(q,t)$ near melting point.

The current correlation functions for the longitudinal and transverse directions, $J_l(q,t)$ and $J_t(q,t)$, respectively, are defined as

$$J_t(q,t) = \frac{1}{2N}\langle \mathbf{j}_t{}^*(q,0).\mathbf{j}_t(q,t)\rangle \tag{5.74}$$

and

$$J_l(q,t) = \frac{1}{N}\langle \mathbf{j}_l{}^*(q,0).\mathbf{j}_l(q,t)\rangle. \tag{5.75}$$

A dynamical magnitude worth exploring is the transverse current time correlation function, or $J_t(q,t)$. Only computer simulations may be used to determine it because it is not connected to any quantifiable quantity. Regarding the shear modes, it provides information.

The shear viscosity coefficient, η, can be expressed in terms of a simple Green-Kubo integral

$$\begin{aligned} \eta &= \frac{1}{k_B T V}\int_0^\infty dt\,\langle\sigma^{zx}(0)\sigma^{zx}(t)\rangle \\ &= \int_0^\infty \eta(t)dt. \end{aligned} \tag{5.76}$$

The quantity $\eta(t) = \eta(q \to 0, t) = \frac{1}{k_B T V}\langle\sigma^{zx}(0)\sigma^{zx}(t)\rangle$, often referred to as the transverse (or shear) stress autocorrelation function [43] with

$$\sigma^{zx} = \sum_{i=1}^{N}\big[m v_{i,z} v_{i,x} - \frac{1}{2}\sum_{i,j\neq i}^{N}\big(\frac{z_{ij}x_{ij}}{r_{ij}}\big)\phi'(r_{ij})\big], \tag{5.77}$$

where, the z-component of a particle's velocity at time t is denoted by the symbol $v_{i,z}$ and $x_{ij} =\mid x_i - x_j \mid$.

The hydrodynamic method for computing the shear viscosity is based on the transverse part of the linearised Naviér-Stokes equation. This formula can be expressed as [130]

$$\frac{\partial}{\partial t}J_t(q,t) = -\frac{q^2\eta}{\rho m}J_t(q,t), \tag{5.78}$$

the time-dependent transverse current correlation function being described as

$$J_t(q,t) = \frac{1}{N}\langle \mathbf{j}_x{}^*(q,0).\mathbf{j}_x(q,t)\rangle, \tag{5.79}$$

and wave number q. The transverse current correlation function's $J_t(q,t)$ short-time characteristics are given by the expression [43]

$$J_t(q,0) = \frac{k_B T}{m} = \frac{1}{\beta m}. \tag{5.80}$$

From equation (5.78), one obtains an exponential decay for the transverse current

correlation function

$$\begin{aligned} J_t(q,t) &= J_t(q,0)\exp\big[-\frac{\eta}{m\rho}q^2 \mid t \mid\big] \\ &= \frac{1}{\beta m}\exp\big[-\frac{\eta}{m\rho}q^2 \mid t \mid\big]. \end{aligned} \tag{5.81}$$

The solution of

$$\frac{\partial}{\partial t}J_t(q\to 0,t) = -\frac{\eta q^2}{\rho m}J_t(q\to 0,t), \tag{5.82}$$

Which arises when the transverse current correlation function reaches a Markovian situation [43] with the hydrodynamic result defined as equation (5.81), gives the ordinary shear viscosity η. Thus we get

$$J_t(q\to 0,t) = \frac{1}{\beta m}\exp\big(-q^2\frac{\eta \mid t \mid}{\rho m}\big), \tag{5.83}$$

where the shear viscosity coefficient η is described as equation (5.76). As a result, for the free-particle limit ($q\to\infty$), $J_t(q,t)$ evolves from a Gaussian in both q and t to a Gaussian in q and an exponential in t for the hydrodynamic limit ($q\to 0$). Because it may oscillate and signal the propagation of shear waves for intermediate values of q, $J_t(q,t)$ displays complex behaviour. The shear viscosity coefficient, η, can be easily determined from the data for $J_t(q,t)$ [43]. On the other hand, the memory function representation of $J_t(q,t)$ is

$$\tilde{J}_t(q,z) = \frac{1}{\beta m}\big[z+\frac{q^2}{\rho m}\tilde{\eta}(q,z)\big]^{-1}, \tag{5.84}$$

where the tilde, which stands for the Laplace transform, adds the generalized shear viscosity coefficient $\tilde{\eta}(q,z)$. Since $\beta m\tilde{J}_t(q,z=0)$ is obtained from the region under the normalized $J_t(q,t)$, values for

$$\tilde{\eta}(q,z=0) = \frac{\rho m}{q^2\beta m\tilde{J}_t(q,z=0)}, \tag{5.85}$$

can be acquired, and the limit $q \to 0$ is used to estimate the shear viscosity coefficient η. This is accomplished by extrapolating the fact that the inversion is the system's symmetry, which enables to approximately [145]

$$\tilde{\eta}(q) = \eta(1 - \alpha q^2). \tag{5.86}$$

The time Fourier transform of the transverse current spectrum, $J_t(q, \omega)$, is given by the equation:

$$J_t(q, \omega) = \frac{1}{2\pi} \int_{-\infty}^{\infty} J_t(q, t) \exp[-i\omega t]. \tag{5.87}$$

The $J_t(q, \omega)$ displays peaks in a particular q-range that are associated with shear waves which are propagating.

Chapter 6

Results and Discussion

6.1 Introduction

We have performed OF-AIMD simulation for Na_xK_{1-x} liquid binary alloys for different concentration at thermodynamic states little above their melting points. All alloys of Na_xK_{1-x} remain in liquid phase at 373 K. We have considered 2000 particles in the present simulation. The size of the cubic periodic cell for simulation is determined by the corresponding atomic number density of the systems at the given thermodynamic state. For a given ionic position at time t the electronic energy functional is minimized with respect to electronic density $\rho(\mathbf{r})$, which is provided by an orbital $\psi(\mathbf{r})$. Here, the number density is defined as $\rho(\mathbf{r}) = |\psi(\mathbf{r})|^2$. An orbital in the OF-AIMD is expanded by a plane wave basis set, truncation of which is determined by a cutoff energy E_{cut}. We have taken the cutoff energy equal to 18.0 Rydberg's for all the systems at different concentrations. The values of the parameters core radius R_c, amplitude A and the softness parameter a that are used in the calculation of electron-ion

interaction are given in Table 6.1. It is known that according to the Coulomb's law the charge-charge interaction energy varies as r^{-1}. But actual potential, V, differs from the original Coulomb's law due to interference of image charges. That is due to chemical and physical interactions. This part is known as the non-Coulombic part of interaction. Figure 6.1, illustrates the non-Coulombic part of the momentum space for the components of liquid Na_xK_{1-x} alloys at different concentrations. The inset of

Table 6.1: The pseudopotential parameters, number density for single component system and alloys, temperature and concentrations used in the simulation. The densities are taken from Waseda [133].

Temp. (K)	Con. (x)	No. density ($Å^{-3}$)			*Rc* (a.u.)		*A* (a.u.)		*a* (a.u.)	
		ρ_1	ρ_2	ρ	Rc_1	Rc_2	A_1	A_2	a_1	a_2
T=373	0.1			0.013246	1.59	2.50	0.30	0.030		
	0.2			0.013949	1.59	2.50	0.13	0.015		
	0.3			0.014732	1.64	2.59	0.35	0.040		
	0.4			0.015608	1.59	2.50	0.30	0.030		
	0.5	0.0243	0.0126	0.016594	1.59	2.50	0.35	0.040	1.0	0.5
	0.6			0.017714	1.59	2.50	0.13	0.015		
	0.7			0.018995	1.68	2.59	0.65	0.070		
	0.8			0.020476	1.59	2.50	0.30	0.030		
	0.9			0.022208	1.59	2.50	0.30	0.030		

the Figure shows the magnified display of the Friedel oscillation at different concentrations. The nature of the phase of the Friedel oscillation is found to be similar for all concentrations. It is also found that the oscillatory behaviour occurs at $q > 3.66$ a.u^{-1}for Na and $q > 2.46$ a.u^{-1} for K. We note here that two separate parameter sets are used to calculate the electron-ion interactions for Na and K. These sets allow us to calculate the non-Coulombic part of interactions for individual elements.

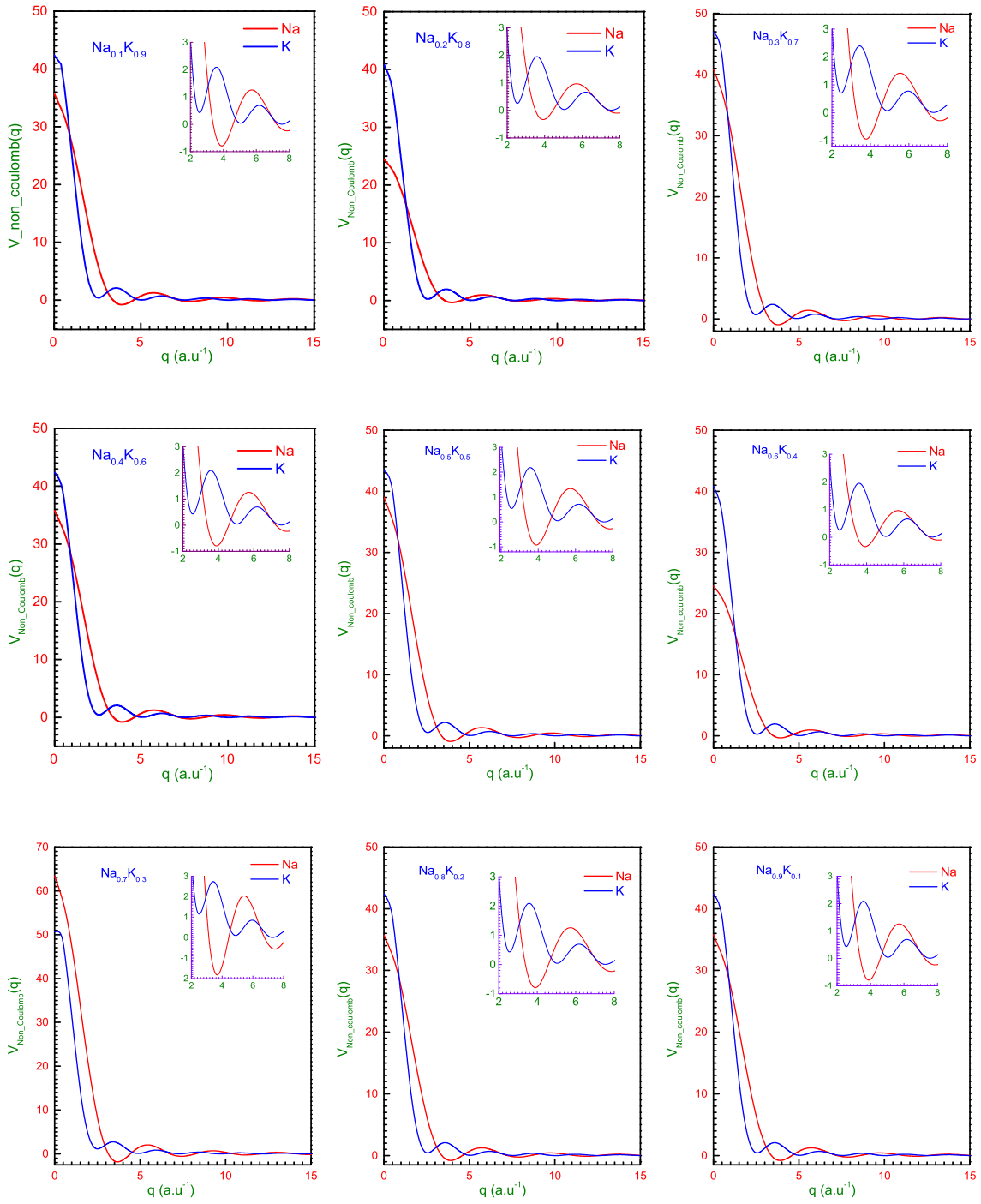

Figure 6.1: Non-Coulombic contribution of the electron-ion potential for the components of Na_xK_{1-x} liquid binary alloys at concentrations, $x_{Na} = 0.1$, 0.2, 0.3, 0.4, 0.5, 0.6, 0.7, 0.8 and 0.9. The inset shows the magnified oscillations.

The minimization of the electronic energy with respect to the Fourier coefficients of expansion is performed at every ionic time step using the quenching method which gives the electron density and energy at the ground state. The ionic forces are essential ingredients to perform the molecular dynamics simulations. These forces are derived from the ground state electronic energy by employing the Hellmann-Feynman theorem [62,63]. The ionic motion specified by the position and velocity are regularly updated at each time step by solving the Newton's equations of motion (NEM). Here, the Verlet Leap-frog algorithm (VLFA) have been used with a finite time step. We have taken finite time step 6×10^{-3} ps for Na_xK_{1-x} binary alloy systems at every concentrations to give a better description of liquid structure. After equillibration, we have performed the calculation for physical properties by averaging over 5000 ionic configurations for the liquid binary systems under study.

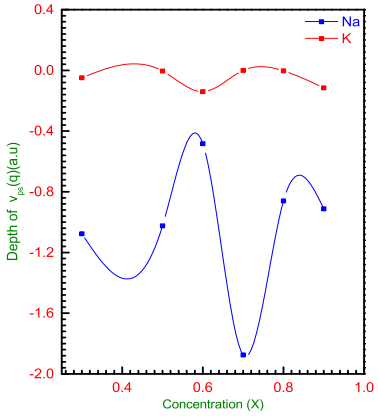

Figure 6.2: Depth of the non-Coulombic contribution of the pseudopotentials for the system under study.

Minimum values of non-Coulombic part for Na and K as a function of x are presented in Figure 6.2. It is noticed that the depth of the V_{ps} versus x curve appears to be oscillatory in nature. For Na amplitude of oscillation is large and for K the amplitude is small. Figure 6.2 also reviews that the pseudopotential for Na shows attractive in

nature for whole concentration range although there is a fluctuations. On the other hand pseudopotential for K exhibits repulsive nature in some concentrations. But one interesting feature is that the maximum of the oscillations for Na and minimum oscillation of K are exhibited at the same concentration. At this stage it is difficult to explain the cause of this fact.

6.2 Structural Properties of *l*-Na_xK_{1-x} Binary Alloys

6.2.1 Pair Correlation Function and Coordination Number

The OF-AIMD simulations allow us to direct evaluation of the partial pair correlation functions (PPCF), $g_{ij}(r)$, and also the corresponding partial AL static structure factors $S_{ij}(q)$. Figure 6.3, shows the $g_{ij}(r)$ calculated by the OF-AIMD method for the liquid Na_xK_{1-x} binary alloys for all nine different concentrations. The major peak height, location, and subsequent oscillations of the $g_{NaK}(r)$ exhibits a behaviour distinct from that of the other two partials. They lie in between those correspond to $g_{NaNa}(r)$ and $g_{KK}(r)$ pairs. It is seen that for $x_{Na} \leq 0.6$, the principal peak of $g_{NaNa}(r)$ is significantly higher than the primary peaks of $g_{NaK}(r)$ or $g_{KK}(r)$. On the other hand, for $x_{Na} = 0.7$, the height of the main peaks of these two ($g_{NaNa}(r)$, $g_{KK}(r)$) are comparable. For concentration, $x_{Na} = 0.8, 0.9$ the situation reverses; *i.e.* the peak of $g_{KK}(r)$ becomes the highest. This behaviour points to the existence of homo-coordinating tendencies, which means the first coordination shell also contain the other species of atoms. The existence of aforementioned ordering tendencies are further examined by calculating the Wagner's [136] short range order (SRO) parameter, α, for the first

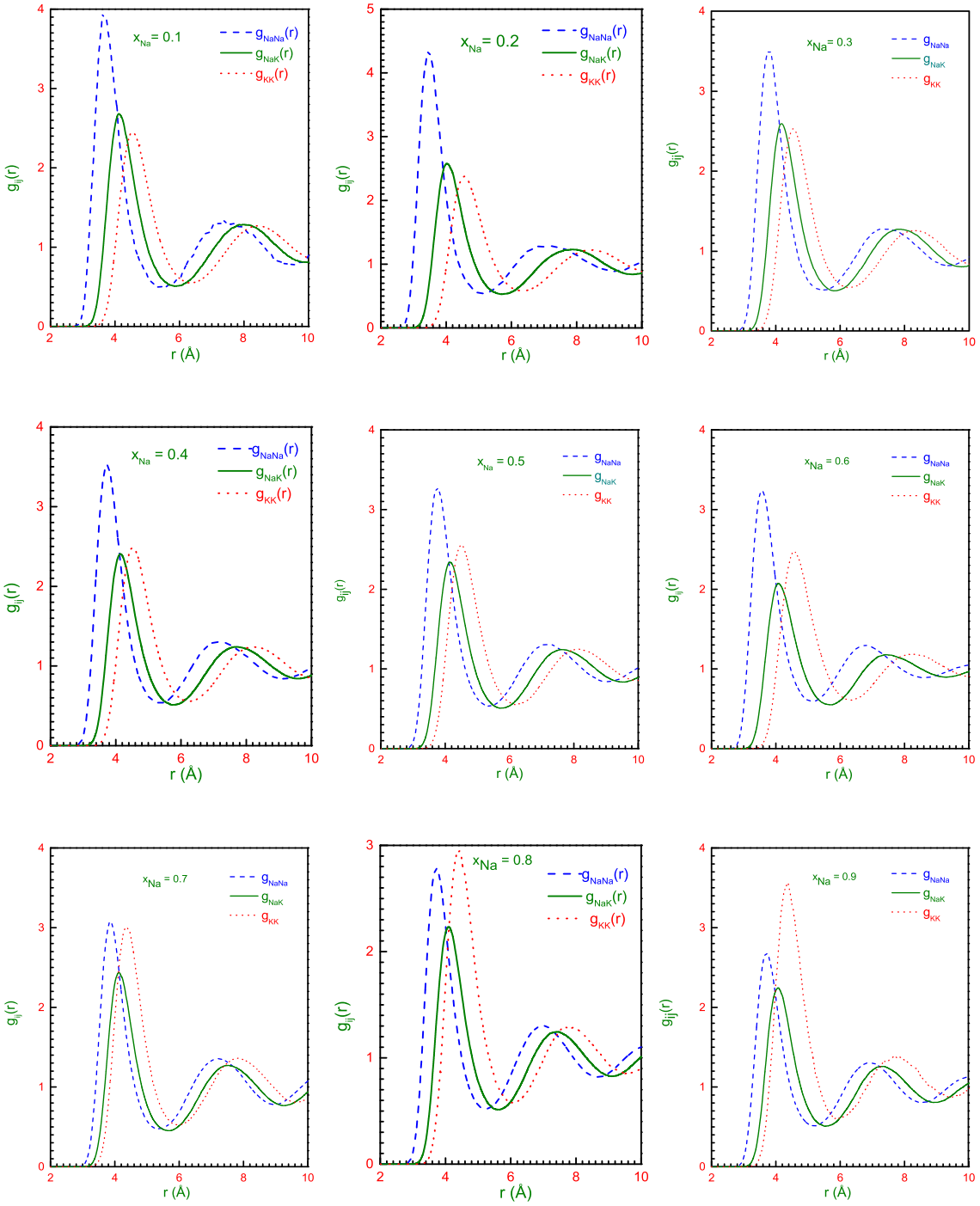

Figure 6.3: Partial pair correlation functions, $g_{\mathrm{ij}}(r)$, for alloys of l-$\mathrm{Na}_x\mathrm{K}_{1-x}$ for all nine concentrations, $x_{\mathrm{Na}} = 0.1$ to 0.9. The blue, olive and orange colours are for $g_{\mathrm{NaNa}}(r)$, $g_{\mathrm{NaK}}(r)$ and $g_{\mathrm{KK}}(r)$, respectively.

neighbour shell, and n_{ij}, the particles number of j-type present around an i-type particles located within a sphere of radius r_{ij}. Note that n_{ij} have been calculated [146–148] from the knowledge of partial pair correlation functions, $g_{ij}(r)$, by performing integration over the radial distribution function (RDF), $4\pi r^2 g_{ij}(r)$ multiplied by density with an upper limit where the position of the first minimum of RDF, r_{ij}, occurs. In Figure 6.3, we have displayed the partial pair correlation functions, $g_{ij}(r)$, for nine concentrations of Na_xK_{1-x} alloys. Total of the partial pair distribution functions (PPDF) behave in the same way as that of pure liquids. The positions of the first peak are related to the size of the atoms. The first peak of $g_{NaK}(r)$ lies in the middle between $g_{NaNa}(r)$ and $g_{KK}(r)$'s principal peaks. It is observed from figures that

Table 6.2: Coordination numbers n_{ij} and the short range order parameter, α, of Warren for l-Na_xK_{1-x} alloys at 373 K.

x_{Na}	n_{NaNa}	n_{NaK}	$n_{K\text{-}Na}$	n_{KK}	n_{Tot}	α
0.1	1.10	9.80	1.05	11.98	12.30	0.02
0.2	2.06	8.18	2.03	10.84	12.20	0.05
0.3	3.46	7.86	3.43	10.01	12.49	0.06
0.4	4.71	6.73	4.45	9.04	12.50	0.09
0.5	5.92	5.79	5.79	7.93	12.69	0.09
0.6	6.11	4.37	6.57	7.23	12.00	0.12
0.7	8.60	3.72	8.50	5.23	12.63	0.07
0.8	9.75	2.58	10.12	4.08	12.46	0.06
0.9	10.95	1.31	12.13	2.44	12.31	0.08

$g_{NaNa}(r)$ undergoes significantly large changes whereas the changes in $g_{NaK}(r)$ and $g_{KK}(r)$ are small when $x \leq 0.6$ and the changes of $g_{KK}(r)$ become significant while $x \geq 0.6$. The heights of the first peaks may exhibit the signature of chemical ordering.

It is found that, when x_{Na} is increased the first peak value of $g_{\mathrm{NaNa}}(r)$ decreases, but its position remains almost same. But the peak of $g_{\mathrm{NaK}}(r)$ remains unchanged while the height of the $g_{\mathrm{KK}}(r)$'s first peak slightly increases. For $x_{\mathrm{Na}} = 0.7$, $g_{\mathrm{NaNa}}(r)$ becomes comparable to $g_{\mathrm{KK}}(r)$. In-case it were significantly lower than others, it would reveal homo-coordination tendencies. Table 6.2 illustrates the calculated results for the coordination numbers and SRO (α) parameters. As we have discussed in Chapter 5, for a random distribution of ions $\alpha = 0$, a positive value of α indicates a homo-coordinating tendency while a negative value of α suggests the hetero-coordination. In our calculation we have found the positive small values for α for all nine concentrations which confirm the existence of homo-coordinating tendencies of our system. But the figures show that for $x_{\mathrm{Na}} \leq 0.6$ $g_{\mathrm{NaK}}(r)$ exhibits peak just between $g_{\mathrm{NaNa}}(r)$ and $g_{\mathrm{KK}}(r)$, and for $x_{\mathrm{Na}} \geq 0.6$ peak of $g_{\mathrm{NaK}}(r)$ falls below the $g_{\mathrm{NaNa}}(r)$ and $g_{\mathrm{KK}}(r)$. This apparently indicates a homo-coordination tendency. The values of $\alpha = 0$ rules out it clearly. The concentration-concentration partial static structure factor, $S_{CC}(q)$, describes how the particles distribute and gather attending to their chemical species. As with equation (5.28), in the limit $q \to 0$ the static structure factors can be related to thermodynamic information. In particular, $S_{CC}(0)$ takes a value equal to $x_{\mathrm{Na}}x_{\mathrm{K}}$ if we have an ideal alloy, while deviations from this value indicate the tendency of the system to be homocoordinating if it tends to form with same pairs of particles ($S_{CC}(0) > x_{\mathrm{Na}}x_{\mathrm{K}}$) or it will be heterocoordinating if it tends to form with different pairs of particles ($S_{CC}(0) < x_{\mathrm{Na}}x_{\mathrm{K}}$). We have found that ($S_{CC}(0) > x_{\mathrm{Na}}x_{\mathrm{K}}$) for all nine concentrations in our calculation. Therefore our system is supose to show homo-coordination tendency.

6.2.2 Static Structure Factor and Isothermal Compressibility

The static structure factor $S(q)$ is related to it's real space counterpart the pair distribution function $g(r)$ through the Fourier transformation (FT). Importantly it can be noted here that the OF-AIMD simulation allows us to direct computation of both $S(q)$ and $g(r)$ on the fly. Therefore, this feature has its own merits to present

Table 6.3: The comparison of OF-AIMD position and peak values of $S(q)$ with Wax data for all nine concentrations and XRD data for three different concentrations.

x_{Na}	q_{p}			q_{m}			$S(q_{\mathrm{p}})$			$S(q_{\mathrm{m}})$		
	Sim	Wax	XRD	Sim	Wax	XRD	Sim	Wax	XRD	Sim	Wax	XRD
0.1	1.66	1.66		2.30	2.30		2.71	2.66		0.62	0.61	
0.2	1.67	1.67		2.32	2.32		2.39	2.59		0.66	0.61	
0.3	1.69	1.69	1.73	2.32	2.32	2.31	2.68	2.45	2.44	0.62	0.63	0.61
0.4	1.75	1.75		2.38	2.38		2.39	2.39		0.64	0.64	
0.5	1.77	1.77	1.78	2.41	2.43	2.52	2.42	2.27	2.30	0.63	0.65	0.66
0.6	1.82	1.82	...	2.47	2.47	...	1.90	2.24	...	0.73	0.65	...
0.7	1.85	1.85	1.88	2.53	2.53	2.54	2.96	2.55	2.54	0.58	0.59	0.60
0.8	1.89	1.89		2.55	2.55		2.67	2.36		0.61	0.61	
0.9	1.96	1.97	...	2.53	2.64	...	2.26	2.55	...	0.71	0.65	...

them with equal importance simultaneously. The static structure factors $S(q)$ for three different concentrations, $x_{\mathrm{Na}} = 0.3, 0.5$ and 0.7 obtained from the simulation and from the x-ray diffraction (XRD) data are shown in Figure 6.4. It is clear from this figure that the OF-AIMD values for the total structure factors $S(q)$ are in very good agreement with XRD data. While for the concentration, $x_{\mathrm{Na}} = 0.7$ a small difference is observed between the OF-AIMD values and the corresponding experimental data

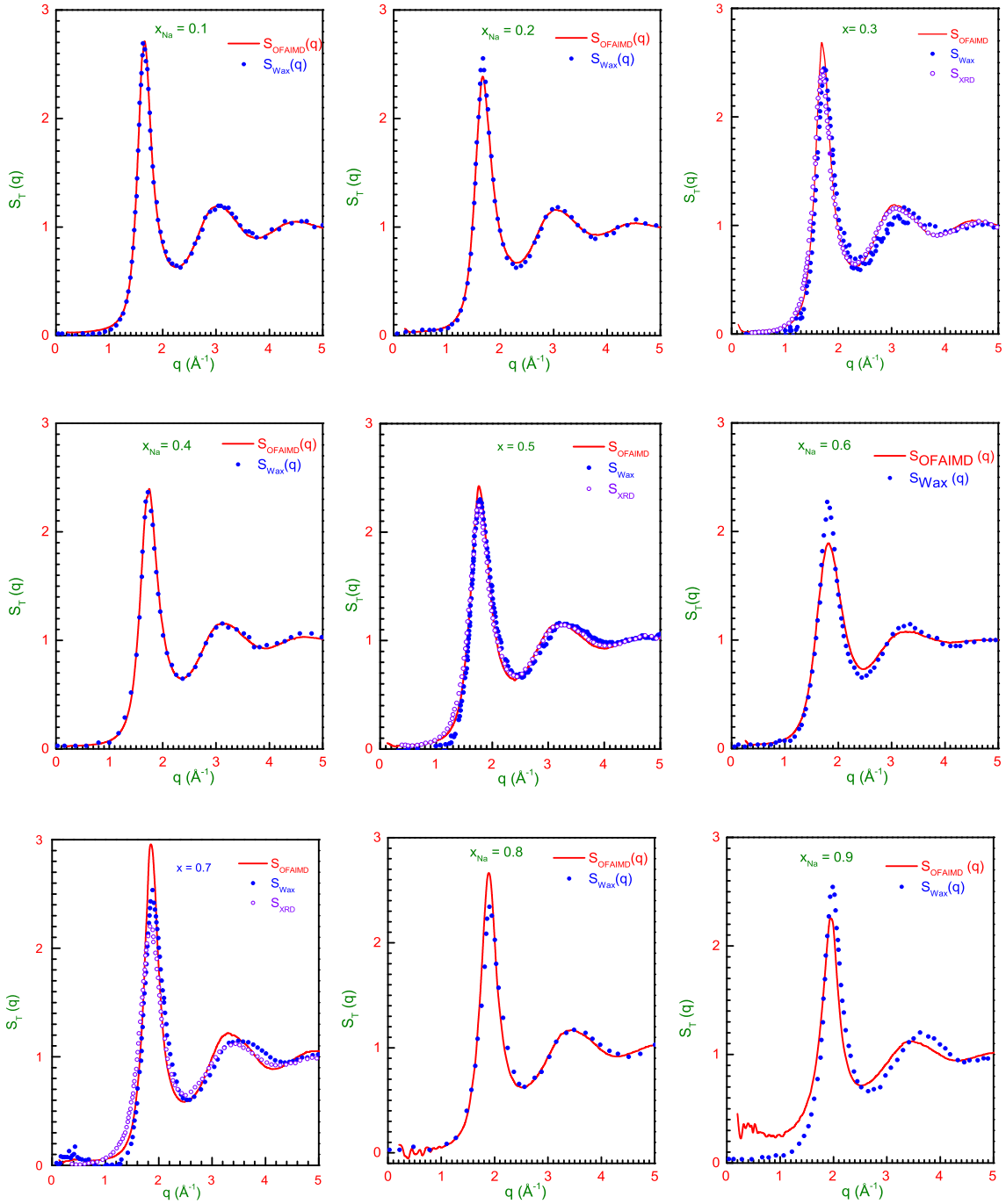

Figure 6.4: Total SSF, $S(q)$ of the liquid Na_xK_{1-x} alloy at x_{Na}= 0.1 to 0.9 at T = 373 K. The continuous line represents OF-AIMD results, the open circles for XRD data [149] and closed circles for calculated values of Wax [150], respectively.

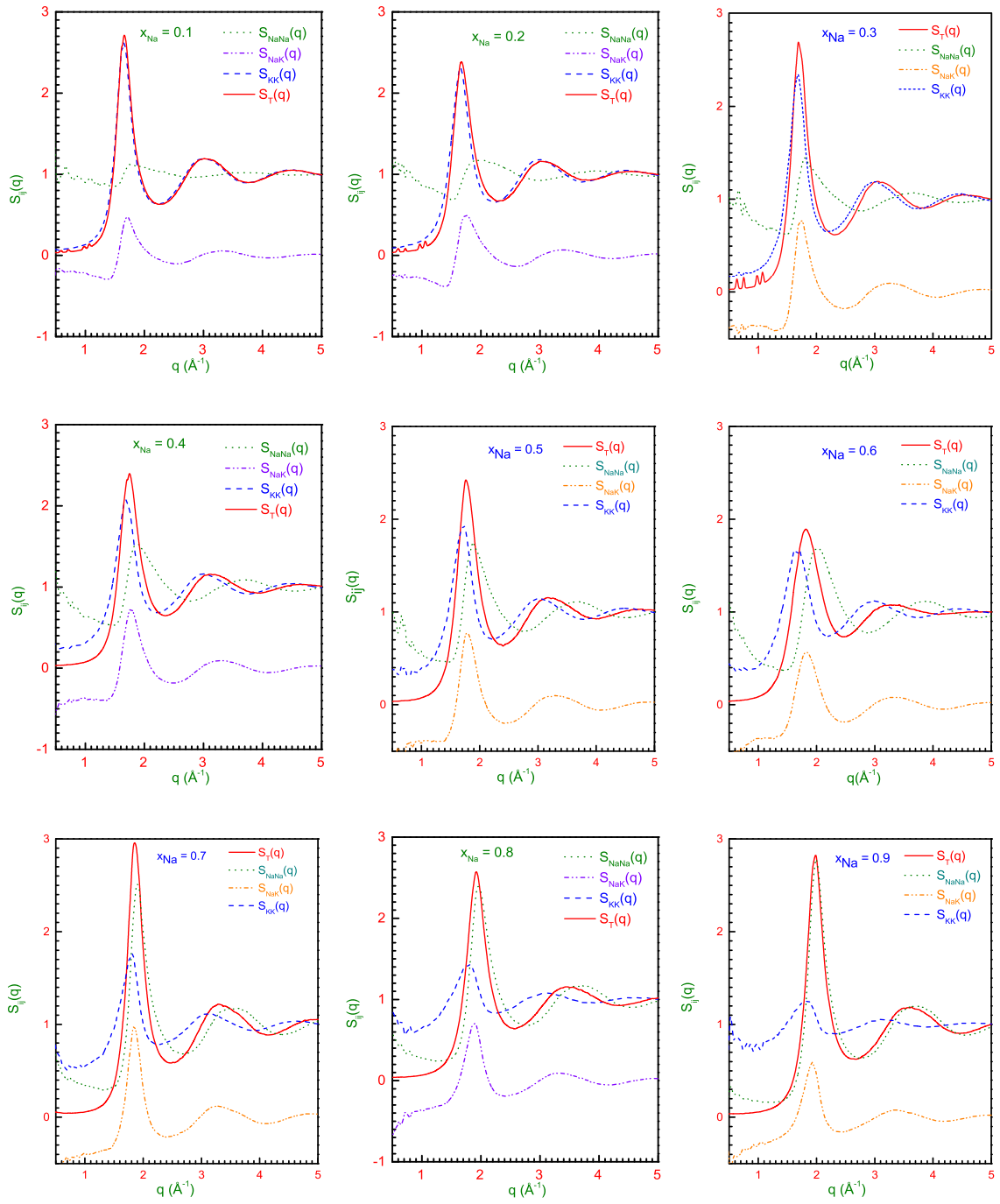

Figure 6.5: AL partial SSF, $S_{\rm ij}(q)$ for the Na_xK_{1-x} liquid alloys for all nine concentrations, $x_{\rm Na}$= 0.1 to 0.9. The green, violet, blue and red colours correspond to $S_{\rm NaNa}(q)$, $S_{\rm NaK}(q)$, $S_{\rm KK}(q)$ and $S_{\rm T}(q)$ respectively.

in the region $q \geq 3$ Å^{-1}. Where a little inward shift is seen in the second OF-AIMD peak. In the region of $q \leq 3$ Å^{-1} values of the OF-AIMD results lie in between Wax and XRD results for all three concentrations. For the concentration, $x_{\mathrm{Na}} = 0.3$ in the region 2.7 Å$^{-1} \leq q \leq 3.8$ Å^{-1} a small deviation from the XRD is found but agreement with Wax data is found to be very good. The principal peak position (q_{p}) of OF-AIMD

Table 6.4: The simulated maximum and minimum position and height of partial static structure factors $S_{\mathrm{ij}}(q)$ at different concentrations.

x	q_{p}			q_{m}			$S(\mathrm{q_p})$			$S(\mathrm{q_m})$		
	q_{11}	q_{12}	q_{22}	q_{11}	q_{12}	q_{22}	S_{11}	S_{12}	S_{22}	S_{11}	S_{12}	S_{22}
0.1	1.78	1.73	1.65	2.78	2.55	2.25	1.12	0.45	2.58	0.94	-0.11	0.62
0.2	1.90	1.76	1.67	2.94	2.61	2.19	1.19	0.50	2.30	0.92	-0.15	0.65
0.3	1.82	1.75	1.68	2.77	2.48	2.19	1.44	0.76	2.33	0.87	-0.18	0.65
0.4	1.86	1.78	1.69	2.79	2.49	2.20	1.53	0.72	2.07	0.82	-0.19	0.68
0.5	1.88	1.78	1.73	2.80	2.43	2.22	1.75	0.77	1.93	0.79	-0.20	0.70
0.6	2.02	1.83	1.66	2.90	2.50	2.18	1.69	0.56	1.66	0.78	-0.19	0.73
0.7	1.90	1.85	1.82	2.73	2.41	2.25	2.50	0.98	1.76	0.68	-0.22	0.78
0.8	1.96	1.90	1.79	2.77	2.38	2.22	2.39	0.69	1.41	0.67	-0.20	0.82
0.9	1.99	1.92	1.83	2.78	2.41	2.23	2.78	0.58	1.27	0.63	-0.16	0.89

fits better with XRD data than that of Wax calculation [149, 150] for $x_{\mathrm{Na}} = 0.3$, 0.5 and 0.7. The OF-AIMD peak height (S_{q_p}) is somewhat overestimated than both XRD and Wax magnitude for all those three concentrations. The comparison of the OF-AIMD magnitude of q_p, q_m, S_{q_p} and S_{q_m} with XRD and Wax are shown in Table 6.3. The principal peak, other peak values, position of the peaks and phase of oscillations also agree well within the uncertainty of the experimental data. This is worth noting that, the Wax calculation sometimes yields larger peak of $S(q)$ than that of the XR diffraction [151]. Now we will analyze the partial structure factors $S_{\mathrm{ij}}(q)$ of liquid

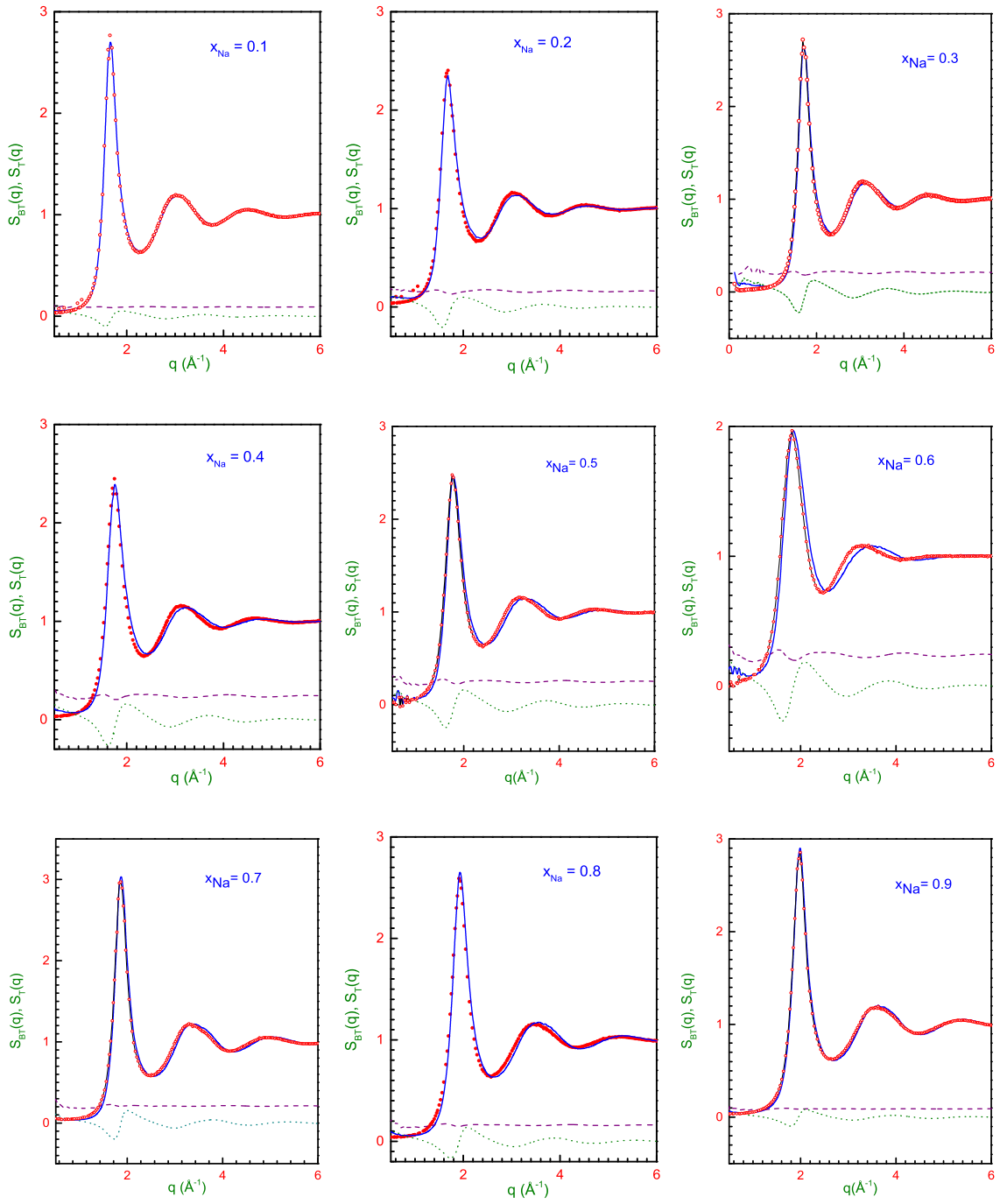

Figure 6.6: BT partial SSF and AL total SSF for Na_xK_{1-x} liquid alloys for all nine concentrations, x_{Na}=0.1 to 0.9. The blue continuous, purple dashed and olive dotted lines correspond to $S_{NN}(q)$, $S_{CC}(q)$, $S_{NC}(q)$, respectively. Full red circles stand for the calculated $S_T(q)$.

Na_xK_{1-x} binary alloys for nine different concentrations. We note here that experimental values are available only for three concentrations. Our main focus is to explain the data obtained from OF-AIMD simulation based on the DFT with LDA approximation [2]. Theoretical results for partial and total static structure factors are shown in Figure 6.5. For all nine concentrations, behaviour at both large and small q values are very good and for large-q a very small inward shift are found in the theoretical results while compared with experimental data. In the intermediate q regime the agreement is less satisfactory. For all concentrations, minimum of $S(q)$ lies in between 2.4 and 3.0 Å^{-1}.

In order to test the reliability and accuracy of our calculation for structure we have derived partial structure factor proposed by Bhatia-Thornton (BT). The BT partial structure factor $S_{\text{NC}}(q)$ oscillation varies from negative to positive region around zero and $S_{\text{CC}}(q)$ oscillates only in the positive region. So, the useful features the BT structure factors are nicely displayed in Figure 6.6. From the figure it appears that the $S_{\text{NN}}(q)$ agrees very well with the total Ashcroft-Langreth (AL) static structure factor. This result indicates that our calculation for AL partial static structure factors are consistent and reliable.

Figure 6.7 shows the isothermal compressibility for different concentrations. The OF-AIMD results overestimate the values when compared with the experimental data. The classical molecular dynamics (CMD) data obtained by J. F. Wax [150] under estimate the values at low concentrations and slightly overestimate at the higher concentrations. But agrees better than the OF-AIMD results although, in principle, theoretically OF-AIMD is more accurate than the CMD. $S_{\text{NN}}(q)$ is the

number-number structure factor mainly provides the structural property of the system. The concentration-concentration structure, $S_{\mathrm{CC}}(q)$, is actually related to the chemical ordering of the system rather than configurational structure. The number-concentration structure, $S_{\mathrm{NC}}(q)$, is actually describe the interplay between the configurational structure and the chemical ordering. So, apparently $S_{\mathrm{NN}}(q)$ structure factor should be closer in magnitude to the total structure factor, $S_{\mathrm{T}}(q)$. The results of my calculation for $S_{\mathrm{T}}(q)$ when compared with the $S_{\mathrm{NN}}(q)$ an excellent agreement is found. This degree of agreement manifest significance of the $S_{\mathrm{NN}}(q)$. The BT partial

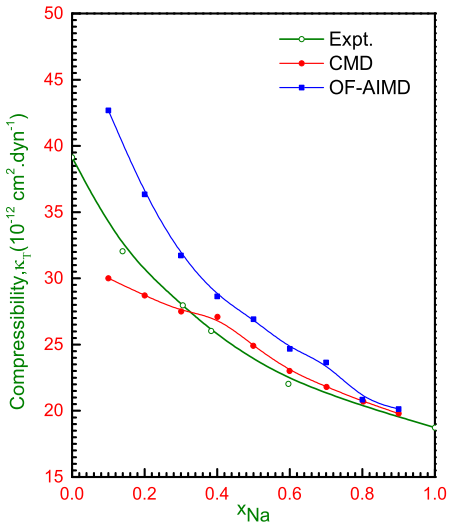

Figure 6.7: χ_T as deduced from the small-q limits OF-AIMD simulation (blue full squres), experimental values (olive open circles) and CMD values (red full circles) [150] of the liquid $\mathrm{Na}_x\mathrm{K}_{1-x}$ alloy.

structure factors in general give the information regarding the chemical and topological ordering in the alloy. Figure 6.6 shows the BT partial structure factors for $\mathrm{Na}_x\mathrm{K}_{1-x}$ alloys calculated for several concentrations. We have found that $S_{\mathrm{NN}}(q)$ displays a typical oscillatory behaviour. But no visible prepeaks or low-q divergences

or shoulders are observed. In the other direction, the long wavelength limit of $S_{\rm CC}$ *i.e* $S_{\rm CC}(q \to 0)$, provides information regarding the existence of the SRO in the alloys. For the Na_xK_{1-x} alloy we have found that $S_{\rm CC}(q \to 0)/x_{\rm Na}x_{\rm K}$ takes values which are grater than unity for all concentrations. This suggests that the homo-coordination tendencies are there in the alloy. Which is consistent with the calculated SRO parameters presented in Table 6.2. The isothermal compressibility, χ_T,

Table 6.5: Compressibility, χ_T $\times 10^{-12}$ cm^2.dyne^{-1} of l-Na_xK_{1-x} alloy at 373 K.

Con.	N. density	$S(0)$	$\frac{S_{\rm CC}(q\to 0)}{x_{\rm Na}x_{\rm K}}$	χ_T (cm^2.dyne^{-1})		
$x_{\rm Na}$	ρ (Å^{-3})			OF-AIMD	Expt.	CMD
0.1	0.0132	0.022	1.08	42.68	34.20	30.00
0.2	0.0139	0.022	1.26	36.34	30.68	28.70
0.3	0.0147	0.022	1.05	31.72	28.05	27.50
0.4	0.0156	0.022	1.09	28.64	25.74	27.10
0.5	0.0166	0.027	1.08	26.92	23.89	24.90
0.6	0.0177	0.035	1.10	24.68	22.51	23.00
0.7	0.0190	0.030	1.45	23.64	21.36	21.80
0.8	0.0204	0.022	1.23	20.85	20.43	20.70
0.9	0.0222	0.021	1.08	20.13	19.51	19.80

for liquid Na_xK_{1-x} alloy have been estimated for nine different concentrations at the thermodynamic states $T = 373$ K. This result has been calculated from the relation $S_T(q \to 0) = \rho_i k_B T \chi_T$, where $k_{\rm B}$ is the Boltzmann's constant. A least-squares fit of $S_T(q) = S_0 + S_2 q^2$ has been employed to calculate $S(q)$ for $(q \to 0)$ which yields the result for χ_T. The obtained results agree within 3.0%- 19.86% of the extrapolated experimental data [152] at the point of theoretical concentrations and 1.6%- 29.7% of the CMD data [150] which are shown in Table 6.5.

6.3 Dynamic Properties

We have evaluated several dynamic properties, both for single-particle (viz self-intermediate scattering functions, self-dynamic structure factors, velocity autocorrelation function and mean square displacement) and for collective ones (viz intermediate scattering functions, dynamic structure factors, longitudinal and transverse currents). The time correlation functions are evaluated by taking time origins every five time steps. In principle, several correlation functions depend on the wave vector $\vec{q}$, but for an isotropic system they sometimes reduces to $q \equiv |\vec{q}|$.

6.4 Dynamic Properties: Single Particle Dynamics

6.4.1 Self-Intermediate Scattering Function

The self-intermediate scattering function, $F_s(q,t)$, gives a complete description of the single-particle properties that probes the single-particle dynamics over different length scales, the range of which varies from the hydrodynamic regime ($q \to 0$) to the free-particle regime ($q \to \infty$). The magnitudes obtained from the equation (5.67), in the present simulations, are shown in Figure 6.8 for a few q values at temperature 373 K. These figures show a typical monotonic decrease of $F_s(q,t)$ with increasing time. The $F_s(q,t)$ is closely related to the velocity autocorrelation function (VACF), $Z(t)$, of the tagged ion in the liquid. The $Z(t)$ can be obtained from the limit ($q \to 0$) of the first-order memory function of the $F_s(q,t)$. It can be easily obtained from its definition given in equation (5.36), which stands for the normalized VACF. The OF-AIMD results for self-intermediate scattering function, $F_s(q,t)$ for the liquid Na_xK_{1-x}

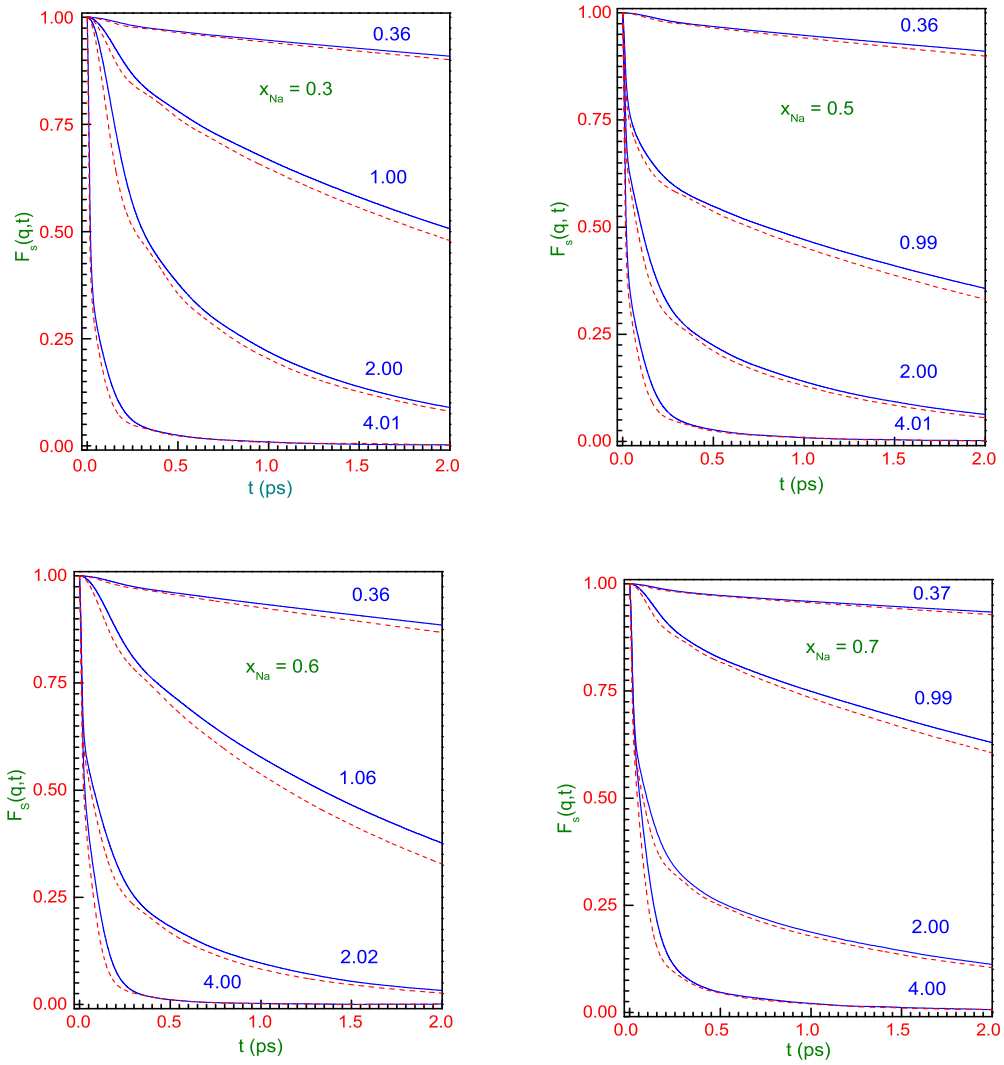

Figure 6.8: Normalized $F_s(q,t)$ at different q's for the l-Na_xK_{1-x} alloys at 373 K for the concentrations, x_{Na}= 0.3, 0.5, 0.6 and 0.7. Dashed (red) and solid (blue) line represent Na and K respectively.

binary alloy at four different concentrations at 373 K are displayed in Figure 6.8. The observed monotonic behaviour of $F_s(q,t)$ as a function of t is found for all concentrations. Here, it is also observed that the decay rate is slow for low q values and it is increased very sharply as q value increases.

6.4.2 Velocity Autocorrelation Function

The OF-AIMD results for the VACF, $Z(t)$, for liquid Na_xK_{1-x} binary alloys for nine different concentrations at 373 K are displayed in Figure 6.9. The most common feature of $Z(t)$ is its oscillatory behaviour. Different magnitudes related to the atomic transport properties of a tagged ion can be evaluated from the normalized velocity autocorrelation function $Z(t)$. The power spectrum of VACF, $Z(\omega)$, is obtained from the Fourier Transformation (FT) of $Z(t)$. The negative values of $Z(t)$ have a first minimum which is followed by rather weak oscillations and indicate typical back-scattering behaviour of ions due to cage effects produced by the nearest neighbours [43]. The $Z^d_{\mathrm{NaK}}(t)$ takes into account the effect of distinct correlations, either between the ions of same kind or different species. The distinct VACF, $Z^d_{\mathrm{NaK}}(t)$, oscillates from negative values for the concentrations $x_{\mathrm{Na}} = 0.3$, 0.5 and 0.8. It is also found from the Figure 6.9 that the VACF $Z^0_{\mathrm{NaK}}(t)$ and $Z_{\mathrm{NaK}}(t)$ are oscillating almost in the same phase for the concentrations, $x_{\mathrm{Na}} = 0.3$, 0.5 and 0.8. While for the concentration, $x_{\mathrm{Na}} = 0.1$, 0.2, 0.4, 0.6 and 0.9 all the $Z^0_{\mathrm{NaK}}(t)$, $Z^d_{\mathrm{NaK}}(t)$ and $Z_{\mathrm{NaK}}(t)$ are oscillating in the same phase. In the case of $x_{\mathrm{Na}} = 0.1$, 0.7, $Z^s_{\mathrm{Na}}(t)$ and $Z^d_{\mathrm{NaK}}(t)$ exactly coincide with each other where $Z^0_{\mathrm{NaK}}(t)$ and $Z_{\mathrm{NaK}}(t)$ is oscillating with a very small difference in phase. For the concentrations, $x_{\mathrm{Na}} = 0.2$, $Z^s_{\mathrm{K}}(t)$, $Z^d_{\mathrm{NaK}}(t)$, and for the concentrations, $x_{\mathrm{Na}} = 0.2$, 0.4 $Z^0_{\mathrm{NaK}}(t)$, $Z_{\mathrm{NaK}}(t)$ are exactly overlap with each other. A quantitative account of the distinct effects is yielded by the γ_{NaK} as defined in equation (5.58). The positive or negative values of γ_{NaK} denote [153–155] that particles of the same or different species have a greater tendency to diffuse together than the distinct or same species.

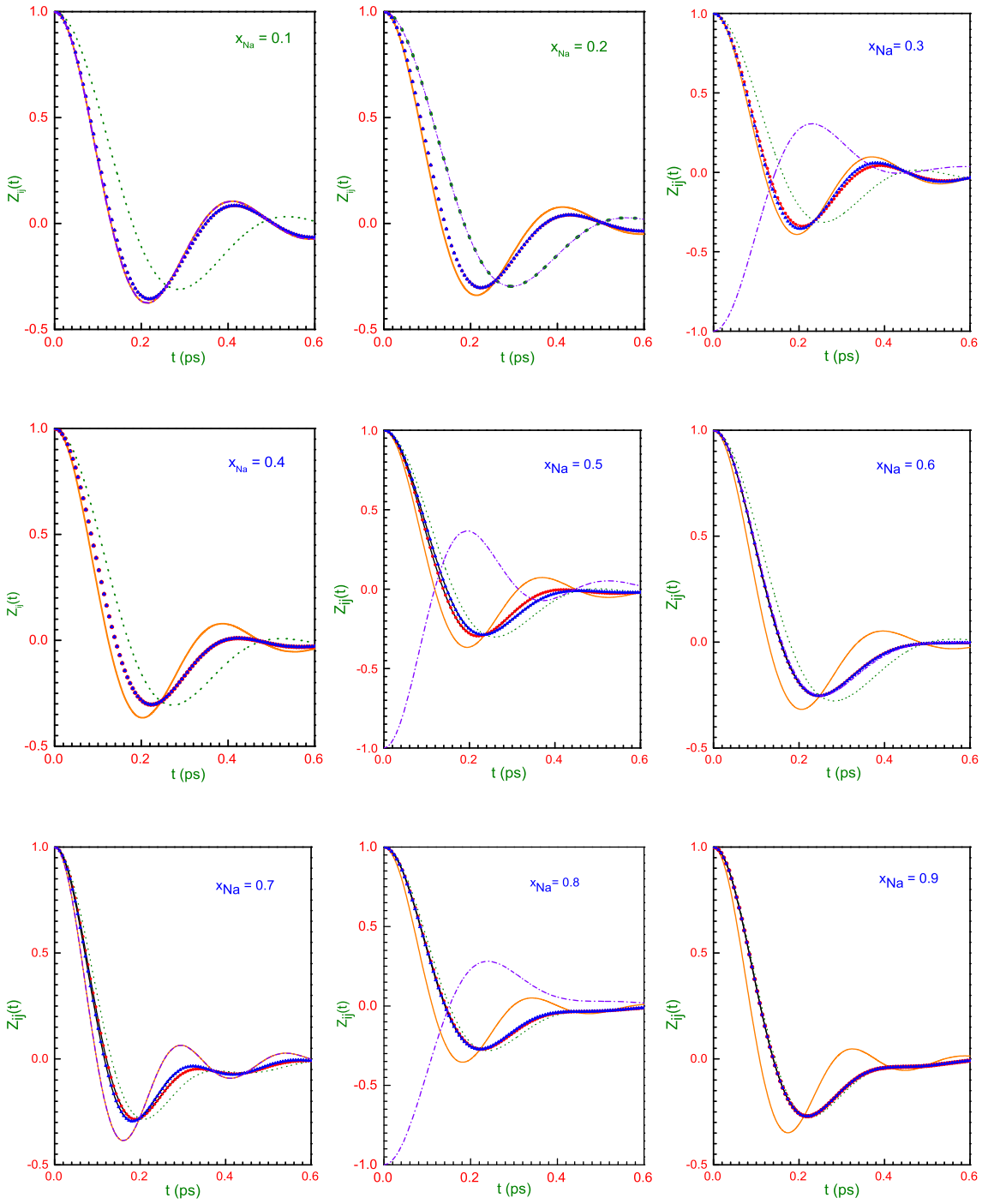

Figure 6.9: Normalized partial VACFs for Na_xK_{1-x} liquid alloy at 373 K and x_{Na} = 0.1 to 0.9. Full orange, dot olive, dash dot violet lines, full red circles and full blue triangles correspond to $Z^s_{Na}(t)$, $Z^s_K(t)$, $Z^d_{NaK}(t)$, $Z^0_{NaK}(t)$ and $Z_{NaK}(t)$, respectively.

6.4.3 Diffusion Coefficients

Atoms of a mixture diffuse into the material, almost like in a pure liquid. This is equivalent to the self-diffusion, which is a unique attribute that is determined by the self-diffusion coefficient. A mixture's associated velocity autocorrelation function (VACF), $Z_{ij}(t)$, can be used to calculate the one coefficient for each chemical species. This function can be calculated with greater accuracy than the mean squared displacement, because relevant information corresponds to short time-range. We can

Table 6.6: Diffusion coefficients, ($\times 10^{-4}$cm^2.s^{-1}) calculated from the Green-Kubo relation of the l-Na$_x$K$_{1-x}$ binary alloys at 373 K. Where w refers to calculated values of J.F. Wax [150]

x_{Na}	D^s_{Na}	$D^s_{\mathrm{Na,w}}$	D^s_{K}	$D^s_{\mathrm{K,w}}$	D_{int}	D^w_{int}	D^0_{NaK}	D_{NaK}	D^d_{NaK}	γ_{NaK}
0.1	0.42	0.50	0.42	0.44	0.39	0.44	0.43	0.43	-0.26	-0.054
0.2	0.47	0.48	0.45	0.42	0.39	0.41	0.49	0.49	-0.49	-0.160
0.3	0.35	0.47	0.31	0.39	0.32	0.36	0.36	0.34	0.32	0.196
0.4	0.40	0.47	0.35	0.38	0.37	0.34	0.38	0.40	0.00	0.000
0.5	0.38	0.46	0.33	0.36	0.37	0.33	0.37	0.40	0.28	0.198
0.6	0.49	0.46	0.43	0.37	0.43	0.31	0.48	0.48	-0.51	-0.267
0.7	0.24	0.45	0.21	0.35	0.14	0.30	0.22	0.21	-0.19	-0.184
0.8	0.36	0.46	0.29	0.35	0.25	0.27	0.31	0.31	0.43	0.158
0.9	0.34	0.46	0.28	0.35	0.27	0.30	0.29	0.29	0.00	0.000

mention here that, the atom's spectrum density, $Z_{ij}(\omega)$, can provide the information regarding to its vibrational behavior. In addition, a phenomenon known as inter-diffusion occurs in mixtures and is associated with the capacity of both species to mix or segregate. This is a collective property, pictured by the inter-diffusion coefficient as stated in equation (5.59). The time correlation functions (TCF) among the atomic velocities gives information about the mobility related transport properties of the system. The relative velocity correlation functions (VCFs), $Z_{ij}(t)$, results and dif-

fusion coefficients, $D^s_{\rm Na}$, $D^s_{\rm K}$, $D^0_{\rm NaK}$, $D_{\rm NaK}$, $D^d_{\rm NaK}$ and inter-diffusion, $D_{\rm int}$ are reported in this section.

The present OF-AIMD results for the diffusion coefficients for Na_xK_{1-x} liquid alloys for all nine concentrations are presented in Table 6.6. The $D^d_{\rm NaK}$ considers the impact of distinct diffusion coefficients for particles of the same or different species. The $\gamma_{\rm NaK}$, as stated in equation (5.58), provides a precise quantitative evaluation of the different effects. The positive or negative values of $\gamma_{\rm NaK}$ signify [153–155] that particles of the same or different species have a stronger tendency to diffuse together

Table 6.7: Diffusion coefficients, ($\times 10^{-4}$cm^2.s^{-1}) calculated from the Einstein relation for l-Na_xK_{1-x} alloys at 373K.

Con.	T(K)	D_s=lim$_{t\to\infty}\frac{\langle \delta r^2(t)\rangle}{6t}$		
$x_{\rm Na}$		$D^s_{\rm Na}$	$D^s_{\rm K}$	$D^0_{\rm NaK}$
0.1		0.53	0.48	0.53
0.2		0.59	0.53	0.58
0.3		0.43	0.39	0.42
0.4		0.49	0.44	0.47
0.5	373	0.50	0.48	0.49
0.6		0.70	0.66	0.68
0.7		0.43	0.44	0.44
0.8		0.69	0.70	0.70
0.9		1.01	1.10	1.09

than those of the same or separate species. We have compared $D^s_{\rm Na}$ and $D^s_{\rm K}$ with $D^s_{\rm Na,w}$ and $D^s_{\rm K,w}$ calculated values of Wax which are found to be good in agreement. For the concentrations, $x_{Na} = 0.1, 0.3$ our results closely fit with the value calculated by Wax. Throughout the wide range of concentrations, the ratio $D^s_{\rm Na}/D^s_{\rm K}$ actually stays essentially constant. Only for the concentrations $x_{\rm Na}$= 0.8 and 0.9 do we observe a slight deviation.

All these quantities are rather slowly varying functions of the concentration. In our calculation we have observed the similar trend except for $x_{\mathrm{Na}} = 0.2, 0.4$ and 0.6 where a small deviation is found from its regular trends. We have calculated inter-diffusion coefficient from the Darken's semiempirical expression $S_{CC}(q \to 0)$ $D_{\mathrm{int}} = x_1 x_2 D_{12}^0$ [156], which is obtained by neglecting the distinct interparticle velocity correlations. Following Darken's argument if we neglect distinct part of the diffusion, the values of γ_{NaK} for all concentrations become positive which indicates a homo-coordinating tendency. γ_{NaK} refers to the deviation from ideal mixture.

We compared our OF-AIMD results for diffusion with the results calculated by J. F. Wax [150], which are presented in Table 6.6. We see from the table that our OF-AIMD simulated results are somewhat good in agreement with the results obtained by Wax. We also estimated the diffusion coefficient using the Einstein relation, and the results are shown in Table 6.7. It is evident from Table 6.6 and Table 6.7 that the self diffusion coefficients D_{NaK}^0 estimated using simulation data and the Green-Kubo relation yield values that are nearly identical to those obtained using the Einstein relation (MSD). The diffusion results of the OF-AIMD calculation lie within 4%-12% that of the magnitude obtained from MSD calculation.

The Stokes-Einstein (SE) relation $\eta D = \frac{k_B T}{2\pi d}$, establishes a link between η and the self-diffusion coefficient D in the context of the Brownian motion of a macroscopic particle with a hard sphere diameter d in a liquid with viscosity η. This relation, which was not created for atoms, has been utilized to calculate D (or η) by matching d to the location of the mean peak of $g(r)$. The Stokes-Einstein relation failing, as described for super-cooled liquid [157, 158], is correlated with the dynamical heterogeneity. The

non-exponential decay of the correlation function, $g(r)$, is one of the markers of this property. Our findings for $g(r)$ suggest that the decay of the correlation function is not purely exponential. Therefore, a departure from the SE relation ($D = \frac{k_B T}{C\pi\eta d}$) may be seen. However, it needs more in-depth research. From the perspective of SE theory, it is fascinating and straightforward which boundary condition—slip or stick—is appropriate for Na_xK_{1-x} liquid binary alloy. Table 6.8 provides values for diffusion coefficients with C= 2 and C= 3, and $d = r_p$ (r_p is the location of the principal peak of $g(r)$), where C= 2 and C= 3, respectively represent the slip and stick

Table 6.8: Diffusion coefficients, ($\times 10^{-4}$cm^2.s^{-1}) calculated from the SE relation for different values of C for l-Na_xK_{1-x} alloy at 373K.

Con.	T(K)	OF-AIMD	$D = \frac{k_B T}{C\pi\eta d}$		OF-AIMD
x_{Na}		η(GPa.ps)	C =2	C =3	D^0_{NaK}
0.1		0.47	0.38	0.25	0.43
0.2		0.47	0.39	0.26	0.49
0.3		0.50	0.37	0.25	0.36
0.4		0.49	0.39	0.26	0.38
0.5	373	0.53	0.37	0.24	0.37
0.6		0.59	0.34	0.23	0.48
0.7		0.59	0.34	0.23	0.22
0.8		0.60	0.35	0.24	0.31
0.9		0.63	0.34	0.23	0.29

boundary conditions [74]. We take note of the fact that a few other writers [157, 158] employed C = 4, 6 for the slide and stick condition for super-cooled liquids. Table 6.8 demonstrates that when C=2, the OF-AIMD produced diffusion agrees more closely with SE values. This makes it possible to deduce that a liquid Na_xK_{1-x} alloy that is close to melting temperature meets the slip boundary condition.

6.5 Dynamic Properties: Collective Dynamics

6.5.1 Intermediate Scattering Function

The collective dynamics due to the density fluctuations in the alloy is generally described through the partial Ashcroft-Langreth (AL) ISF, $F_{\rm ij}(q,t)$. ISF, $F(q,t)$, provides information regarding the time evolution of the collective excitation's (propagation and damping). $F(q,t)$ is directly obtained from the MD simulations through the wave vectors $\vec{q}$ allowed by the size of the simulation box and the time evolution of the ionic positions. The $F(q,t)$ is usually defined by the relation of equation (5.69). When q-values are small $F_{\rm ij}(q,t)$ oscillates in a typical manner. The amplitude of the oscillations gets weaker as q-value increases. Furthermore, the oscillatory shape is superposed on a weak diffusive component. The $F(q,t)$ exhibit a slow decay at $q \approx q_p$. This is actually induced by the strong spatial correlations at around that q-values and this phenomenon is known as de Gennes narrowing. Minimum q values allowed by the present OF-AIMD simulation are q_{min}= 0.117, 0.120, 0.122, 0.124, 0.127, 0.129, 0.133, 0.136 and 0.140 Å^{-1} for $x_{\rm Na}$ = 0.1 to 0.9 respectively. Figure 6.10-6.11 show the nature of $F_{\rm ij}(q,t)$ for a few q values and for nine different concentrations. The observed slow decay that is dominated by the diffusive contributions for small q's in the partial $F_{\rm NaNa}(q,t)$, $F_{\rm KK}(q,t)$ and $F_{\rm NaK}(q,t)$, due to the effect of screening of the oscillations is connected to the flow of the density fluctuations. Whereas for some q values the $F_{\rm NaK}(q,t)$ takes on negative values for all concentrations. However, with increasing value of q the decay rate becomes faster at small t.

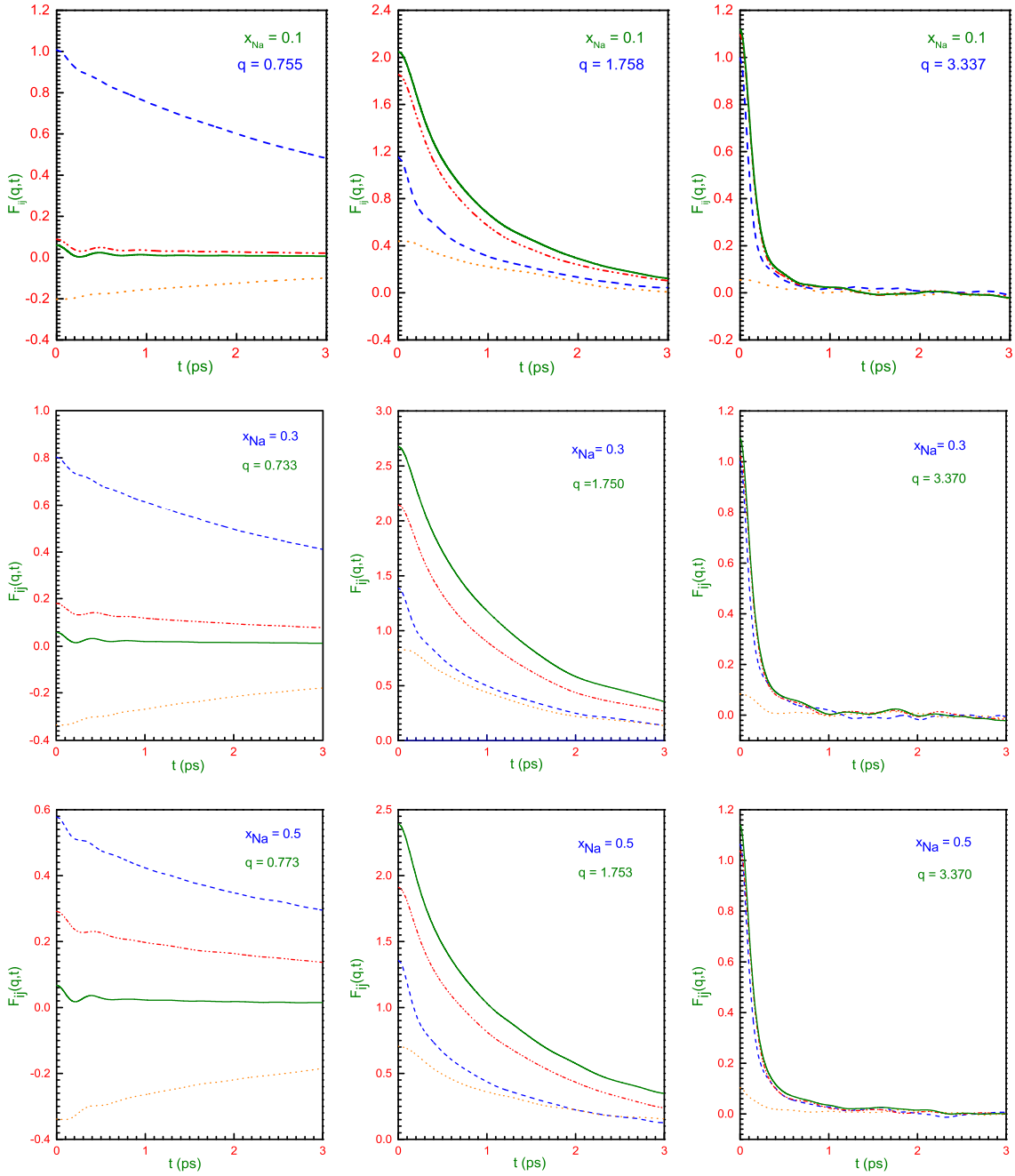

Figure 6.10: Partial ISF, $F_{ij}(\mathbf{q},t)$ of the Na_xK_{1-x} liquid alloy at several q values for x_{Na}= 0.1, 0.3 and 0.5 at T = 373 K. The blue, red, orange and olive colours are for $F_{\mathrm{NaNa}}(\mathbf{q},t)$, $F_{\mathrm{KK}}(\mathbf{q},t)$, $F_{\mathrm{NaK}}(\mathbf{q},t)$ and $F_{\mathrm{NN}}(\mathbf{q},t)$, respectively.

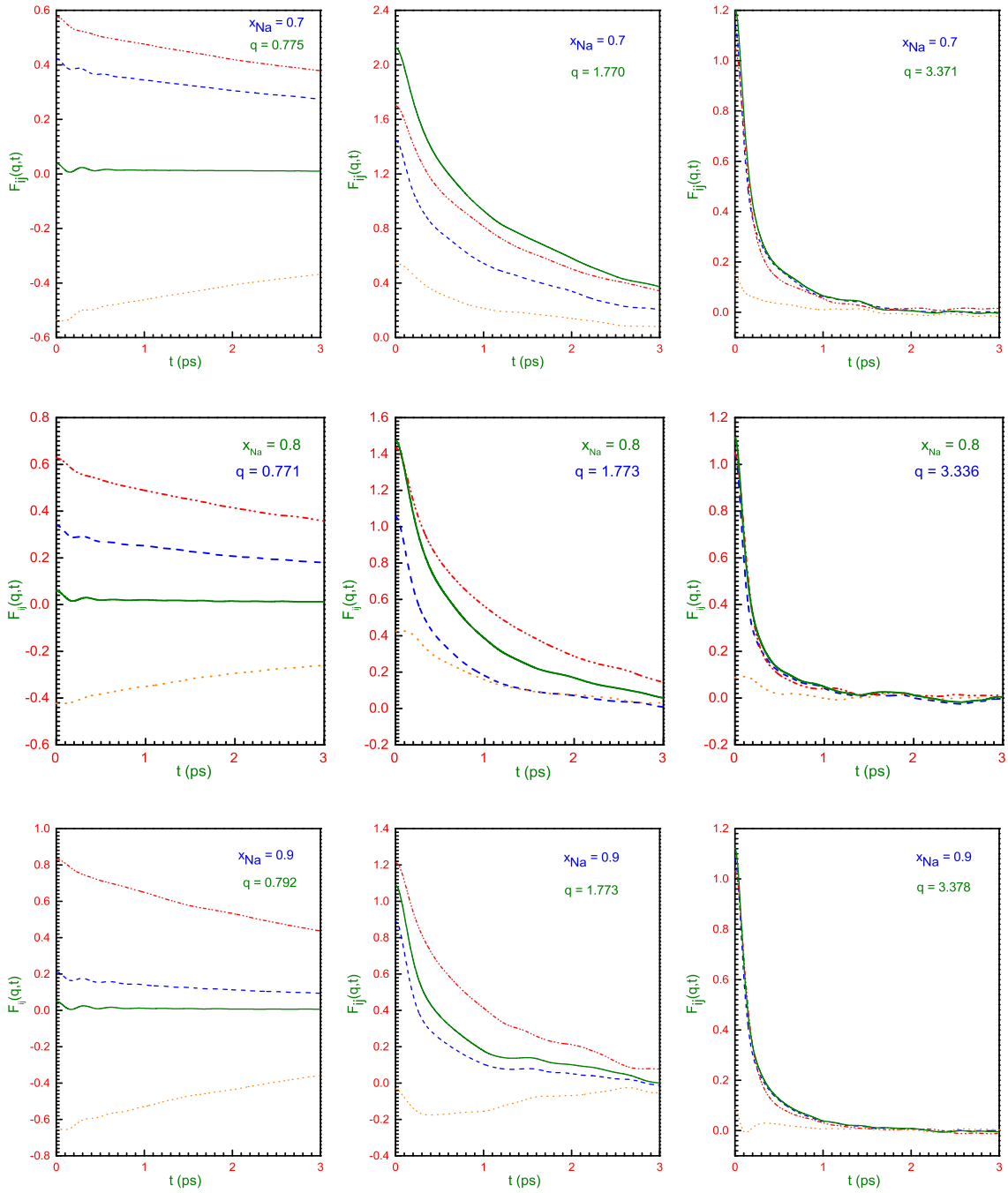

Figure 6.11: Partial ISF, $F_{ij}(\mathbf{q},t)$ of the Na_xK_{1-x} liquid alloy at several q values for x_{Na}=0.7, 0.8 and 0.9 at $T = 373$ K. The blue, red, orange and olive colours are for $F_{\mathrm{NaNa}}(\mathbf{q},t)$, $F_{\mathrm{KK}}(\mathbf{q},t)$, $F_{\mathrm{NaK}}(\mathbf{q},t)$ and $F_{\mathrm{NN}}(\mathbf{q},t)$, respectively.

6.5.2 Dynamic Structure Factors

The dynamic structure factor $S(\mathbf{q},\omega)$ is closely connected with $F(q,t)$. The time Fourier Transformation (FT) of the OF-AIMD $F_{ij}(q,t)$ in the ω-domain yields the partial dynamic structure factors (PDSF) $S_{ij}(\mathbf{q},\omega)$ (with an appropriate window to smooth out truncation effects). Its importance lies in its direct connection to the inelastic neutron scattering or the IXS data. The intensity observed in an inelastic x-ray scattering (IXS) experiment and, the coherent component of the intensity in inelastic neutron scattering (INS) have direct relations with $S_{ij}(\mathbf{q},\omega)$. To the best of our knowledge only a few preliminary measurements for $S(q,\omega)$ through INS and IXS for different concentrations of liquid Na_xK_{1-x} alloys are available. So we have intended to compare our OF-AIMD value with those data where appropriate. We noticed that for small q's, $S_{\mathrm{NN}}(q,\omega)$ show Rayleigh-Brillouin type structure which is similar to that of the one component systems near to the hydrodynamic region, except the extended central line caused by the inter-diffusion processes. We have reported the results for the $S_{ij}(\mathbf{q},\omega)$ for several q values in Figure 6.12. Calculated $S_{ij}(q,\omega)$ shows the following general trends: (i) show side-peaks, indicative of collective density excitation's, for small q and (ii) for large q-values, $S_{ij}(q,\omega)$ decreases monotonically. The appearance of the side peaks depends on the range of concentrations, as depicted in Figure 6.12.

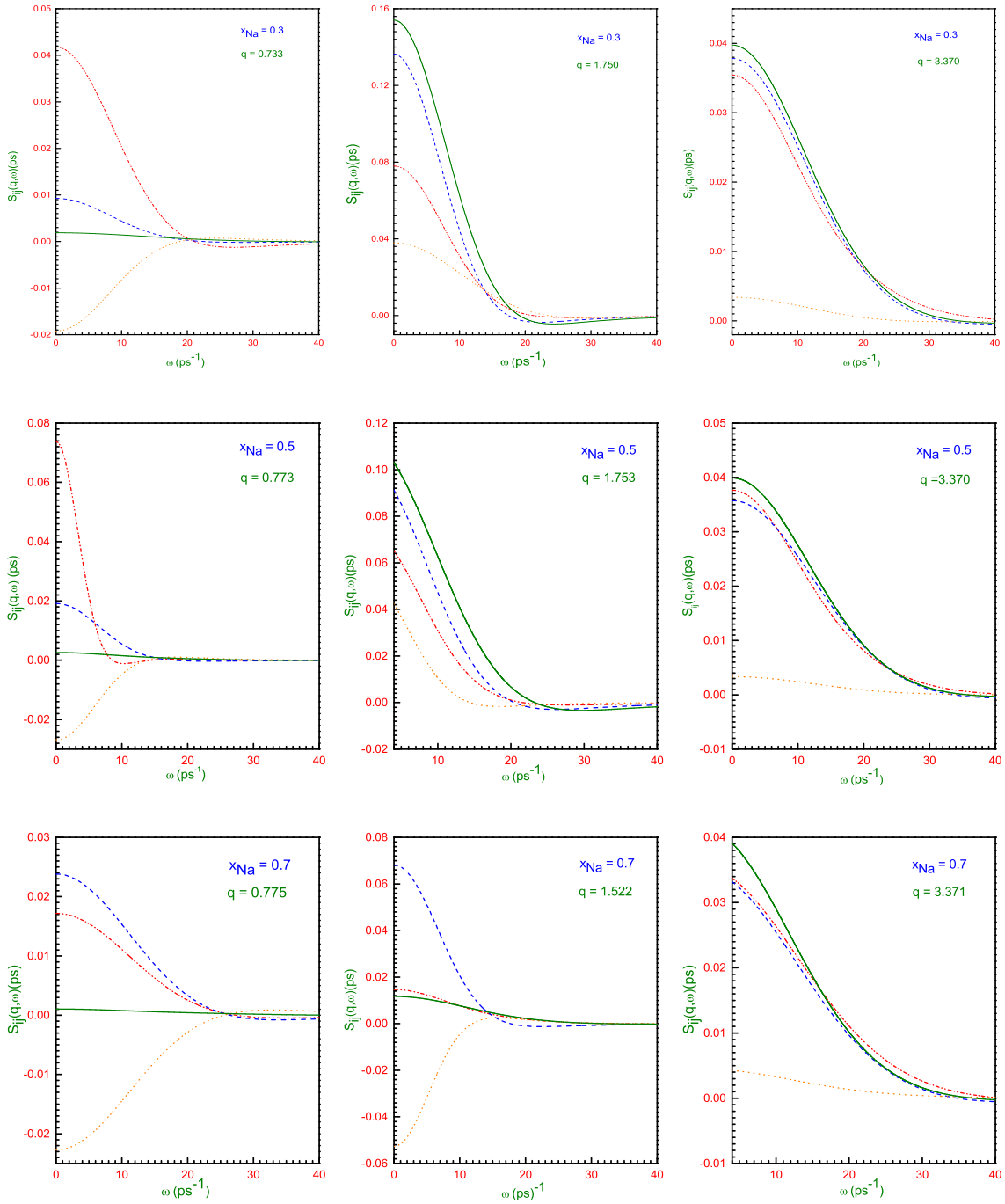

Figure 6.12: PDSF, $S_{ij}(\mathbf{q},\omega)$ of Na_xK_{1-x} liquid alloy for $x_{\rm Na} = 0.3$, 0.5 and 0.7. Red dash dot dot, blue dash, orange dot and olive lines are for $S_{\rm NaNa}(\mathbf{q},\omega)$, $S_{\rm KK}(\mathbf{q},\omega)$, $S_{\rm NaK}(\mathbf{q},\omega)$ and $S_{\rm NN}(\mathbf{q},\omega)$, respectively.

6.5.3 Longitudinal Current Correlation Functions, Dispersion Relations and Adiabatic Sound Velocity

The particle current with the j-type component [147] $\mathbf{j}_j(\mathbf{q},t)$ is often divided into a longitudinal component $\mathbf{j}_j^L(\mathbf{q},t)$, and a transverse component $\mathbf{j}_j^T(\mathbf{q},t)$. The former one is parallel and the latter one is perpendicular to $\mathbf{q}$ and these are also interesting dynamical functions. The partial longitudinal current correlation functions (PLCCF) and transverse current correlation functions (TCCF), $C_{\rm ij}^{\rm L}(\mathbf{q},t)$ and $C_{ij}^T(\mathbf{q},t)$ to be acquired from the relation $C_{\rm ij}^{\rm L}(\mathbf{q},t) = \langle \mathbf{j}_{\rm j}^{\rm L}(\mathbf{q},t).\mathbf{j}_{\rm j}^{\rm L}*(\mathbf{q},0)\rangle$ and $C_{\rm ij}^{\rm T}(\mathbf{q},t) = \frac{1}{2}\langle \mathbf{j}_{\rm j}^{\rm T}(\mathbf{q},t).\mathbf{j}_{\rm j}^{\rm T}*(\mathbf{q},0)\rangle$. The related time FT results in the corresponding spectrum of $C_L(q,\omega)$ and $C_T(q,\omega)$, where $C_L(q,\omega) = \frac{\omega^2 S(q,\omega)}{q^2}$. These dynamical magnitudes were computed from the configurations produced in the current OF-AIMD simulations. All of the previous correlation functions for isotropic systems rely solely on the equation $q = |\mathbf{q}|$.

The estimated PLCCF, $C_{\rm ij}^{\rm L}(\mathbf{q},t)$ are displayed in Figure 6.13 for the concentrations $x_{{\rm Na}a}$ = 0.3, 0.5 and 0.7 for various q values. The partial current correlation function $C_{\rm KK}^{\rm L}(\mathbf{q},t)$ and $C_{\rm NaK}^{\rm L}(\mathbf{q},t)$ oscillate precisely at similar phase for concentrations of $x_{\rm Na}$ = 0.3, 0.5 and 0.7 for all q's as shown in the figure. Contrarily, for the concentration of $x_{{\rm Na}a}$ = 0.3 (q = 0.423, 1.305) and 0.5 (q = 0.421, 1.321) oscillations of $C_{\rm NN}^{\rm L}(\mathbf{q},t)$ shifts to the right side from $C_{\rm NaNa}^{\rm L}(\mathbf{q},t)$. For $x_{\rm Na}$ = 0.7 and q = 0.420 the oscillation of $C_{\rm NN}^{\rm L}(\mathbf{q},t)$ shifts toward the right from $C_{\rm NaNa}^{\rm L}(\mathbf{q},t)$ but for q = 1.013 oscillation of $C_{\rm NaNa}^{\rm L}(\mathbf{q},t)$ and $C_{\rm NN}^{\rm L}(\mathbf{q},t)$ are in phase. In this case, we observe that as time t increases, the oscillation's amplitude monotonically decreases to zero.

Figure 6.14 illustrate the PLCCF for the four distinct concentrations of $x_{{\rm Na}a}$ = 0.3, 0.5, 0.6 and 0.7 that are originated from the OF-AIMD simulations. Longitudinal

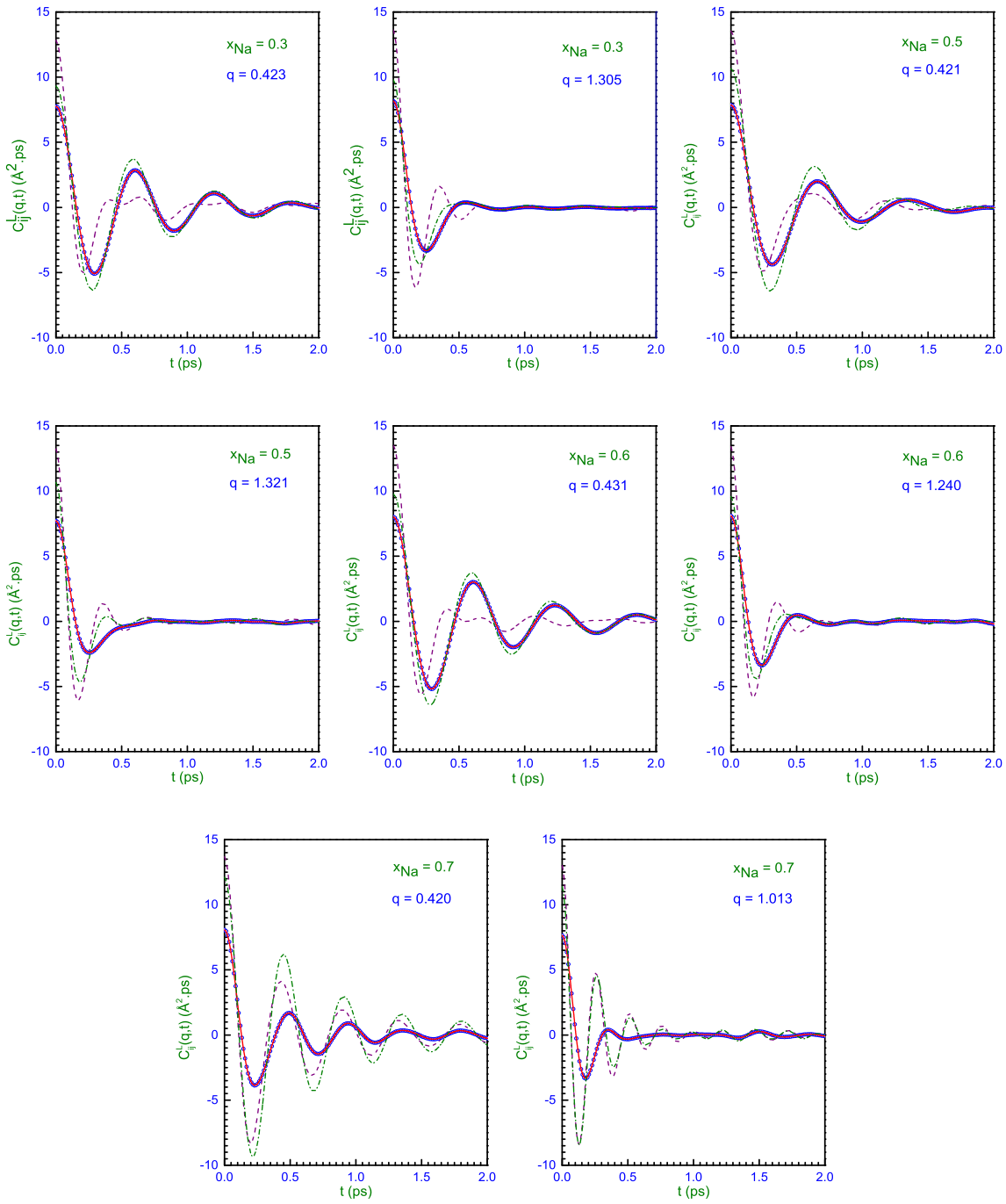

Figure 6.13: PLCCF, $C^L_{\rm ij}(q,t)$ for Na_xK_{1-x} liquid alloy at 373 K for $x_{\rm Na}$= 0.3, 0.5, 0.6 and 0.7. The purple dashed, red solid line, blue open circle and olive dot dashed represent $C^L_{\rm NaNa}(q,t)$, $C^L_{\rm KK}(q,t)$, $C^L_{\rm NaK}(q,t)$ and $C^L_{\rm NN}(q,t)$ respectively.

current correlation functions $C^{\mathrm{L}}_{\mathrm{ij}}(\mathbf{q},\omega)$ can be used to gather data regarding the longitudinal collective modes. For all q's, we can see that, there is at least one peak of $C^{\mathrm{L}}_{\mathrm{KK}}(\mathbf{q},\omega)$ and $C^{\mathrm{L}}_{\mathrm{NaK}}(\mathbf{q},\omega)$ coincides at a certain frequency.

Figure 6.14 shows that for $x_{\mathrm{Na}} = 0.3$ and $q = 0.423$, the peaks of $C^{\mathrm{L}}_{\mathrm{KK}}(\mathbf{q},\omega)$, $C^{\mathrm{L}}_{\mathrm{NaK}}(\mathbf{q},\omega)$ and $C^{\mathrm{L}}_{\mathrm{NN}}(\mathbf{q},\omega)$ appear at the same frequency $\omega = 10.16$ ps^{-1}. But the peak of $C^{\mathrm{L}}_{\mathrm{NaNa}}(\mathbf{q},\omega)$ shifts to the right and located at $\omega = 12.70$ ps^{-1}. It is also noticed that for $x_{\mathrm{Na}} = 0.3$ and $q = 1.305$ peaks of $C^{\mathrm{L}}_{\mathrm{KK}}(\mathbf{q},\omega)$, $C^{\mathrm{L}}_{\mathrm{NaK}}(\mathbf{q},\omega)$ remain at the same ω but of $C^{\mathrm{L}}_{\mathrm{NaNa}}(\mathbf{q},\omega)$ and $C^{\mathrm{L}}_{\mathrm{NN}}(\mathbf{q},\omega)$ shift toward the right side. For the concentration $x_{\mathrm{Na}} = 0.5$ and $q = 0.421$, the peaks of $C^{\mathrm{L}}_{\mathrm{KK}}(\mathbf{q},\omega)$, $C^{\mathrm{L}}_{\mathrm{NaK}}(\mathbf{q},\omega)$ and $C^{\mathrm{L}}_{\mathrm{NN}}(\mathbf{q},\omega)$ appear at the same frequency $\omega = 9.48$ ps $^{-1}$. But the peak of $C^{\mathrm{L}}_{\mathrm{NaNa}}(\mathbf{q},\omega)$ shifts to the right and located at the frequency $\omega = 10.65$ ps^{-1}. It is further noted that for $x_{\mathrm{Na}} = 0.5$ and $q = 1.321$ peaks of $C^{\mathrm{L}}_{\mathrm{KK}}(\mathbf{q},\omega)$ and $C^{\mathrm{L}}_{\mathrm{NaK}}(\mathbf{q},\omega)$ remain at the same ω but $C^{\mathrm{L}}_{\mathrm{NaNa}}(\mathbf{q},\omega)$ and $C^{\mathrm{L}}_{\mathrm{NN}}(\mathbf{q},\omega)$ shift toward the right side.

Figure 6.14 shows that for $x_{\mathrm{Na}} = 0.6$ and $q = 0.431$, the peaks of $C^{\mathrm{L}}_{\mathrm{KK}}(\mathbf{q},\omega)$, $C^{\mathrm{L}}_{\mathrm{NaK}}(\mathbf{q},\omega)$ and $C^{\mathrm{L}}_{\mathrm{NN}}(\mathbf{q},\omega)$ appear at the same frequency $\omega = 10.23$ ps^{-1}. But the peak of $C^{\mathrm{L}}_{\mathrm{NaNa}}(\mathbf{q},\omega)$ shifts to the right and appears at $\omega = 13.06$ ps^{-1}. Additionally, it is noted for $x_{\mathrm{Na}} = 0.6$ and $q = 1.240$ that peaks of $C^{\mathrm{L}}_{\mathrm{KK}}(\mathbf{q},\omega)$, $C^{\mathrm{L}}_{\mathrm{NaK}}(\mathbf{q},\omega)$ keeping the same ω but $C^{\mathrm{L}}_{\mathrm{NaNa}}(\mathbf{q},\omega)$ and $C^{\mathrm{L}}_{\mathrm{NN}}(\mathbf{q},\omega)$ shift toward the right side. For the concentration $x_{\mathrm{Na}} = 0.7$ and $q = 0.420$, the peaks of $C^{\mathrm{L}}_{\mathrm{KK}}(\mathbf{q},\omega)$ and $C^{\mathrm{L}}_{\mathrm{NaK}}(\mathbf{q},\omega)$ appear at the same frequency $\omega = 12.48$ ps^{-1} but of $C^{\mathrm{L}}_{\mathrm{NaNa}}(\mathbf{q},\omega)$ and $C^{\mathrm{L}}_{\mathrm{NN}}(\mathbf{q},\omega)$ are slightly shifted toward right and appear at $\omega = 14.06$ ps^{-1}. On the other hand, for $x_{\mathrm{Na}} = 0.7$ and $q = 1.013$ peaks of $C^{\mathrm{L}}_{\mathrm{KK}}(\mathbf{q},\omega)$ and $C^{\mathrm{L}}_{\mathrm{NaK}}(\mathbf{q},\omega)$ show up at $\omega = 15.60$ ps^{-1} but $C^{\mathrm{L}}_{\mathrm{NaNa}}(\mathbf{q},\omega)$ and $C^{\mathrm{L}}_{\mathrm{NN}}(\mathbf{q},\omega)$ shifts toward the right side with $\omega = 23.58$ ps^{-1}.

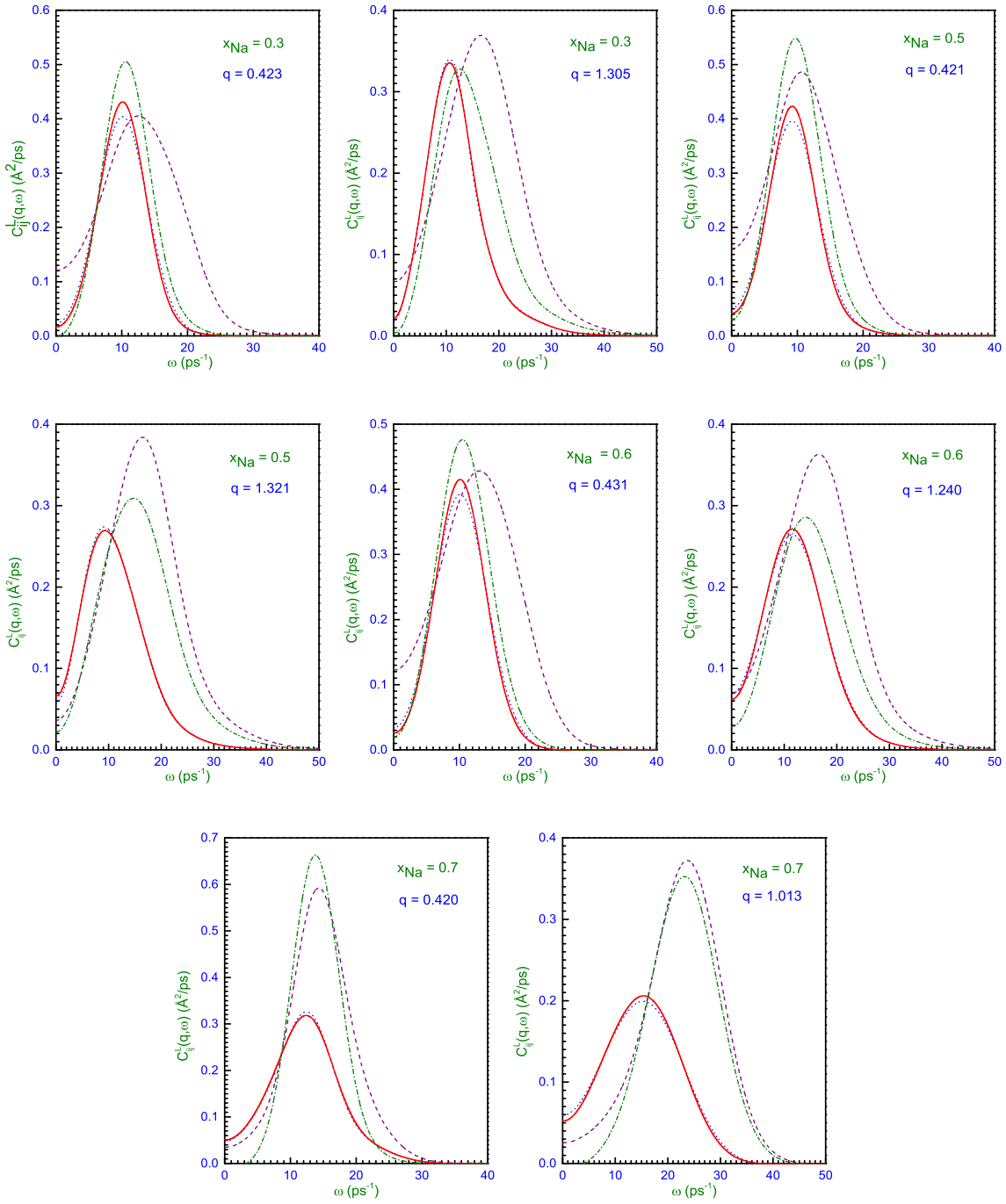

Figure 6.14: PLCCF spectra $C^L_{ij}(q,\omega)$ for Na_xK_{1-x} liquid alloy at 373 K for x_{Na} = 0.3, 0.5, 0.6 and 0.7. The purple dashed, red solid line, blue dot and olive dot dashed represent $C^L_{NaNa}(q,\omega)$, $C^L_{KK}(q,\omega)$, $C^L_{NaK}(q,\omega)$ and $C^L_{NN}(q,\omega)$ respectively.

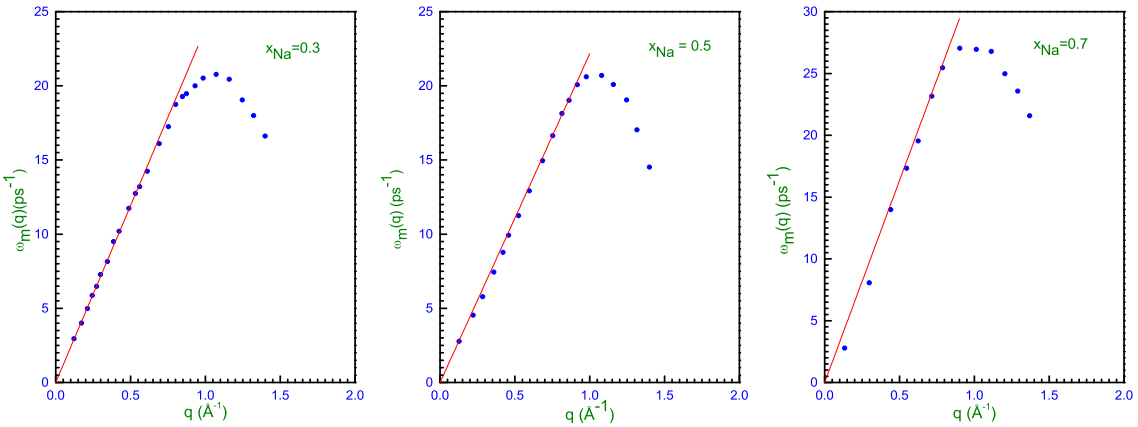

Figure 6.15: Longitudinal dispersion relation for the liquid Na_xK_{1-x} alloy at 373 K for the concentration, $x_{\rm Na}$= 0.3, 0.5 and 0.7. Full circles: peak positions $\omega_m(q)$ from the OF-AIMD $C_L(q,\omega)$. Solid line: linear dispersion for the adiabatic sound velocities.

Table 6.9: Adiabatic sound velocities, c_s, for $l-$ Na_xK_{1-x} alloy at 373K.

Concent.	Temperature	c_s (m/s)	
$x_{\rm Na}$	K	OF-AIMD	Expt.
0.1		3652.83±3.45	.....
0.2		4424.11±1.62	.....
0.3		2504.30±3.13	.....
0.4		4477.30±1.74	2023±5
0.5	373	2271.30±9.57	1998.00
0.6		2414.23±1.35	2145±5
0.7		3250.90±1.70	2196±5
0.8		4461.02±2.20	.....
0.9		2504.30±1.13	2345±5

The longitudinal dispersion relation $\omega^L_{\rm NN}(q)$ (average frequency) for the concentrations, $x_{\rm Na}$ = 0.3, 0.5 and 0.7 is depicted in Figure 6.15. We have estimated the adiabatic sound velocity of these modes employing the relation $c_s = \frac{\omega_B(q_{min})}{q_{min}}$. Here it is estimated on the basis of the location of the Brillouin peak at q_{min}, $\omega_B(q_{min})$. Table 6.9 presents the computed adiabatic sound velocity c_s. We notice that, for the

concentration of $x_{\mathrm{Na}} = 0.5$, the experimentally determined value of adiabatic sound velocity [159] is quite close to the value calculated by our OF-AIMD method. For the concentration of $x_{\mathrm{Na}} = 0.4$, 0.6, 0.7 and 0.9 the experimental results are taken from Abowitz *et al.* [152], which are favourable to our calculated results. The experimental adiabatic sound velocity for other four concentrations are not available to us.

6.5.4 Transverse Current Correlation Functions and Shear Viscosity

The total transverse current correlation function can be used to calculate the shear viscosity, η of alloys. The total transverse current correlation function is defined by $C_t^T(q,t) = \langle j_t^T(q,t) * j_t^T(q,0)\rangle$, where the total transverse current is $j_t^T(q,t) = x_1^{1/2} m_1 j_1^T(q,t) + x_2^{1/2} m_2 j_2^T(q,t)$. Simple liquid alloys exhibit η variations with concentration. This is either linear or slightly deviated from linearity; positive deviations are typically observed in those alloys with pronounced homo-coordination tendencies. The partial transverse current correlation function (PTCCF), $C_{ij}^T(q,t)$ is shown in Figure 6.16 for $x_{Na} = 0.3$, 0.5, 0.6, and 0.7 for several different q values. The transverse current correlation function exhibits oscillating behaviour, as seen from the figure at low q. When q is large the amplitude of oscillation's decreases with increasing time.

The partial current correlation spectrum $C_{ij}^T(q,\omega)$ is provided by the time FT of $C_{ij}^T(q,t)$. The PTCCF spectrum $C_{ij}^T(q,\omega)$ can be used to identify whether the shear modes are present in the system or not. These modes are not directly related to any observable parameter. Hence the only tools available for their investigation are

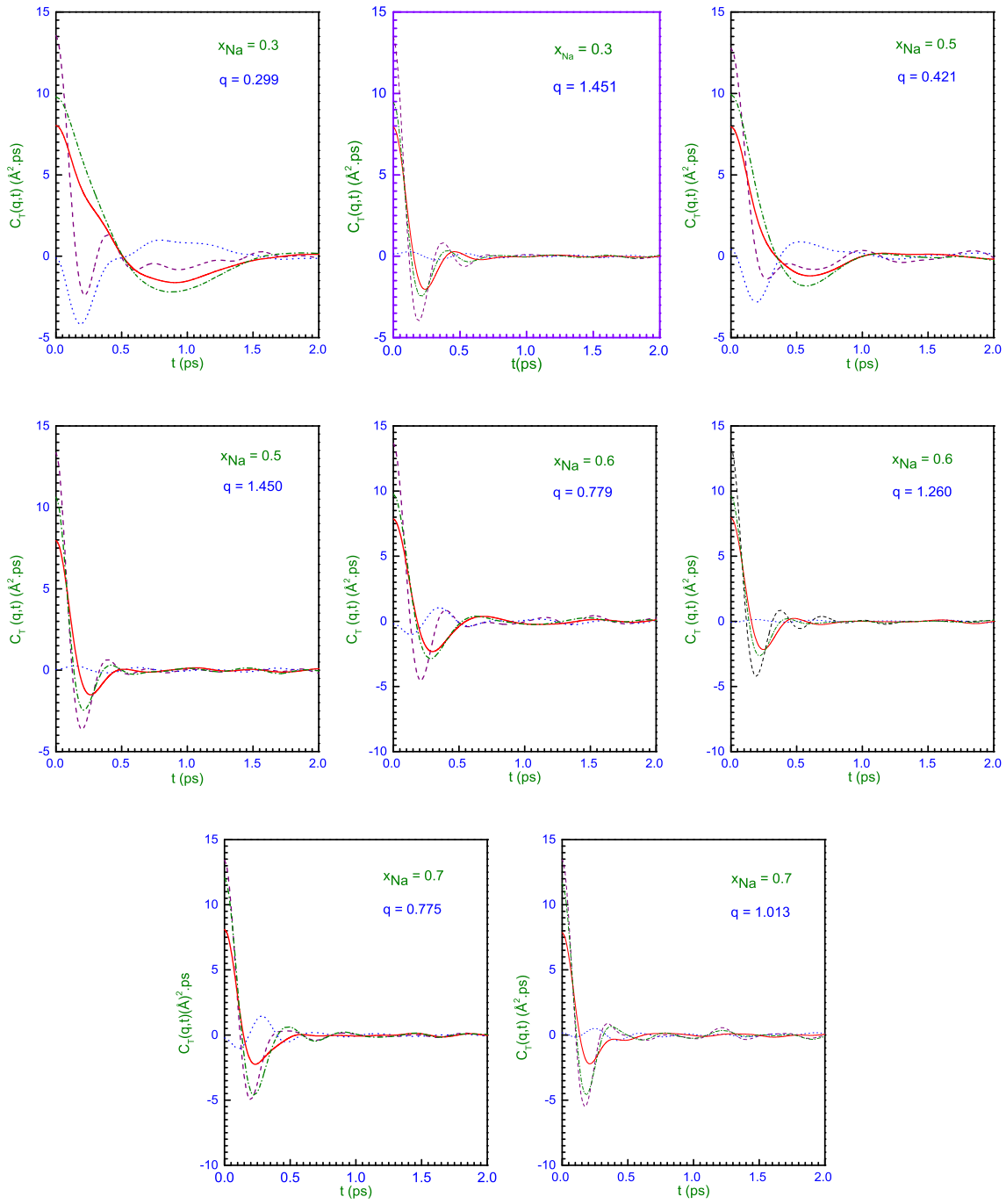

Figure 6.16: PTCCF, $C_{ij}^{T}(q,t)$ for Na_xK_{1-x} liquid binary alloy at 373 K for the concentrations, $x_{\mathrm{Na}} = 0.3$, 0.5, 0.6 and 0.7 at several q values. The purple dashed, red solid line, blue dot and olive dot dashed represent $C_{\mathrm{NaNa}}^{T}(q,t)$, $C_{\mathrm{KK}}^{T}(q,t)$, $C_{\mathrm{NaK}}^{T}(q,t)$ and $C_{\mathrm{NN}}^{T}(q,t)$ respectively.

theoretical models or MD simulations. A few investigations on transverse currents in liquids have been conducted, and those that have intended to focus on one-component systems have discovered that $C^T(q,\omega)$ evolves [43,44] as a function of ω from a Gaussian (when $q \to \infty$) toward a Lorentzian curve (when $q \to 0$). Transverse modes are unable to spread in these harsh conditions, but at intermediate q's, the $C^T(q,\omega)$, may have a peak that is associated with propagating shear waves. The first CMD simulations of transverse current correlations in binary liquids were performed on molten salts. The peak of $C^T_{\mathrm{NN}}(q,\omega)$ was at intermediate q's, just like in single component liquids. Furthermore, a peak in the charge-charge transverse current correlation curves was seen for both small and intermediate q's. The hydrodynamic limit revealed a connection between this peak and transverse optical modes with a finite frequency.

Table 6.10: Calculated OF-AIMD viscosity, η is compaired with KS-AIMD value computed by J. F. Wax, the experimental results of Kitajima and Potter [160] of l-$\mathrm{Na}_x\mathrm{K}_{1-x}$ alloy at thermodynamic state 373K.

Con.	Temp.	η (GPa.ps)				
x_{Na}	K	OF-AIMD	LT app.	Wax Sim.	Kitajima exp.	Potter exp.
0.1		0.47	...	0.36	0.42	0.46
0.2		0.47	...	0.37	0.44	0.47
0.3		0.50	0.48	0.39	...	0.45
0.4		0.49	...	0.41	...	0.49
0.5	373	0.53	0.53	0.43	0.48	0.51
0.6		0.59	0.56	0.46	0.51	0.55
0.7		0.59	0.59	0.49	...	0.56
0.8		0.60	...	0.49	...	0.59
0.9		0.63	0.65	0.49	0.57	0.63

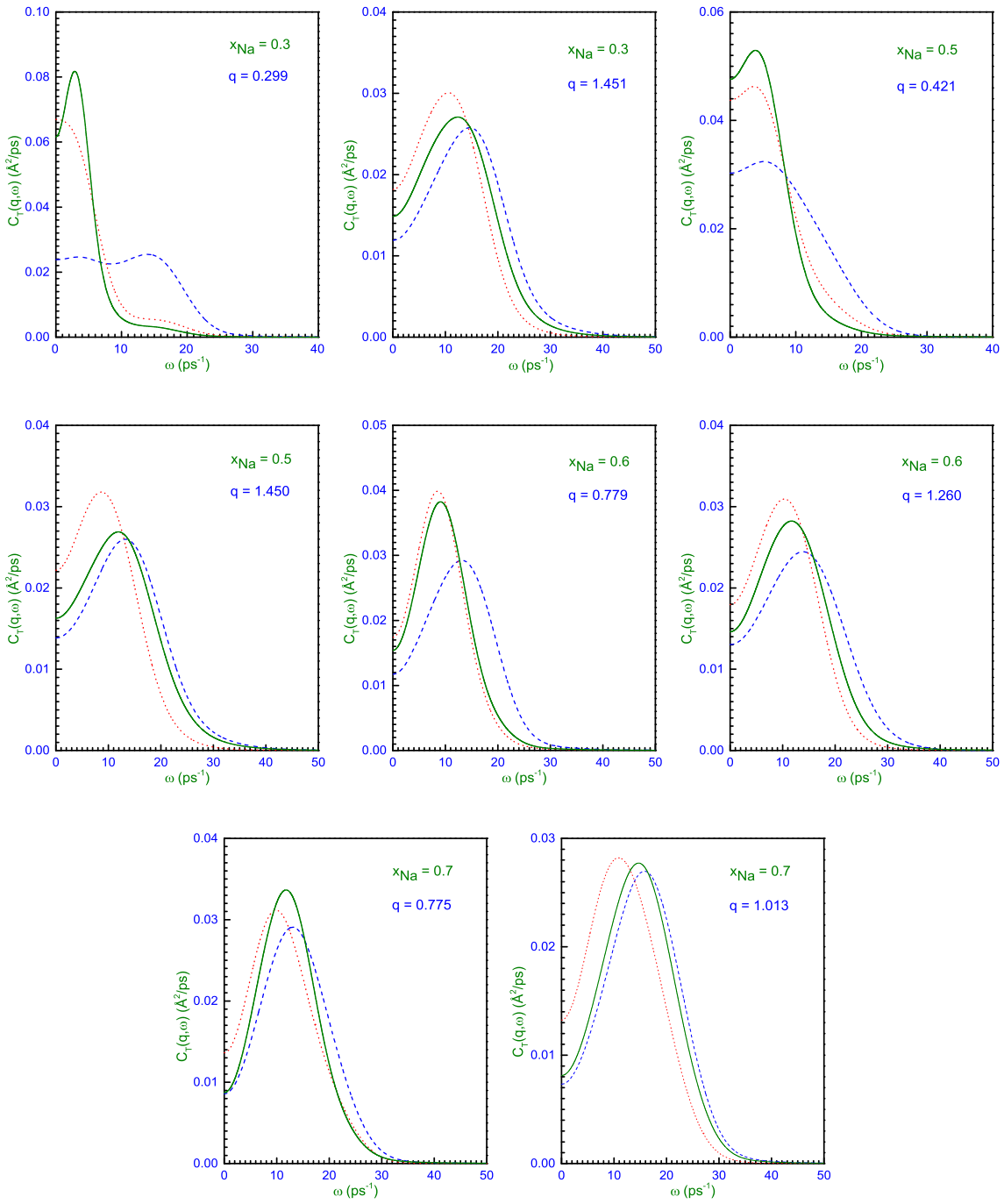

Figure 6.17: PTCCF spectrum, $C_{ij}^{T}(q,\omega)$ for Na_xK_{1-x} liquid binary alloy at 373K for the concentrations, $x_{\mathrm{Na}} = 0.3$, 0.5, 0.6 and 0.7 at several q values. The blue dashed, red dot and olive solid line represent PTCCF namely, $C_{\mathrm{NaNa}}^{T}(q,\omega)$, $C_{\mathrm{KK}}^{T}(q,\omega)$ and $C_{\mathrm{NN}}^{T}(q,\omega)$ respectively.

For binary Lennard-Jones systems and metallic alloys, additional CMD research has identified optical-like modes associated with $C^T_{\rm CC}(q,\omega)$. Figure 6.17 shows some calculated $C^T_{ij}(q,\omega)$ for different q values at concentrations, $x_{\rm Na}$ = 0.3, 0.5, 0.6 and 0.7. As can be seen from the figures that $C^T_{\rm NaNa}(q,\omega)$ and $C^T_{\rm KK}(q,\omega)$ for the smallest q's achieved in the simulations as mentioned in section 6.5.1 do not exhibit a peak. However, for $q = 0.299$ Å^{-1} and $x_{\rm Na} = 0.3$, $C^T_{\rm NN}(q,\omega)$ strat to exhibits a peak. Whereas all components $C^T_{\rm NaNa}(q,\omega)$, $C^T_{\rm KK}(q,\omega)$ and $C^T_{\rm NN}(q,\omega)$ for q>0.299 the spectrum display distinct and clear peak. It is also found from the same figure that for, $x_{\rm Na}$ = 0.6 and 0.7 the pre peaks of $C^T_{\rm NaNa}(q,\omega)$, $C^T_{\rm KK}(q,\omega)$ and $C^T_{\rm NN}(q,\omega)$ are just appear for q = 0.779 Å^{-1} and 0.775Å^{-1} respectively. While peaks of all components become very prominent for q = 1.260 Å^{-1} and 1.013Å^{-1} for concentrations, $x_{\rm Na}$ = 0.6 and 0.7 respectively. It is interestingly observed that as q rises, $C^T_{\rm NN}(q,\omega)$ rapidly decreases. It is to be note here that for convinience we do not present the figures for concentrations, $x_{\rm Na}$ = 0.1, 0.2, 0.4, 0.8 and 0.9.

The $C^T_{\rm NN}(q,t)$ provides details on the typical behaviour of the system. It already displays a high frequency peak at q_{min} that is comparable to that of $C^T_{\rm NaNa}(q,\omega)$. We consider the influence of the composition on the viscosity of alloys. Our results at 373K for nine concentrations are displayed in Table 6.10, as well as experimental data from S. Becker *et. al* [160]. We simulated nine regularly varying compositions at 373K to explore the properties *e.g.* viscosity of Na_xK_{1-x} liquid binary alloys at those states. Our calculated results are very good in agreement with the experimental data [31] within the uncertainty of experiment. Our calculation exactly reproduce experimental data [31] for the concentration, $x_{\rm Na} = 0.2, 0.4$ and 0.9. For the concentrations, $x_{\rm Na}$ =

$0.1, 0.3, 0.5, 0.6, 0.7$ and 0.8 our claculated results are slightly overestimated which lies in between 1.69% to 11.11%. Whereas the calculated results of Wax is under estimated by 12.5% to 22.22% in the whole concentrations range. The trends of the experimental and all simulated results are similar.

We have also presented experimental results of Kitajima although we do not have the results for all concentrations. Whatever the results we have, we see that the Kitajima's results are slightly under estimated from the potter results [31]. We do not have any information regarding the experimental uncertainties between these two experiments. But our results mostly reproduced the Potter's experimental data [31]. The evolution of the viscosity of Na_xK_{1-x} vs concentration curve is rather smooth due to the additivity of the pair interactions which leads to homocoordination tendencies in the alloy.

We have calculated the shear viscosity of the alloy from the OF-AIMD results from the $C_t^T(q,t)$. Table 6.10 illustrates the OF-AIMD values for the shear viscosity. Similar trends are also seen in the results obtained from Linear trajectory (LT) approximation method by Helfhand [161]. OF-AIMD results for $x_{\mathrm{Na}} = 0.5$, 0.7 exactly coincide with the values that are calculated by using the LT approximation method. Here, we would like to note that our OF-AIMD results agreed very well with the LT approximation [161].

Chapter 7

Conclusions

7.1 Conclusions

We have presented results of the OF-AIMD simulation study for some static properties and dynamic properties of Na_xK_{1-x} liquid binay alloys for nine different concentrations near their melting temperatures. Here, $E_{xc}[n]$ functionals are treated by using the LDA and, the electron -ion interaction by a local pseudopotential. Present OF-AIMD results are reliable and accurate as much as the DFT and as the LDA are valid.

The OF-AIMD total static structure factor, $S_T(q)$, is quite good in agreement with the x-ray diffraction data [149]. A detailed analysis of the ionic configurational data of the atoms generated by the OF-AIMD for the alloy indicates the presence of the homo-coordinate tendency. This trend becomes more marked with the increase of Na concentration in the alloy. The above tendencies are farther confirmed by calculating the well-known SRO parameters.

In the case of single particle dynamics, we have started with the VACF $Z_{ij}(t)$ which illustrates the back scattering effects when t is small. The diffusion coefficients calculated from time integral of $Z_{ij}(t)$ and from the Stoke-Einstein relation are very close to each other in magnitude for the system under study. The agreement found in this case is within a few percent of experimental values. The present OF-AIMD results allows us to say that the slip boundary condition associated with the Stokes-Einstein (SE) theory is appropriate for liquid Na_xK_{1-x} binary alloy. This result also indicates that, the molecules in the liquid binary alloys under study are exhibiting different kind of Brownian motion than that of the suppercooled liquid or glass. It is informative that the structural relaxation time τ can be derived from the equation $F_s(q,\tau) = \frac{1}{e}$ for any $\vec{q}$. As $F_s(q,t)$ is controlled by the self-diffusion coefficients, the knowledge of τ is sometimes useful to examine the break down limit of the Stokes-Einstein relation.

Effects of the collective dynamics, for example dynamical structure factor $S_{ij}(q,\omega)$ or adiabatic sound velocity (ASV) show the appropriate physical trends, and agree well with the corresponding experimental values. For instance, the positions of the side peak of $S_{ij}(q,\omega)$ for different values of q yields a dispersion curve. The slope of this dispersion curve at $q \to 0$ provides the value for the ASV. ASV thus obtained is found to be good in agreement for the liquid Na_xK_{1-x} binary alloy. The OF-AIMD shear viscosity, η, also agree well with the available experimental values and also with the values of some model calculations. We can infere that $C^T_{ij}(q,\omega)$ displays prepeak for all component with increasing q values, but at smallest possible q prepeaks are not seen for all concentrations under study.

Structural properties predicted by the present simulation study are having the same accuracy as that of the AIMD [149] as far as the agreement with experimental values is concerned. From a careful look it appears that, values obtained from the $S(q)$ and $g(r)$ (for instance, coordination number, isothermal compressibility etc.) are found to be even better in agreement with the available experimental data than that of AIMD [150]. In the case of dynamics namely the self diffusion coefficients (SDC) and ASV. Similar trends are also observed. These evidences, however, do not allow us to claim that OF-AIMD is better in accuracy than AIMD, but we can say that we are fortunate in selecting the potential parameters.

Finally, in the Conclusion we can say that the OF-AIMD simulation technique is very much reliable and, can predict the static properties and dynamic properties of liquid Na_xK_{1-x} binary alloys well at near its melting point. Comparison of the OF-AIMD and AIMD results from the point of view of the agreement with experiment suggests that accuracy of the former method is as good as the latter one for the case of Na_xK_{1-x} liquid binary alloys. This might happaned due to the advantage of taking more particles in the sample for the OF-AIMD than AIMD. The simulation work on other liquid alkali metal alloys is also in progress. Results of these will be published when completed.

The OF-AIMD simulation results presented in this thesis provide a useful information and better understanding on the static and the dynamic properties of Na_xK_{1-x} liquid binary alloys. So, it is natural to expect that these information can be useful for those who are interested to have a better understanding of the alkali metal alloy, in particular, to use liquid alkali metal alloys as a coolant in the nuclear reactors.

Appendix A

Collective Dynamics in Liquid Alloys

The definitions of the magnitudes used in this study are provided here. Some of them are rather common and are covered in a wide range of reliable references. We take into account a binary system with N_1 and N_2 particles of each type. Concentrations $x_i = \frac{N_i}{(N_1+N_2)} = \frac{N_i}{N}$, and the total number density, $\rho = \frac{N}{V}$ with a volume V.

Starting in Fourier space, where the average is calculated over wavevectors and time origins using the same module, we begin with partial microscopic number densities.

$$\rho_{ij}(q,t) = \frac{1}{\sqrt{N_j}} \sum_{l=1}^{N_j} e^{[-i\mathbf{q}.\mathbf{r}_l^{(j)}(t)]} \qquad (j = 1, 2) \tag{A.1}$$

The definition of AL partial intermediate scattering functions, $F_{ij}(q,t)$ is

$$\begin{aligned} F_{ij}(q,t) &= \langle \rho_i(\mathbf{q}, t+t_0)\rho_j(-\mathbf{q}, t_0)\rangle \\ &= \frac{1}{\sqrt{N_i N_j}} \langle \sum_{l=1}^{N_i} e^{[-i\mathbf{q}.\mathbf{r}_l^{(i)}(t+t_0)]} \sum_{n=1}^{N_j} e^{[-i\mathbf{q}.\mathbf{r}_n^{(j)}(t_0)]} \rangle \end{aligned} \tag{A.2}$$

These functions' initial values are the static AL partial structure factors, $S_{ij}(q) = F_{ij}(q, t = 0)$, which are connected to the partial PDF, $g_{ij}(r)$, through the time FT.

$$S_{ij}(q) = \delta_{ij} + \rho\sqrt{(x_i x_j)} \int [g_{ij}(r) - 1] e^{[-\mathbf{q}.\mathbf{r}]} d\mathbf{r}. \tag{A.3}$$

The ISF can also be separated in a similar manner, as

$$F_{ij}(q,t) = F_j^s(q,t)\delta_{ij} + \sqrt{(x_i x_j)} F_{ij}^d(q,t). \tag{A.4}$$

where $F_j^s(q,t)$ indicates the self part, this relates to the autocorrelation of the j-type single-particle density, $\rho_j^s(q,t) = e^{[-i\mathbf{q}.\mathbf{r}_n^j(t)]}$. Here, n can have any value between 1 to N_j, and $F_j^s(q,t) = \langle \rho_j^s(\mathbf{q}, t+t_0)\rho_j^s(-\mathbf{q}, t_0)\rangle$ includes an additional average over similar-type particles. The second component in equation (A.4) corresponds to the terms in $F_{ij}(q,t)$ that do not share any particles in the double sum that defines equation (A.2).

The PDSF for AL are defined by the time FT into frequency domain,

$$S_{ij}(q,\omega) = \frac{1}{2\pi} \int F_{ij}(q,t) e^{[i\omega t]} dt. \tag{A.5}$$

Appendix B

Total Static Structure Factor

The system can be configured repeatedly through molecular dynamic (MD) simulations. As a result, it is possible to calculate the partial pair distribution functions (PDF), $g_{ij}(r)$, given the positions of the atoms in the simulation box. Both the topological and chemical order are described by these functions. Bathia and Thornton's [162] partial structural factors provide an excellent illustration of these characteristics.

The BT partials are defined as the sum of the magnitudes of the AL partials

$$\begin{aligned} S_{\mathrm{NN}}(q) &= x_1 S_{11}(q) + x_2 S_{22}(q) + 2\sqrt{(x_1 x_2)} S_{12}(q) \\ S_{\mathrm{CC}}(q) &= x_1 x_2 [x_2 S_{11}(q) + x_1 S_{22}(q) - 2\sqrt{(x_1 x_2)} S_{12}(q)] \\ S_{\mathrm{NC}}(q) &= S_{11}(q) - S_{22}(q) + (x_2 - x_1)/\sqrt{(x_1 x_2)} S_{12}(q). \end{aligned} \tag{B.1}$$

The first one calculates the relationship between the local density of atoms, regardless of their chemical composition. As a result, it is connected to the topological order. The second one gauges the relationship between the local composition and is

connected to the chemical order, while the third one relates to the cross-correlation between concentration and atomic density.

All these functions can be connected to experimental measurements in several ways. First, total structure factors as measured in x-ray or neutron diffusion experiments can be reconstructed from the partial ones as

$$S(q) = \frac{x_1 f_1^2 S_{11}(q) + 2\sqrt{(x_1 x_2)} f_2 S_{12}(q) + x_2 f_2^2 S_{22}(q)}{x_1 f_1^2 + x_2 f_2^2} \tag{B.2}$$

where f_1 and f_2 corresponds to the x-ray or neutron scattering form factor of i type atom. From the partial AL static structure factors $S_{ij}(q)$, the total neutron weighted static structure factor $S_T(q)$ is readily evaluated using the expression

$$\langle b^2 \rangle S_T^{(\mathrm{INS})}(q) = \sum_{i=1}^{2} \left(\langle b_i^2 \rangle - \langle b_i \rangle^2 \right) x_i + \sum_{i,j=1}^{2} (x_i x_j)^{1/2} \langle b_i \rangle \langle b_j \rangle S_{ij}(q) \tag{B.3}$$

where, $\langle b_i \rangle$ is the coherent scattering length, $4\pi \langle b_i \rangle^2$ is the total scattering cross-section and $\langle b \rangle^2 = \sum_{i=1}^{2} x_i \langle b_i^2 \rangle$ is the average cross-section per atom. In the case of IXS, the total static structure factor only presents the coherent term, namely,

$$S_T^{(\mathrm{INS})}(q) = \sum_{i,j=1}^{2} (x_i x_j)^{1/2} \frac{f_i(q) f_j(q)}{\langle f^2(q) \rangle} S_{ij}(q) \tag{B.4}$$

where, $f_i(q)$ are the atomic scattering form factors and $\langle f^2(q) \rangle = \sum_{i=1}^{2} x_i f_i^2(q)$.

Appendix C

Average Kinetic Energy Density Functional

We think of kinetic energy as a functional

$$T_s[\rho] = T_\beta[\rho] + T_W[\rho], \tag{C.1}$$

here, $T_W[\rho(\mathbf{r})]$, $T_\beta[\rho]$, $\tilde{k}(\mathbf{r})$ and $k(\mathbf{r})$ are defined in equations 4.86, 4.87, 4.88 and 4.89 respectively. We want to restore the LRT outcome in the case of minor deviations from a homogeneous system. The weight function is obtained by equating the FT of the second functional derivative of $T_s[\rho]$ with regard to $\rho(\mathbf{r})$ when $\rho(\mathbf{r}) = \rho_0$, to the inverse of the Lindhard response function

$$(6\beta^2 - \frac{20}{3}\beta + \frac{10}{9}) + 4\beta(\frac{5}{3} - 2\beta)\bar{\omega}_\beta(\eta) + 2\beta^2\bar{\omega}_\beta(\eta)^2 = \frac{10}{9}(\frac{1}{\pi_L(\eta)} - 3\eta^2) \tag{C.2}$$

where $\eta = q/2k_F^0$,and $\bar{\omega}_\beta$ are the FT of ω_β, respectively and

$$\pi_L(\eta) = \frac{1}{2}(1 + \frac{1-\eta^2}{2\eta} ln|\frac{1+\eta}{1-\eta}|). \tag{C.3}$$

is the response function for a homogeneous electron gas without interactions. When the solution to equation (C.2) is taken into consideration and β is within the range $0 \leq \beta \leq \frac{5}{6}$ so that the power of $\rho(\mathbf{r})$ in equation (4.87) is positive, the weight function is provided by

$$\bar{\omega}_\beta(\eta) = 2 - \frac{5}{3\beta} + \frac{1}{3\beta}\sqrt{(5-3\beta)^2 + 5(\pi_L^{-1}(\eta) - 1 - 3\eta^2)} \tag{C.4}$$

A stronger limit on $\beta : \beta \leq 0.5991$ is imposed by the requirement that $\bar{\omega}_\beta$ be genuine. The functional reduces to the Thomas-Fermi functional in the limit of uniform density when using this weight function, recovering the LRT limit. The limit $\eta \to \infty$ contains the following

$$\bar{\omega}_\beta(\eta) \to C_1 + A/\eta^2 + ... \tag{C.5}$$

where

$$C_1 = 2 - \frac{5}{3\beta} + \frac{1}{3\beta}\sqrt{17 - 30\beta + 9\beta^2} \tag{C.6}$$

It is practical to design a weight function that is "modified" since the constant C_1 results in a Dirac delta function in real space

$$\tilde{\omega}_\beta(\eta) = \bar{\omega}_\beta(\eta) - C_1 \tag{C.7}$$

in order for every convolution containing ω_β, such as in equation (**??**), to become

$$G(\mathbf{r}) * \omega_\beta(2k_F^0 r) = C_1 G(\mathbf{r}) + G(\mathbf{r}) * \omega_\beta(2k_F^0 r) \tag{C.8}$$

The point at which the mean electron density and, consequently, k_F^0, vanish, as in the case of a finite system, is a crucial limit. As a result of $\eta = q/2k_F^0 \to \infty$ and $\tilde{\omega}_\beta(\eta)$ disappearing, the convolutions using the "modified" weight function are no longer present. Therefore, $\tilde{k}(\mathbf{r} = C_1 k(\mathbf{r}))$, the kinetic energy functional changes to $T_s[\rho] = T_w[\rho] + C_1^2 T_{TF}[\rho]$, and for $\beta = 4/9, C_1 = 0$.

Bibliography

[1] P. Hohenberg, and W. Kohn. *Phys. Rev.*, **136**:864, 1964.

[2] W. Kohn, and L. J. Sham. *Phys. Rev. A*, **140**:1133, 1965.

[3] R. G. Parr, and W. Yang. *Density-functional theory of atoms and molecules*. Oxford University Press, New York, 1989.

[4] R. N. Singh, and F. Sommer. Segregation and Immiscibility in Liquid Binary Alloys. *Rep. Prog. Phys.*, **60**:57, 1997.

[5] A. Meyer, M. Silbert, and W. H. Young. A Simplified WCA Theory of Liquid Structure. *Chemical Physics*, **49**:147, 1980.

[6] M. P. Allen, and D. J. Tidesley. *Computer Simulation of Liquid*. Clarendon Press, Oxford, 1987.

[7] B. J. Alder, and T. E. Wainwright. Phase transition for hard sphere system. *J. Chem. Phys.*, **27**:1208, 1957.

[8] B. J. Alder, and T. E. Wainwright. Studies in Molecular Dynamics. I. General Method. *J. Chem. Phys.*, **31**:459, 1959.

[9] A. Rahman. Correlations in the motion of atoms in liquid argon. *Phys. Rev.*, **136**:A 405, 1964.

[10] N. W. Ashcroft, and N. D. Mermin. *Solid State Physics*. W. B. Saunders, Philadelphia, 1976.

[11] L. Verlet. Computer "experiments" on classical fluids. II. Equilibrium Correlation Function. *Phys. Rev.*, **165**:201, 1968.

[12] L. Verlet. Computer "experiments" on classical fluids. I. Thermodynamical properties of Lennard-Jones molecules. *Phys. Rev.*, **159**:98, 1967.

[13] J. R. D. Copley and S. W. Lovesey. The dynamic properties of monatomic liquids. *Reports on progress in physics*, **38**:461, 1975.

[14] F. H. Stillinger and A. Rahman. Improved simulation of liquid water by molecular dynamics. *J. Chem. Phys.*, **60**:1545, 1974.

[15] M. S. Daw and M. I. Baskes. Semiempirical, Quantum Mechanical Calculation of Hydrogen Embrittlement in Metals. *Phys. Rev. Lett.*, **50**:1285, 1983.

[16] M. Levitt and A. Warshel. Computer simulation of protein folding. *Nature*, **253**:694, 1975.

[17] R. Car, and M. Parrinello. *Phys. Rev. Lett.*, **55**:2471, 1985.

[18] K. Laasonen, M. Sprik, M. Parrinello and R. Carr. *J. Chem. Phys.*, **99**:9080, 1993.

[19] Björn O. Roos, Roland Lindh, Per Åke Malmqvist, Valera Veryazov, Per-Olof Widmark. *Multiconfigurational Quantum Chemistry*. John Wiley & Sons, New Jersey, USA, 2016.

[20] R. M. Dreizler, and E. K. U. Gross. *Density Functional Theory*. Springer-Verlag, Berlin, 1990.

[21] M. R. Molla, A. Z. Z. Ahmed, H. Sarker, G. M. Bhuiyan, M. R. Amin, L. E. González, and D. J. González. *J. Non-Crys. Solids*, **406**:45, 2014.

[22] M. J. Gillan. *Contemporary Physics*, **38**:115, 1997.

[23] D. Max and J. Hutter. *Ab initio Molecular Dynamics*. Cambridge University Press, Cambridge, 2009.

[24] Josef Hansson and Torbjörn M. J. Nilsson and Lilei Ye and Johan Liu. *Int. Mater. Rev.*, **63**:22, 2017.

[25] J. W. Boley, E. L. White, and R. K. Karmer. *Adv. Mater*, **27**:14, 2015.

[26] J. A. Pryde. *The Liquid State*. Hutchinson University Library, London, 1966.

[27] J. S. Rowlinson. *Liquids and Liquid Mixtures*. Butterworth, London, 2nd edition, 1971.

[28] P. A. Egelstall. *An Introduction to the Liquid State*. Academic Press, New York, 1967.

[29] T. E. Faber. *An Introduction to the Theory of Liquid Metals*. Cambridge University Press, London, 1972.

[30] Kanaev, A. A. and Andreev, P. A. U. S. Department of Commerce, Office of Technical Services, USA, 1960.

[31] P. E. Potter, and M. H. Rand. Handbook of Thermodynamic and Transport of Alkali Metals. Blackwell Scientific, Oxford, 1985.

[32] R. Hultgren, R. D. Desai, T. D. Hawkins, M. Gleiser, and kelley. *Selected Values of the Thermodynamic properties of Binary Alloys*. American Society for Metals, Metals Park, Ohio, 1973.

[33] Piyush Sabharwall, Vivek Utgukar, Akira Tokuhiro, Fred Gunnerson. *Journal of Nuclear Science and Technology*, **46**:534, 2009.

[34] Mohamed S. El-Genk. Space nuclear reactor power system concepts with static and dynamic energy conversion. *Energy Conversion and Management*, **49**:402, 2008.

[35] Chenglong Wang and Zhangpeng Guo and Dalin Zhang and Suizheng Qiu and Wenxi Tian and Yingwei Wu and Guanghui Su. *Progress in Nuclear Energy*, 68:142, 2013.

[36] D. Marx, and J. Hutter. *Modern Methods and Algorithms of Quantum Chemistry*. J. Grotendorst(Ed.), John von Neumann Institute for Computing, Jülich, NIC series, Vol.1, ISBN 3-00-005618-1, Germany, 2000.

[37] M. E. Tuckerman. *J. Phys. B Condens. Matter*, **14**:R1297, 2002.

[38] R. Iftimie, P. Minary, and M. E. Tuckerman. *Proc. Natl. Acad. Sci. USA*, **102(19)**:6654, 2005.

[39] D. G. Kanhere, and V. Shah. *Ab initio, orbital free molecular dynamics: Technique and applications, in Electronic Structure of Alloys, Surfaces and Clusters*. Chap. 10, Taylor and Francis, eds., Hardcover, 2002.

[40] R. Car, and M. Parrinello. *Simple Molecular Systems at Very High Density, in NATO Advanced Study Institute*. Series B: Physics 186, A. Polian, P. Lebouyre and N. Boccaraeds, Plenum, 1989.

[41] H. Chen, and A. Zhou. *Numer. Math. Theor. Meth. Appl.*, **1(1)**:1, 2008.

[42] A. R. Leach. *Molecular Modelling Principles and Applications*. Longman, Edinburg, 1996.

[43] U. Balucani, and M. Zoppi. *Dynamics of the liquid State*. Clarendon Press, Oxford, UK, 1994.

[44] J. P. Hansen, and I. R. McDonald. *Theory of Simple Liquids*. Academic Press, London, UK, 3rd edition, 2006.

[45] J. P. Mithen. *Molecular dynamics simulations of the equilibrium dynamics of non-ideal plasmas*. PhD Thesis, Trinity College, University of Oxford, 2012.

[46] P. P. Ewald. *Ann. Phys. (Leipzig)*, **64**:253, 1921.

[47] C. David Sherrill. *Introduction to Electronic Structure Theory*. Georiga Institute of Technology, Georiga, USA, 2003.

[48] L. I. Schiff. *Quantum Mechanics*. McGraw-Hill, 1968.

[49] M. Born, and J. R. Oppenheimer. *Ann. Phys.*, **84**:457, 1927.

[50] J. Perdew, and A. Zunger. Self-interaction correction to density-functional approximations for many-electron systems. *Phys. Rev. B*, **23**:5048, 1981.

[51] M. Bhuiyan, L. E. González, and D. J. González. *Euro. Phys. J. Web of Conference*, **15**:01011, 2011.

[52] D. J. González, L. E. González, and J. M. López, M. J. Stott. *Phys. Rev. B*, **65**:184201, 2002.

[53] E. Schrödinger. *Phys. Rev.*, **28**:1049, 1926.

[54] D. J. Griffiths. *Introduction to Quantum Mechanics*. Pearson, UK, 2005.

[55] M. Born. *Zeitschrift fuer Physik*, **37**:863, 1926.

[56] Wolfram Koch, and Max C. Holthausen. *A Chemists's Guide to Density Functional Theory*. Wiley-VCH, Germany, 2001.

[57] N. Zettili. *Quantum Mechanic: Concepts and Applications*. Wiley-VCH, jacksonville, USA.

[58] K. Capelle. *A bird's-eye view of density-functional theory*. arXiv:cond-mat, 0211443v5, 2006.

[59] W. Kohn. *Rev. Mod. Phys.*, **71**:1253, 1999.

[60] W. Kock, and M. C. Holthausen. *A Chemists Guide to Density Functional Theory*. Wiley-VCH, 2001.

[61] B. Santra. *Density-Functional Theory Exchange-Correlation Functionals for Hydrogen Bonds in Water*. PhD thesis, der Technischen Universität, Berlin, Germany, August 2010.

[62] H. Hellmann. *Einführung in die Quantenchemie*. Leipzig, Franz Deuticke, 1937.

[63] R. P. Feynman. *Phys. Rev.*, **56 (4)**:340, 1939.

[64] L. H. Thomas. *Proc. Cambridge Phil. Soc.*, **23**:542, 1927.

[65] E. Fermi. *Rend. Accad. Naz. Lincei*, **6**:602, 1927.

[66] V. F. Petrenko, and R. W. Whitworth. *Physics of Ice*. Oxford University Press, Inc., New York, 2003.

[67] P. A. M. Dirac. *Proc. Cambridge Phil. Soc.*, **26**:376, 1930.

[68] D. M. Ceperley, and B.J. Alder. *Phys. Rev. Lett.*, **45**:566, 1980.

[69] J. P. Perdew, and Y. Wang. *Phys. Rev. B*, **45**:13244, 1992.

[70] J. P. Perdew, and A. Zunger. *Phys. Rev. B*, **23**:5048, 1981.

[71] S. J. Vosko, L. Wilk, and M. Nusair. *Can. J. Phys.*, **58**:1200, 1980.

[72] J. P. Perdew, K. Burke, and M. Ernzerhof. *Phys. Rev. Lett. E*, **78**:1396, 1997.

[73] J. P. Perdew, and Y. Wang. *Phys. Rev. B*, **46**:12947, 1992.

[74] J. P. Perdew, K. Burke, and M. Ernzerhof. *Phys. Rev. Lett.*, **77**:3865, 1996.

[75] A. D. Becke. *J. Chem. Phys.*, **38**:3098, 1998.

[76] P. P. Rushton. *Towards a Non-local Description of Exchnage and Corrlation*. PhD Thesis, University of Durham, 2002.

[77] J. S. Lin, A. Qteish, M. C. Payne, and V. Heine. *Phys. Rev. B*, **47**:4174, 1993.

[78] D. Marx, and J. Hutter. *Ab initio Molecular Dynamics: Basic Theory and Advanced Methods*. Cambridge University Press, UK, 2009.

[79] J. M. Ziman. *Principals of the Theory of Solids*. II ed., Cambridge University Press, London, 1972.

[80] N. Troullier, and J. L. Martins. *Phys. Rev. B*, **43**:1993, 1991.

[81] G. P. Kerker. *J. Phys. C*, **13**:L189, 1980.

[82] D. R. Hamann, M. Schl´uter, and C. Chiang. *Phys. Rev. Lett.*, **43**:1494, 1979.

[83] D. Vanderbilt. *Phys. Rev. B*, **32**:8412, 1985.

[84] S. Goedecker, M. Teter, and J. Hutter. *Phys. Rev. B*, **54**:1703, 1996.

[85] W. E. Pickett. Pseudopotential methods in condensed matter applications. *Comp. Phys. Rep.*, **9**:115, 1989.

[86] L. Calderin, D. J. González, L. E. González, and J. M. López. *J. Chem. Phys.*, **129**:194506, 2008.

[87] L. Calderin, L. E. González, and D. J. González. *Phys. Rev. B*, **80**:115403, 2009.

[88] T Itami, S Munejiri, T Masaki, H. Aoki, Ishil, T. Kamiyama, Y. Senda, F. Shimojo, and K. Hoshino. *Phys. Rev. B*, **67**:064201, 2003.

[89] M. Pearson, E. Smargiassi, and P. A. Madden. *J. Phys. Condens Matter*, **5**:3221, 1993.

[90] Y. A. Wang, and E. A. Carter. *Theoritical Methods in Condensed Phase Chemistry*. Kluwer, Dordrecht, 2000.

[91] B. Zhou, V. L. Ligneres, and E. A. Carter. *J. Chem. Phys.*, **122**:044103, 2005.

[92] E. Smargiassi, and P. A. Madden . *Phys. Rev. B*, **49**:5220, 1994.

[93] E. Smargiassi, and P. A. Madden . *Phys. Rev. B*, **51**:117, 1995.

[94] M. Foley, E. Smargiassi, and P. A. Madden . *J. Phys. Condens Matter*, **6**:5231, 1994.

[95] M. Foley. *Developments in the ab initio simulation of metallic systems*. D. Phil. Thesis, Oxford University, UK, 1996.

[96] M. Foley, and P. A. Madden . *Phys. Rev. B*, **53**:10589, 1996.

[97] S. C. Watson. *Structural relaxation at defects by ab initio molecular dynamics*. D. Phil. Thesis, Oxford University, UK, 1996.

[98] Q. Wang, M. D. Gossman, M. P. Iñiguez, and J. A. Alonso. *Phil. Mag. B*, **69**:1045, 1993.

[99] S. C. Watson, and P. A. Madden . *Phys. Chem. Comm.*, **1**:1, 1998.

[100] S. C. Watson, and E. A. Carter . *Comput. Phys. Commun.*, **128**:67, 2000.

[101] D. R. Hartree. *Proc. Cambridge Phil. Soc.*, **24**:89, 1928.

[102] V. Fock. *Z. Phys.*, **61**:126, 1930.

[103] C. C. J. Roothaan. *Rev. Mod. Phys.*, **23**:69, 1951.

[104] C. F. von Weizsäcker. *Z. Phys.*, **96**:431, 1935.

[105] R. O. Jones, and O. Gunnarsson. *Rev. Mod. Phys.*, **61**:689, 1989.

[106] F. Perrot. *J. Phys. Condens Matter*, **6**:431, 1993.

[107] E .V. Ludeña, and V. V. Karasiev. *Reviews of Modern Quantum Chemistry: a Celebration of the Contributions of Robert Parr*. World Scientific, Singapore, 2002.

[108] W. Jones. *Phys. Lett. A*, **34**:351, 1971.

[109] W. Jones, and W. H. Young. *J. Phys. C: Solid State Phys.*, **4**:1332, 1971.

[110] J. Lindhard. *K. Dan. Vidensk. Selsk. Mat-Fys. Medd*, **28**:8, 1954.

[111] E. Smargiassi, and P. A. Madden. *Phys. Rev. B*, **49**:5220, 1994.

[112] M. Foley, and P. A. Madden. *J. Phys. Condens Matter*, *ibid* **53**:10589, 1996.

[113] Y. A. Wang, N. Govind, and E. A. Carter. *Phys. Rev. B*, **58**:13 465, 1998.

[114] Y. A. Wang, N. Govind, and E. A. Carter. *Phys. Rev. B*, **60**:16 350, 1999.

[115] E. Chacón, J. E. Alvarellos, and P. Tarazona. *Phys. Rev. B*, **32**:7868, 1985.

[116] P. García-Gonález, J. E. Alvarellos, and E. Chacón. *Phys. Rev. A*, **54**:1897, 1996.

[117] P. García-Gonález, J. E. Alvarellos, and E. Chacón. *Phys. Rev. B*, **53**:9509, 1996.

[118] P. García-Gonález, J. E. Alvarellos, and E. Chacón. *Phys. Rev. B*, **57**:4857, 1998.

[119] D. J. González, L. E. González, J. M. Lopez, and M. J. Stott. *J. Chem. Phys.*, **115**:2373, 2001.

[120] S. Gómez, L. E. González, D. J. González, M. J. Stott, S. Dalgic, and M. Silbert. *J. Non-Crys. Solids*, **163**:250, 1999.

[121] S. R. Bickham, O. Pfaffenzeller, L. A. Collins, J. D. Kress, and D. Hohl. *Phys. Rev. B*, **58**:R11813, 1998.

[122] N. Govind, J. L. Mozos, and H. Guo. *Phys. Rev. B*, **51**:7101, 1995.

[123] P. Blaise, S. A. Blundell, and C. Guet. *Phys. Rev. B*, **55**:15856, 1997.

[124] M. Foley, E. Smargiassi, and P. A. Madden. *J. Phys. Condens Matter*, **6**:5231, 1994.

[125] E. Smargiassi, and P. A. Madden. *Phys. Rev. B*, **51**:117, 1995.

[126] E. Smargiassi, and P. A. Madden. *Phys. Rev. B*, *ibid* **51**:129, 1995.

[127] B. J. Jesson, M. Foley, and P. A. Madden. *J. Phys. Condens Matter*, *ibid* **55**:4941, 1997.

[128] F. J. Rogers and D. A. Young. New Thermodynamically Consistent Integral-Equation for Simple fluids. *Phys. Rev. A*, **30**:999–1007, 1984.

[129] S. K. Lai, W. Li, and M. P. Tosi. Evalution of Liquid Structure for Potassium, Zinc, and Cadmium. *Phys. Rev. A*, **42**:7289–7303, 1990.

[130] J. P. Boon, and S. Yip. *Molecular Hydrodynamics*. Dover Publications, Inc., New York, 1991.

[131] N. W. Ashcroft and D. C. Langreth. Structure of Binary Liquid Mixtures. *Phys. Rev.*, **156**:685–691, 1967.

[132] P. A. Doyle and P. S. Turner. Relativistic Hartree-Fock X-Ray and Electron Scattering Factors. *Acta Cryst.*, **24**:390–397, 1968.

[133] Y. Waseda. *The Structure of Non-Crystaline Materials*. McGraw-Hill Inc., USA, 1980.

[134] R. L. McGreevy, A. Baranyai, and I. Ruff. *Phys. Rev. B*, **16**:47, 1986.

[135] N. E. Cusak. *The Physics of Structurally Disordered Matter*. Adam-Hilger, Bristol, 1987.

[136] C. N. J. Wagner and H. Ruppersberg. *At. Energy Rev.*, **1**:101, 1981.

[137] R. B. Bird, W. E. Stewart, and E. N. Lightfoot. *Transport phenomena*. 2nd ed., John Wiley and Sons, New York, 2002.

[138] L. Wei-Zhong, C. Cong, and Y. Jian. *Asian Research*, **37(2)**:86, 2008.

[139] J. M. Haile. *Molecular Dynamics Simulation*. John Wiley and Sons, New York, 1992.

[140] L. Van Hove. *Phys. Rev.*, **95**:249, 1954.

[141] M. Shimoji. *Liquid Metals An Introduction to the Physics and Chemistry of Metals in the Liquid States*. Academic Press, London, 1977.

[142] S. J. Blundell, and K. M. Blundell. *Concepts in Thermal Physics*. Oxford University Press, UK, 2006.

[143] D. M. Heyes. *The Liquid state: Application of Molecular Simulations*. Wiley, West Sussex-England, 1998.

[144] N. Jakse, J. F. Wax, and A. Pasturel. *J. Chem. Phys.*, **126**:234508, 2007.

[145] B. J. Palmer. *Phys. Rev. E*, **49**:359, 1994.

[146] R. L. McGreevy, A. Baranyai and I. Ruff. *Phys. Chem. Liq.*, **16**:47, 1986.

[147] J. Souto, M. M. G. Alemany, L. J. Gallego, L. E. González and D. J. González. *J. Nuc. Matter*, **411**:163, 2011.

[148] J. Souto, M. M. G. Alemany, L. J. Gallego, L. E. González and D. J. González. *Modelling Simul. Mater. Sci. Eng.*, **21**:075006, 2013.

[149] B. P. Alblas, W. Van Der Lugt, E. G. Visser, and J. Th. M. De Hosson. *Physica B+C*, **114**:59, 1982.

[150] J. F. Wax. Molecular dynamics study of the Static Structure of Liquid Na-K Alloys. *Physica B*, **403**:4241–4248, 2008.

[151] G. Bhuiyan, L. E. González, and D. J. González. *Condens. Matt. Phys.*, **15(3)**:33604, 1, 2012.

[152] G. Abowitz, and R. B. Gordon. *J. Chem. Phys.*, **37**:125, 1962.

[153] J. Trullàs, and J. A. Padró. *Phys. Rev. E*, **50**:1162, 1994.

[154] J. Trullàs, and J. A. Padró. *J. Chem. Phys.*, **99**:3983, 1993.

[155] Tadashi Kato. *J. Phys. Chem.*, **89**:5750, 1985.

[156] L. S. Darken and R. W. Gurry. *Physical Chemistry of Metals*. McGraw-Hill series in materials science and engineering. McGraw-Hill, Michigan, 1953.

[157] Z. Shi, P. G. Debenedetti, and F. H. Stillinger. *J. Chem. Phys.*, **138**:12A526, 2013.

[158] S. Sengupta, S. Karmakar, C. Dasgupta, and S. Sastry. *J. Chem. Phys.*, **138**:12A548, 2013.

[159] O. J. Foust. *Sodium-NaK Engineering Handbook*, volume 1. Gordon and Breach, Science Publishers, Inc., New York, USA, 1972.

[160] S. Becker, N. Meyer, H. Xu and J. -F. Wax. Viscosity of liquid Na–K alloys from molecular dynamics simulations. *J. Phys. Condens Matter*, **32**:194005, 2020.

[161] R V Gopala Rao and A K Murthy. Self Diffusion in liquid Na-K alloy. **9**:587, 1977.

[162] A. B. Bhatia, and D. E. Thornton. Structural Aspects of the Electrical Resistivity of Binary Alloys. *Phys. Rev. B*, **2**:3004, 1970.